Photofunctions of Intercalation Compounds

Makoto Ogawa*

The Institute of Physical and Chemical Research (RIKEN), Hirosawa 2-1, Wako-shi, Saitama 351-01, Japan

Kazuyuki Kuroda*

Department of Applied Chemistry, Waseda University, Ohkubo-3, Shinjuku-ku, Tokyo 169, Japan

Received June 30, 1994 (Revised Manuscript Received November 1, 1994)

Contents

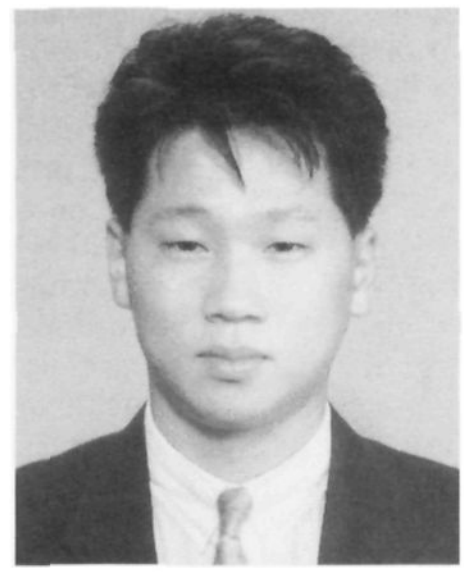

Makoto Ogawa was born in Shizuoka, Japan, in 1964. He received his B. and M. degrees in Applied Chemistry from Waseda University in 1987 and 1989. His Dr. degree was earned at Waseda University in 1992 under Professor Chuzo Kato. He is currently a special researcher for the basic science program, Science and Technology Agency, Japan (postdoctoral status) at The Institute of Physical and Chemical Research (RIKEN). His research interests include the organization of molecules at inorganic–organic interfaces.

Kazuyuki Kuroda is presently professor of Department of Applied Chemistry at Waseda University where he has been since 1989. He received his Ph.D. degree from Waseda University in 1979 under the direction of Professor C. Kato. His research interests include intercalation chemistry of layered inorganic materials, silicate chemistry, inorganic polymers for ceramic precursors, novel synthetic methods of inorganic materials utilizing inorganic–organic interactions, and functional inorganic materials.

I. Introduction

Photophysical and photochemical reactions in heterogeneous media may differ significantly from analogous reactions in a homogeneous solution.[1-3] The important role of reaction media in control rates, product distributions, and stereochemistry has long been recognized. Therefore, the study of the photoprocesses of organic and inorganic photoactive species in restricted geometry is a growing new field which yields a wide variety of useful applications in such areas as reaction media for controlled photochemical reactions and molecular devices for optics.[1-19] For this purpose, nanomaterials with an ordered structure have an advantage in that the properties of

0009-2665/95/0795-0399$15.50/0

Table 1. Characteristics of Host–Guest Systems Studied for Photofunctional Materials

host	layered materials	sol–gel derived materials	organic polymers
dopant concentration	very high	low[a]	low[a]
stability	thermally chemically very good	thermally chemically good	relatively low
processing	powder, oriented film, single crystal	film, fiber, monolith etc.	film, fiber, monolith etc.
film preparation	from suspension	from precursor solution	from solution
characterization	microscopic information can be obtained	porosity can be measured	geometrical characterization is difficult
optical quality	good	very good	very good
variation	wide	limited	relatively wide

[a] Dopant should be miscible in starting solution and high concentration of dopant may result in the aggregation.

immobilized species can be discussed on the basis of their defined nanoscopic structures. Their structure–property relationships will provide indispensable information on designing materials with novel chemical, physical, and mechanical properties. In other words, one can control the attractive properties, such as photochromic and photocatalytic ones, by organizing photoactive species into matrices with appropriate geometry and chemical environments. The notable systems with molecularly ordered structures utilized to organize reactants are surfactant aggregates such as micelles,[9] and inclusion compounds of both organics[10,11] and inorganics.[12–14] Organized assemblies such as Langmuir–Blodgett (LB) films[15] and liquid crystals[16] have extensively been studied because of their applicability as molecular devices.

Among the many ordered or constrained systems utilized to organize reactants, crystalline inorganic solids such as layered materials and zeolites occupy a special position owing to their adsorptive properties, ion exchange ability, thermal and chemical stability, and so on.[20–23] Zeolites have been utilized as a reaction vessel at molecular level due to their defined and interconnected microporous structures.[12–14,24] The well-confined size of the pore enables us to prepare and characterize metal and semiconductor clusters[25,26] and to obtain highly efficient charge separation in artificial photosynthetic systems.[27] The interconnected micropore has been applied to prepare conjugated polymer (so-called molecular wire)[28] and to align dipoles for the second harmonic generation.[29] The processing of zeolites into films[30] or larger crystals[31] and the preparation of solids with different porous structures,[32–36] etc., are currently being investigated for wider application.

In contrast, layered materials offer two-dimensional expandable interlayer space for organizing guest species.[21,37] Intercalation means the reversible insertion of guest species into layered host materials while maintaining the structural features of the host. (Figure 1 schematically represents intercalation.) Various layered materials such as graphite, clay minerals, transition metal dichalcogenides, layered double hydroxides, metal phosphates and phosphonates, and transition metal oxides have been known as host materials for intercalation compounds. The motivation to study intercalation reactions is that the optical and electronic properties of both guest and host can be altered by the reactions. On this basis, intercalation compounds have been studied as catalysts and their supports,[38] shape-selective adsorbents,[22,39] ion exchangers,[40] ionic conductors,[40,41] electrodes,[42] photofunctional materials,[37] etc., and a wide variety of host–guest systems with unique structures and properties have been reported. Compared with zeolites, one of the most important characteristics of intercalation compounds is the expandability of interlayer space. The microscopic structure can be tailored by selecting and designing both the guests and hosts and also by coadsorption. From X-ray diffraction studies, interlayer distance can be measured and the orientation of the intercalated species can be roughly estimated. Moreover, some materials have been processed into single crystals or oriented films, in which case microscopic anisotropy can be converted into a macroscopic one. Those structural features make it possible to discuss structure–property relationships.

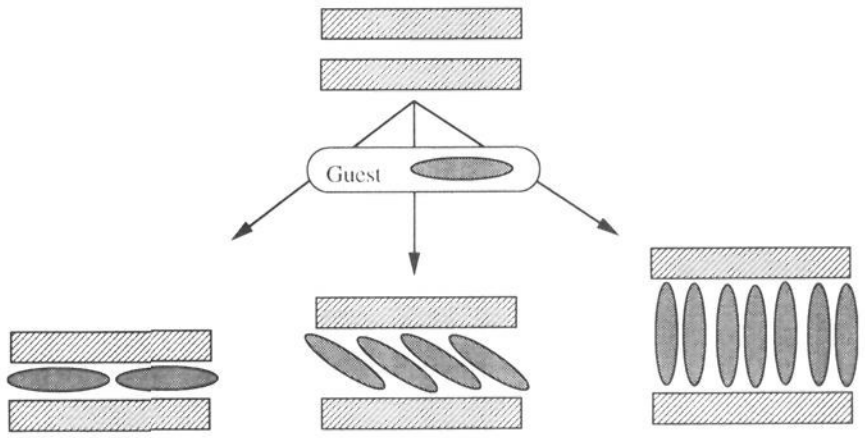

Figure 1. Schematic representation of intercalation.

In this article, we will review the studies on the photofunctions of intercalation compounds. (The structures and properties of host materials which have been used for immobilizing photoactive species have been summarized in the following section.) Some of these studies are for the purpose of characterizing the properties of host materials and host–guest systems, and others are for the purpose of contributing to future practical applications. The well-defined layered structures as well as the ability to accommodate guest species on the surface of the layers are very useful for organizing photoactive species to evaluate and control the photofunctions. Table 1 summarizes the characteristics of typical host–guest systems studied for immobilizing photoactive species. Our attention will be mainly focused on the role of layered structure on the organization of photoactive species; the photofunctions of intercalation compounds will be discussed only in connection with the microscopic structures.

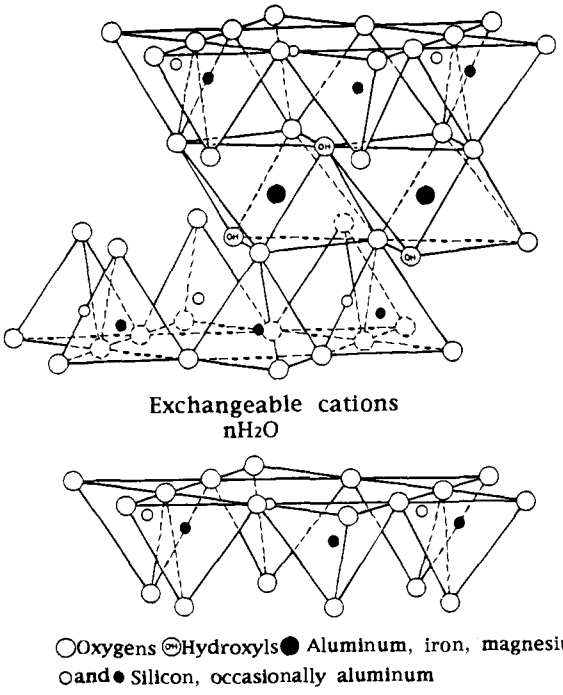

Figure 2. Schematic structure of montmorillonite.

II. Characteristics of Hosts and Preparation and Characterization of Intercalation Compounds

Table 2 summarizes the layered host–guest systems which have been studied for immobilizing photoactive species.

A. Smectites

Smectite is a group of 2:1-type layered clay mineral consisting of negatively charged silicate layers and readily exchangeable interlayer cations.[43-45] Figure 2 shows the layered structure of montmorillonite, which is a typical smectite. The silicate layers are essentially made up of layers formed by a 2:1 condensation of sheets of linked $M_{2-3}(OH)_6$ octahedra, where M is either a divalent or trivalent cation, being sandwiched between two sheets of inward pointing $Si(O,OH)_4$ tetrahedra (the mica-type layer structure) giving a layer with the formula of $M_{2-3}Si_4O_{10}(OH)_2$.

Isomorphous substitution of metal cations with similar size and lower valency, such as $Si^{4+}-Al^{3+}$, $Al^{3+}-Mg^{2+}$, and $Mg^{2+}-Li^{+}$, generates a net negative charge for layers. To compensate for the negative charge, metal cations (generally Na^+ or Ca^{2+}) occupy the interlayer space. The amount as well as the site of the isomorphous substitution influences the surface and colloidal properties of the layered silicates, since they determine the density of charge and the cation–silicate sheet interactions. Smectites are classified by the charge per formula unit of 0.25 to 0.6.

One of the most unique and attractive properties of smectites is their swelling property.[45] By dispersion in water, smectites form a stable thixotropic gel. When the gel is evaporated moderately, the clay particles pile up with their *ab* plane parallel to the substrate to form a transparent self-supporting film.

The mechanism of the intercalation of guest species into smectites is roughly classified into two. One is cation exchange with interlayer exchangeable cations and the other is adsorption of polar molecules such as alcohols, ketones, and amides by ion–dipole interactions with interlayer cations and/or hydrogen bonding with the surface oxygen atom of the silicate sheets. These reactions have been carried out in solid–liquid or solid–gas reactions. Recently, we have reported that solid–solid reactions can be applied to the preparation of intercalation compounds.[46-49] When transition metal ions are substituted for interlayer Na ions, charge transfer between the interlayer transition metal ions and guest species can be a driving force for the intercalation.[50-55]

Synthetic analogues of smectites, i.e. saponite (Sumecton SA, Kunimine Ind. Co.), hectorite (Laponite, Laporte Ind. Co.),[56] and swelling mica (sodium fluortetrasilicic mica, Topy Ind. Co.),[57] have attracted increasing interest since natural clay minerals contain impurities, the amounts of which depend on the source of the clay minerals, both within the structure and on the surface.

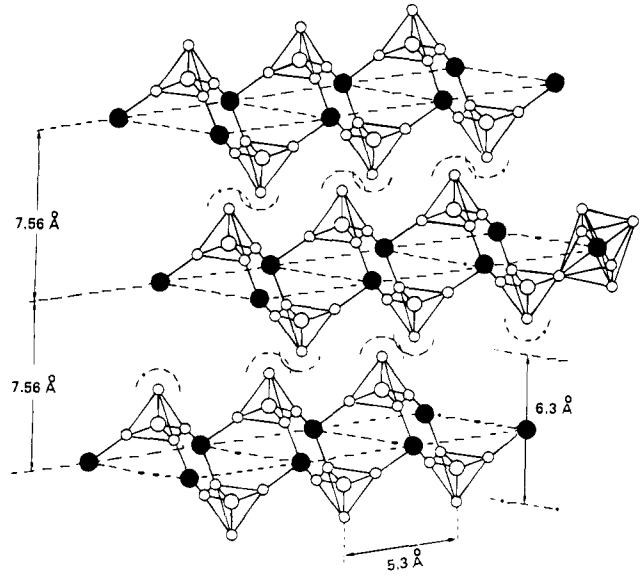

Figure 3. Schematic structure of α-ZrP: (●) Zr, (○) P, (○) O.

B. Zirconium Phosphate and Related Materials

Layered metal phosphates and arsenates have been known to form intercalation compounds.[40,58-60] The best known members of this group are zirconium phosphate, $H_2[Zr(PO_4)_2]H_2O$ and other M^{IV} phosphates and arsenates (M^{IV} = Zr, Ti, Ge, etc.). The α phase of zirconium hydrogen phosphate, $Zr(O_3POH)_2H_2O$ (α-ZrP, the schematic structure is shown in Figure 3), has a layered structure in which zirconium atoms lie in a plane and are bridged by phosphate groups. Three oxygens of each tetrahedral phosphate are linked to three zirconium atoms so that each zirconium is octahedrally coordinated with six oxygens of six different phosphate groups. The fourth oxygen of each phosphate group bears a proton and the proton can be replaced with another cation. Cationic and basic guest species have been intercalated into ZrP through ion exchange and acid–base reactions, respectively.

Since they exhibit swelling behavior in water, photoprocesses in colloidal ZrP systems have been

Table 2. Layered Host–Guest Systems Studied for Immobilizing Photoactive Species

host	guest	photofunctions (refs)	host	guest	photofunctions (refs)
montmorillonite and/or hectorite	ruthenium polypyridine complexes	probe (122–125, 133–136) photocatalysts (233–240)	synthetic saponite synthetic saponite	*p*-nitroaniline rhodamine 590	nonlinear optics (320) emission (277)
montmorillonite and/or hectorite	pyrenes and anthracene	probe (155–166)	synthetic saponite synthetic saponite	pyronin Y coumarine	emission (277) emission (278)
montmorillonite	methylene blue	methachromasy (179, 181–184) surface area determination (178, 180) photosensitizer (225)	synthetic mica (TSM) ZrP ZrP	$Ru(bpy)_3^{2+}$ $Ru(bpy)_3^{2+}$ acridine orange	emission (279, 280) probe (138, 139) (192)
montmorillonite	proflavin	metachromasy (176)	ZrP	porphyrins	(87) photoinduced electron transfer (273)
montmorillonite	acridine orange	metachromasy (186, 187)			
montmorillonite	thionines	metachromasy (188, 189)	ZrP	CdS	(260)
montomorillonite	pyronin Y	metachromasy (185)	ZrP	viologens	photoinduced electron transfer (271–273)
montmorillonite	crystal violet	metachromasy (190)			
montmorillonite	rhodamines	luminescence (171, 276)	ZrP	pyrene, anthracene,	photoinduced electron transfer
montmorillonite	chloridazone	(220)		naphthalene	(275)
montmorillonite	*N*-methyl-8-hydroxy-quinoline methyl sulfate	UV radiation collector (221)	ZrP	manganese carbonyl complex	(226)
montmorillonite	pyrethroid bioresmethrin	energy transfer (222)	ZrP derivative	$Ru(bpy)_3^{2+}$	probe (140, 141)
montmorillonite	rose bengal	photosensitizer (225)	$K_2Ti_4O_9$	methylene blue	(194)
montmorillonite	viologens	photochromism (293) probe (169, 170)	$K_2Ti_4O_9$ $H_2Ti_3O_7$ and $H_2Ti_4O_9$	porphine Eu^{3+}, Tb^{3+}	(202) luminescence (282)
montmorillonite	fulgide	photochromism (288)	$K_2Ti_4O_9$	methylviologen	photochromism (296)
montmorillonite	spiropyranes	photochromism (289–291)	KNb_3O_8	methylviologen	photochromism (299)
montmorillonite	*p*-aminoazobenzene	photochromism (48)	$K_4Nb_6O_{17}$	methylviologen	photochromism (298, 299)
montmorillonite and/or hectorite	porphines	(195–201, 205–210)	$K_4Nb_6O_{17}$ $K_4Nb_6O_{17}$	$Ru(bpy)_3^{2+}$ Ni	photosensitizer (69, 269, 270) photocatalysts (262–266)
montmorillonite and/or hectorite	phthalocyanines	catalysts (211–214)	$K_4Nb_6O_{17}$ $KTiNbO_5$	Pt methylviologen	photocatalysts (267–270) photochromism (297)
montmorillonite and hectorite	dioxorhenium(V) ion	excited state properties (241)	$HA_{n-1}Nb_nO_{3n+1}$ $HA_{n-1}Nb_nO_{3n+1}$	methylviologen	photochromism (300) photocatalysts (268)
montmorillonite	UO^{2+}	photocatalysts (242, 243)	$MnPS_3$	$Ru(bpy)_3^{2+}$	probe (143,144)
montmorillonite	TiO_2	photocatalysts (249–252)	MPS_3	stilbazolium	nonlinear optics (312, 313)
montmorillonite	Fe_2O_3,	photocatalysts (253, 254)	(M = Cd^{2+} and Mn^{2+})		
montmorillonite	CdS	photocatalysts (255)	CdI_2 and $CdCl_2$	stilbazolium	nonlinear optics (311)
montmorillonite and hectorite	Eu^{3+}, Tb^{3+}	luminescence (281)	PbI_2 PbI_2	alkylammonium aniline	(77–79) (80)
laponite	$Ru(bpy)_3^{2+}$	probe (125–129)	LDH (Mg/Al)	ruthenium polypyridine complex	probe (142)
laponite	pyrenes	probe (156–160, 163–166) photoinduced electron transfer (164, 165)	LDH (Mg/Al)	new coccine, indigo carmine	(84)
laponite	rhodamines	metachromasy (170, 171, 175, 176)	LDH (Mg/Al)	naphthol yellow S	(193)
laponite	rhodamine B and 6G, thinone, cresyl violet	photosensitizer (177)	LDH (Zn/Al)	porphine and phthalocyanines	(211–214)
laponite	crystal violet	metachromasy (191)	LDH (Mg/Al)	cinnamic acid	photochemical cycloaddition (231)
laponite	CdS	photocatalysts (256–258)			
synthetic saponite	stilbazolium	photochemical cycloaddition (227–230)	LDH (Mg/Al)	dioxorhenium(V) ion	excited state properties (241)
synthetic saponite	quinizarin	photochemical hole burning (302)	LDH (Mg/Al) LDH (Mg/Al)	CdS spiropyrane	photocatalysts (259) photochromism (292)
synthetic saponite	porphine	photochemical hole burning (204)	LDH (Li/Al)	4-nitrohippuric acid	nonlinear optics (310)

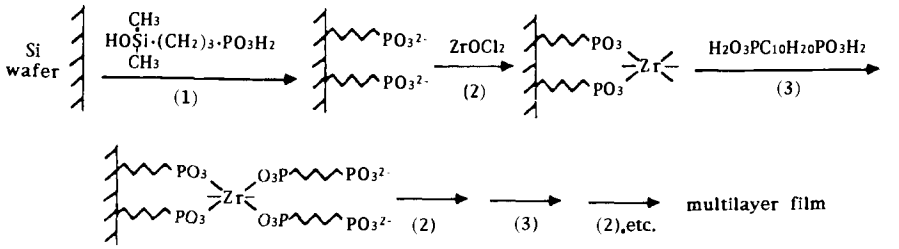

Figure 4. Sequential adsorption scheme for growing metal phosphonate multilayer films on surfaces. (Reprinted from ref 62. Copyright 1988 American Chemical Society.)

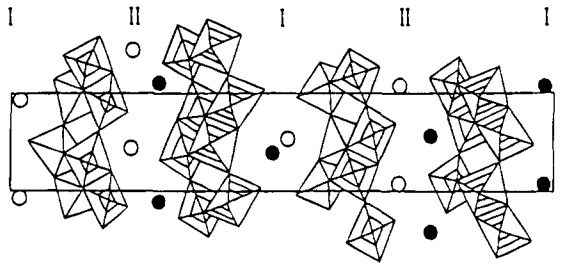

Figure 5. Schematic structure of $K_4Nb_6O_{17}·3H_2O$.

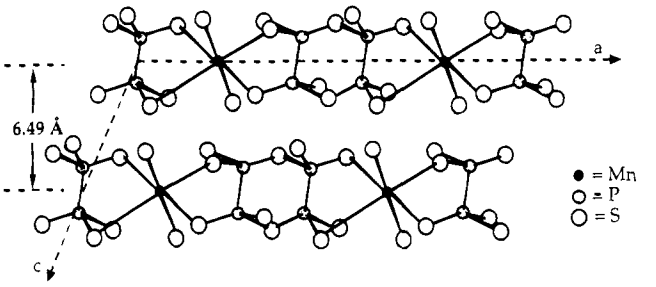

Figure 6. Schematic structure of MPS_3.

investigated. One of the most notable features of this class of materials is the property that organic substituents can be attached to the phosphate groups to form their organic derivatives. Recently, various tetravalent or divalent metal organophosphonates have been synthesized and the layered structures have been characterized.[60]

The powdered nature of the samples leads to severe scattering losses in optical studies. In order to overcome the scattering problem associated with powder, multilayer thin films of zirconium phosphonates are grown directly onto fused silica substrates[61,62] as is shown in Figure 4. The substrate surface is first derivatized with phosphonate groups. When the derivatized substrate is treated with an aqueous solution of Zr^{4+}, the Zr^{4+} binds to the phosphonate groups on the surface, giving a zirconium-rich surface. The substrate is again treated with a solution of biphosphonic acid. Then, one of the phosphonate groups binds to the zirconium rich surfaces, while the other is left uncoordinated. Repeated sequential treatments with the biphosphonic acid and zirconium solutions lead to layer-by-layer growth of zirconium phosphonate film on both sides of the substrate simultaneously.

C. Transition Metal Oxides

Transition metal oxides such as titanates and niobates have been known to form intercalation compounds.[63-69] $K_4Nb_6O_{17}·3H_2O$, $KNbO_3$, $KTiNbO_5$, $K_2Ti_4O_9$ and perovskite-type layered niobates $H[An_{n-1}Nb_nO_{3n+1}]$(A = Ca, La, etc.) are known as ion exchangeable layered solids. One of their most important characteristics is the semiconducting properties of the host layers.

Among them, $K_4Nb_6O_{17}·3H_2O$ is the material studied most extensively because it has two types of alternating interlayers (interlayer I and interlayer II) with different reactivity.[66] The layered structure of $K_4Nb_6O_{17}$ consists of stacked $[Nb_6O_{17}]^{4-}$ layers as is shown in Figure 5. In interlayer I, K^+ ions are present in "more open" cavities than those in interlayer II.

Intercalation of cationic guest species has been introduced by mixing the aqueous solution of guest species and host materials. In order to accelerate the reactions, the reactions are carried out at elevated temperatures. In some cases, a guest exchange method, in which organoammonium-exchanged materials have been used as intermediates, was conducted.[69]

D. Metal Phosphorous Trichalcogenides

MPS_3 (where M = Mn^{2+}, Cd^{2+}, etc.) is a class of layered semiconducting materials which is known as a structural analogue of transition metal calcogenides to intercalate electron donor species such as amines.[70-73] The schematic structure is shown in Figure 6. Certain cationic species can also be intercalated into MPS_3 from their solution and the electric charges are balanced by the loss of cations. They exhibit unique properties such as magnetism and metallic behavior.

E. Perovskite-type Metal Halides

Heavy metal halides are composed of three planes of atoms and are structurally similar to transition metal dichalcogenides.[74-81] The bonding between the adjacent molecular layers is a weak, van der Waals type. As a result, guest species can be introduced in the interlayer space thus modifying many of the physical properties (such as electronic and optical ones) of hosts. The introduction of organic species into the layered structures is carried out by reactions between host and guest vapor or coprecipitation from solutions which contain metal halide and guest. Lead iodide, which is one of the heavy metal iodides, is a direct-band-gap semiconductor with a hexagonal layered structure (Figure 7). Alkylammonium intercalated perovskite-type metal halides $(C_nH_{2n+1}NH_3)_2MX_4$ are candidates of "natural quantum wells" in which the dielectric confinements are important because the alkylammonium layers have a wide band gap.

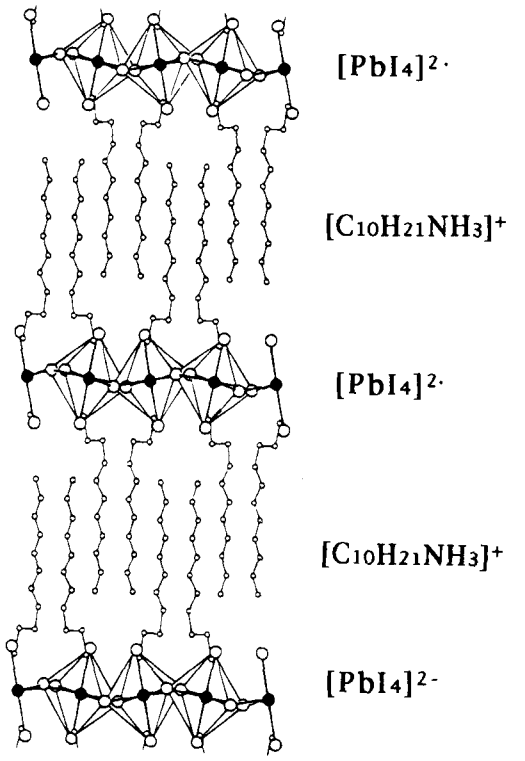

Figure 7. Schematic structure of $(C_{10}H_{21}NH_3)_2PbI_4$: (●) Pb^{2-}, (○) I^-.

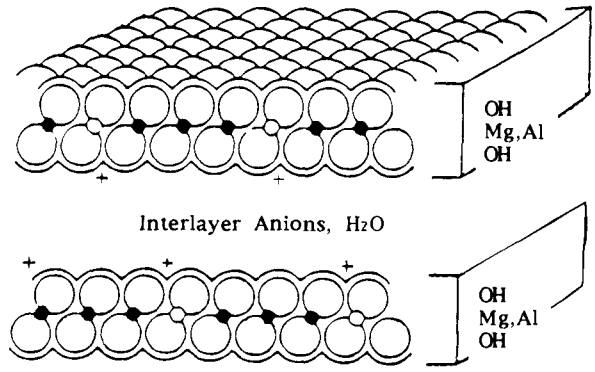

Figure 8. Schematic structure of LDH.

F. Layered Double Hydroxides (LDHs)

Layered double hydroxides (LDHs) are minerals and synthetic materials with positively charged brucite-type layers of mixed-metal hydroxides.[82,83] The schematic structure of the LDH is shown in Figure 8. Exchangeable anions located in the interlayer spaces compensate for the positive charge of the brucite-type layers. The chemical composition of the LDHs is generally expressed as $[M^{2+}_{1-x}M'^{3+}_x(OH)_2][A^{n-}_{x/n}]^{x-}$ where $M^{2+} = Mg^{2+}$, Co^{2+}, Ni^{2+}, etc., $M^{3+} = Al^{3+}$, Cr^{3+}, Fe^{3+}, etc., and A^{n-} is an interlayer exchangeable anion such as CO_3^{2-}, Cl^-, etc. This group of materials has been extensively studied as anion exchangers, adsorbents, catalyst, and so on.

Anionic species have been introduced into the interlayer spaces of LDHs by three methods. The conventional anion exchange reaction using an aqueous solution of guest species has been used widely. Compared with the cation exchange of smectites, the ion exchange reaction for the LDHs is not easily achievable because of their high selectivity to carbonate anions and the large anion exchange capacity. Therefore, CO_2 should be excluded during the sample preparation. Intercalation compounds have also been prepared via direct synthesis in which a LDH phase precipitate forms in the presence of a guest species.[84] The treatment of a mixed-metal oxide solid solution, obtained by the heat treatment of LDH–carbonate, with an aqueous solution of guest results in its reconstitution into an LDH intercalation compound.[85]

G. Characterization of Intercalation Compounds

Intercalation compounds have been characterized by a variety of instrumental analysis techniques including X-ray diffraction, infrared (IR) and Raman spectroscopy, electron micrography, nuclear magnetic resonance (NMR) spectroscopy, electron paramagnetic spectroscopy (EPR), Mössbauer spectroscopy, X-ray photoelectron (XPS) spectroscopy, thermal analyses, and UV–visible and luminescence spectroscopy.

Since the orientations of the guest species correlate directly with the properties of intercalation compounds, a discussion of them is very important. The basal spacings of the intercalation compounds have been determined from X-ray diffraction patterns and the arrangements of the intercalated species can be discussed by the basal spacings and the size of the guest species. Spectroscopic studies on the intercalation compounds have been done to study the states of the adsorbed species and hosts. A variable-temperature solid-state ^2H NMR study of 2H-TaS_2-$\{Co(\eta\text{-}C_5D_5)_2\}_{0.25}$ showed the orientations of the guest species.[86] EPR spectra of uniaxially oriented films of porphyrins intercalated compounds showed the tilt angle of the porphyrins in the interlayer spaces[87] (see section III.E).

Changes in optical, electronic, and magnetic properties upon intercalation may give important information on the structure of intercalation compounds. Among them, photoprocesses of the adsorbed photoactive species, which are very sensitive to the environment, may give insight into the microscopic structures of host–guest systems, to which conventional instrumental analysis does not have access. (Photoprocesses of photoactive species adsorbed on layered solids are discussed in section III.)

H. Representative Examples of Two-Dimensional Organization of Organic Species and Their Applications

n-Alkylammonium ions are the guest cations which have been used widely and the quantitative exchange of the interlayer cation by alkylammonium ions has provided a method for the characterization of smectites and the determination of their layer charge.[88-90] Figure 9 shows the schematic structures of *n*-alkylammonium-intercalated compounds with different cation exchange capacity (CEC). Since the charge density of smectites is relatively low, the intercalated alkylammonium ions can be lying flat. Higher layer charge density results in the paraffin-type arrangements of the intercalated alkylammonium ions. This indicates that the intercalation compounds with the desired geometry of the guest species can be obtained by selecting a host with the appropriate layer charge

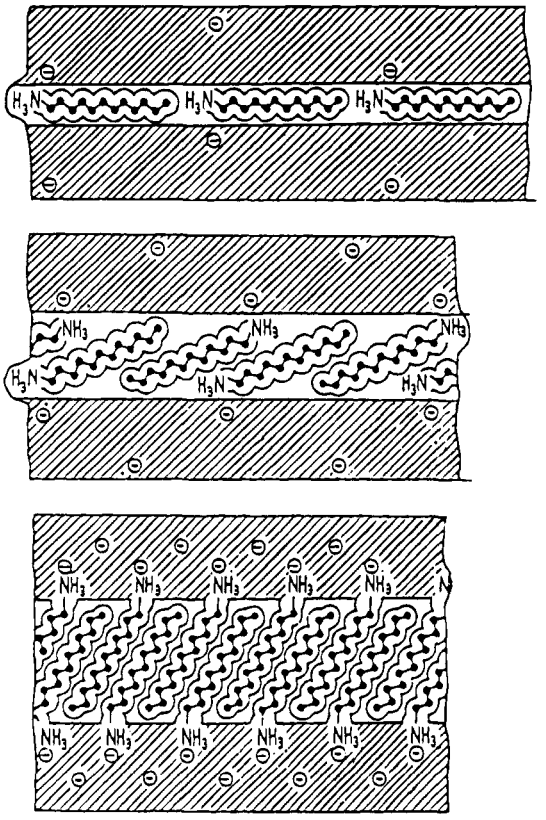

Figure 9. Schematic structure of alkylammonium ions in the interlayer space of layered materials with different layer charge density.

density and a guest with the appropriate sizes. The paraffin-type arrangements formed in the interlayer space of layered materials can be regarded as structural analogues to Langmuir–Blodgett films, self-assembled multilayers,[15,91] and biomembranes,[92,93] which have been investigated widely to construct novel molecular assembly. Besides the cation exchange reactions, acid–base reactions between interlayer proton-donating sites with alkylamines and anion exchange reactions between LDHs and aliphatic sulfates have been reported.

When the interlayer metal cations are replaced by organoammonium cations, the hydrophilic surfaces of the clays are substantially modified to become strongly organophilic.[94] The organophilic clays have been studied as adsorbates,[22,95] chromatographic stationary phase,[96] catalysts,[97] rheology controlling agent,[98] and so on.[99] Recently, immobilization of photoactive species in the interlayer spaces of the alkylammonium exchanged montmorillonites and the unique behavior of the intercalated species have been reported. (See sections III and IV.)

The organization of organic polymers on the layered materials has been investigated widely in order to impart ordered structures to the polymers and to control their electronic and mechanical properties.[41,100] Ruiz-Hitzky et al. have prepared poly(ethylene oxide)–mica intercalation compounds and examined the ionic conductivity of the intercalation compound.[101] The intercalation of water-soluble polymers into semiconducting layered host materials has also been investigated.[102]

Polymerization of organic monomers in sterically limited environments may lead to polymers with novel structures or conformations. By utilizing a two-dimensional opening between the lamellae of montmorillonite, poly(acrylonitrile) (PAN) was carbonized without developing the three-dimensional cross-linked network structure.[103,104] The resultant carbon was found to consist of planar macromolecules and to be easily graphitized by further heat treatment. Most intriguing is the fact that nongraphitizing polymer such as poly(furfuryl alcohol) and poly(vinyl acetate) can be converted to carbon by utilizing the method of carbonization in the interlayer space of montmorillonite.[105] Steric constraint in the interlayer space has been assumed to play a dominant role in the unusual reactions.

The insertion of conjugated polymers into layered solids is a topic of considerable interest because the resulting organic/inorganic nanostructures may exhibit novel electronic and optical properties. Conjugated polymers have attracted increasing interest because of their unique electronic and optical properties.[106] Owing to the amorphous nature and limited processability of conjugated polymers, anisotropic studies are lacking. Immobilization of them into solid matrices seems to be a way of controlling their properties as well as processing them into films. Electrochemical polymerization of aniline in the interlayer space of montmorillonite has been reported.[107] Kanatzidis et al. have reported intercalation and *in situ* polymerization of aniline, pyrrole, and 2,2′-bithiophene in the interlayer spaces of layered transition metal oxides, chalcogenide, oxyhalide, etc.[40,108] Polymerization of diacetylenes intercalated in the interlayer spaces of metal halides[109] and metal phosphate[110] has also been reported. Besides the electronic conductivity of the resulting intercalation compounds, the study of their optical properties seems to be interesting because the polymers have been confined in a two-dimensional nanospace.

So-called pillared clay is a class of porous solids formed by the intercalation of robust cations in the interlayer spaces of layered materials.[111] In order to obtain stable micropores with appropriate geometry, much effort has been made to prepare and evaluate various pillared layered materials.

Thus, layered materials offer a two-dimensional opening for constructing nanocomposite materials with unique microstructures and properties.

III. Photoprocesses of Adsorbed Photoactive Species on Layered Solids as a Probe

Intercalation compounds have been characterized by a wide variety of instrumental analysis. Spectroscopic properties of the adsorbed species, which are very sensitive to the environment, have given insight to the microscopic structures of the host–guest systems, to which conventional instrumental analysis does not have access.[112] By utilizing photoprocesses of adsorbed photoactive species, one can obtain microscopic information such as the distribution and mobility of the guest species. Besides the scientific importance, these studies are of practical significance because they provide indispensable information on designing photofunctional materials using layered solids. In this chapter, photoprocesses of photoactive

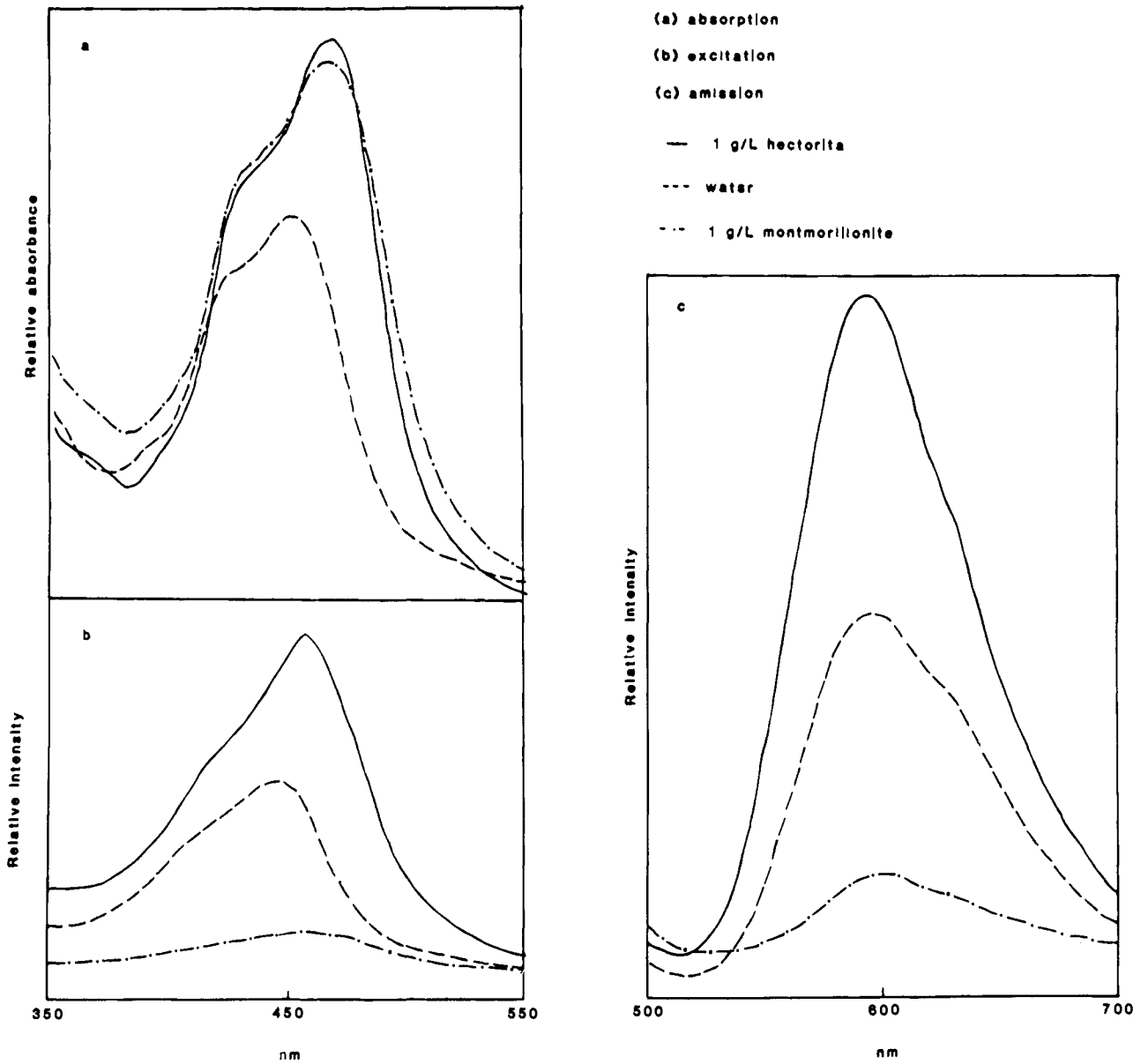

Figure 10. (a) Absorption, (b) excitation (recorded by monitoring the emission at 610 nm), and (c) emission (460 nm excitation) spectra of 2×10^{-5} M Ru(II) in water, sodium hectorite, and sodium montmorillonite. (Reprinted from ref 122. Copyright 1984 American Chemical Society.)

species adsorbed on layered solids are discussed in order to clarify the characteristics of hosts and host–guest systems. Chemical environments, such as polarity and rigidity as well as geometrical features such as distances between reactants and orientation of organic species on the surfaces, can be changed in layered host–guest systems.

A. Luminescence of Ruthenium Poly(pyridine) Complexes

In the study of organized assemblies, photoluminescence is quite a powerful tool which provides information on the compositional, structural, and dynamic characteristics of the media.[9,112] There are two commonly encountered kinds of luminescence: fluorescence and phosphorescence. Fluorescence is generally associated with the emission of light accompanying the transition of excited singlet states to the ground state while phosphorescence is generally associated with the emission of light from the lowest triplet state to the ground state. Luminescence parameters are sensitive to changes in the microenvironment of the probe so that a luminescence probe in different microenvironments will display distinct luminescence properties. Emission spectrum, luminescence decay, quantum efficiency of luminescence, polarization of luminescence (the orientation of the emitted light vector relative to the orientation of the absorbed light vector), and excitation spectrum have been employed to obtain information on microenvironments. Quenching, sensitization, and energy transfer, which have been observed by adding a second component or changing the microenvironment, also provide information especially on dynamics.

Tris(2,2′-bipyridine)ruthenium(II); $[[Ru(bpy)_3]^{2+}$, abbreviated as Ru(II)] is the probe molecule used most extensively because of its unique combination of chemical stability, long excited-state lifetime, redox properties, and so on.[113] The absorption spectrum of Ru(II) in aqueous solution has a metal–ligand (d–π) charge transfer (MLCT) band around 460 nm and

a $\pi-\pi^*$ transition for the ligands around 300 nm. The luminescence of Ru(II) on ion exchange resins,[114] micelles,[115] cellulose,[116] porous Vycor glass,[117] oxides,[118] semiconductors,[119] zeolites,[120] and layered materials has been investigated and valuable information on microscopic structures has been obtained. Studies on the photoprocesses of Ru(II) on layered systems with well-defined separation between an excited probe molecule and a quencher can provide insights into the distance dependence of electron transfer.

The cation exchange ability of smectites has been utilized to incorporate Ru(II) cations. The luminescence probe studies have mainly been carried out in colloidal clay systems in which an aqueous solution of Ru(II) is mixed with an aqueous suspension of smectites. In some cases, a species which quenches the excited state of Ru(II) has been added. The concentrations of hosts, Ru(II), and quenchers in the suspensions have been changed in order to see the dynamics of the reactions. The photoprocesses of the Ru(II)–smectite systems have revealed that the steady-state and time-resolved luminescence properties of Ru(II) are not simple, and various interpretations of the unusual properties have been proposed.

X-ray diffraction studies of the metal tris(2,2′-bipyridine) complex–smectite intercalation compounds, which have been prepared by a conventional ion exchange method, showed the basal spacings of ca. 1.8 nm when the complexes substitute the interlayer exchangeable cation quantitatively.[121] Considering the size and shape of the complexes, it has been concluded that the intercalated tris(2,2′-bipyridine) complexes are arranged as a monomolecular coverage of the silicate sheets with their 3-fold axis perpendicular to the silicate sheets.

In the absorption spectra of the Ru(II) adsorbed on smectites, the MLCT band appeared at around 460 nm which is red-shifted from that observed for an aqueous Ru(II) solution.[122] Figure 10 shows an example of the absorption and luminescence spectra of the Ru(II)–smectite systems. From the observed spectral shifts, both MLCT and $\pi-\pi^*$ band of bipyridine, as well as Raman and XPS studies, it has been proposed that covalently hydrated or slightly distorted bipyridine ligands due to steric constraints are formed when Ru(II) is adsorbed on montmorillonite. The formation of partially oxidized Ru(II) has also been reported.[123] Judging from the surface charge density of the silicate sheets and the size of Ru(II), the Ru(II) ions were arranged in close contact with adjacent Ru(II) ions in the interlayer space when the interlayer exchangeable cations were replaced by the Ru(II) quantitatively. This close proximity may cause the distortion of bipyridine ligand. The spectral shifts in the absorption and luminescence spectra have been observed even when the loaded amounts of Ru(II) are far below the cation exchange capacity of smectites.

It has been reported by Ghosh and Bard that the montmorillonite interlayer segregates Ru(II) from exchangeable Na^+ ions, resulting in high local concentrations of the complex ions in the interlayer space even when the added concentration of Ru(II) is only 1–2% of the cation exchange capacity.[122] (See Figure 11.) Very efficient self-quenching due to the high local concentration has been observed. When Zn(bpy)$_3^{2+}$ was coadsorbed with Ru(II) on hectorite, the effective self-quenching rate was dramatically reduced, presumably due to dilution of Ru(II) in the interlayer (surface dilution, Figure 11). One important observation in this segregation behavior is that MV^{2+} does not quench the excited state of Ru(II) even though such a quenching is readily observed for the neutral viologen, propyl viologensulfonate (abbreviated as PVS). The results were attributed to ion segreation; i.e., MV^{2+} and Ru(II) are located in different regions of the clay interlayers. Steady-state Stern–Volmer plots of Ru(II) quenching by MV^{2+} and PVS are shown in Figure 12. The origin of the ion segregation process is unclear. Nonuniform charge distribution among different layers or weak interactions between Ru(II) may be involved.

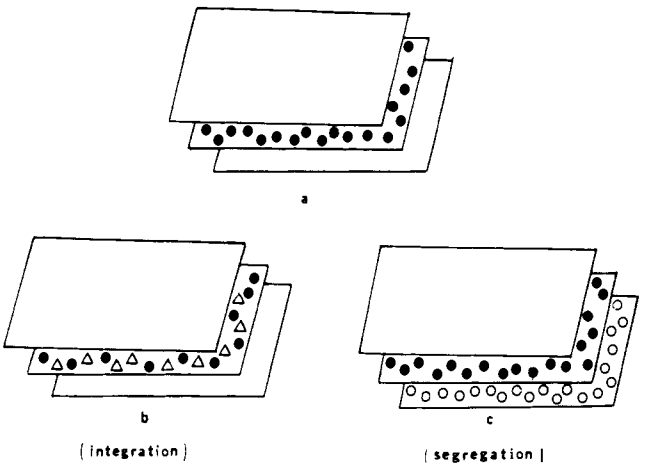

Figure 11. Schematics of the different modes of intercalation of exchangeable cations in colloidal sodium hectorite suspensions: (●) Ru(II), (△) Zn(bpy)$_3^{2+}$, and (○) MV^{2+}. Na^+ ions are not shown. (Reprinted from ref 122. Copyright 1984 American Chemical Society.)

Steady-state and time-resolved studies of the excited properties of the Ru(II) adsorbed on a variety of clay minerals have been carried out by some research groups in order to understand the adsorbed states of Ru(II) more clearly.[122-129] Habti et al. have reported nonexponential decay of the excited state of Ru(II) adsorbed on a variety of clay minerals with different iron contents.[123] Normalized luminescence decay profiles are shown in Figure 13. From the effects of iron contents on the decay profiles, they pointed out the quenching effect of the irons within the lattice of the minerals and the essentially immobile character of adsorbed Ru(II) on the microsecond time scale. Each adsorbed probe ion is able to interact with a very limited number of neighboring quencher ions around the adsorption sites. The total quenching probability for a particular probe is determined by the quencher concentration in the solid and by the number of solid particles in contact with the probe. They have also mentioned that the degree of swelling affects the quenching.

DellaGuardia and Thomas reported similar decay profiles for Ru(II) bound to montmorillonite and attributed the components to two species, one at the outer surface and edges and one between the silicate sheets (intercalated).[124] Schoonheydt et al. also

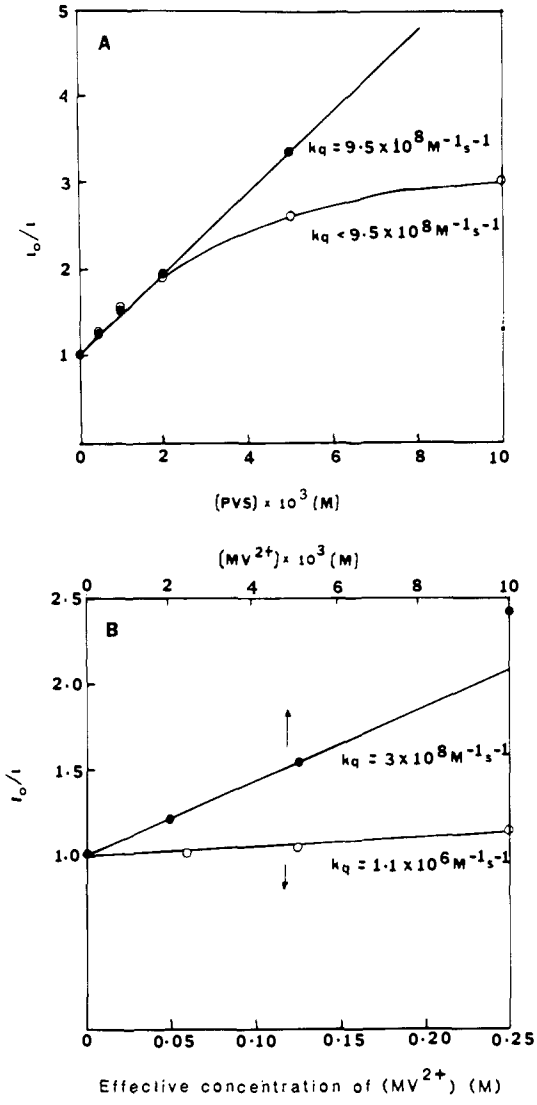

Figure 12. Steady-state Stern–Volmer plots of Ru(II)* quenching in water (●) and in 2 g/L sodium hectorite (○). (A) PVS and (B) MV^{2+}; Ru(II) (2×10^{-5} M) and the quencher ions were premixed and then added to the clay suspension. (Reprinted from ref 122. Copyright 1984 American Chemical Society.)

pointed out that Ru(II) is adsorbed on the external (edge sites) and interlamellar surfaces (planar sites) even at the small loadings of Ru(II), as is shown in Figure 14,[125] which was proposed by Turro et al.[126] The occupancy of edge sites with respect to planar sites increases with decreasing particular size of the clay minerals. Nakamura and Thomas also reported two different adsorption sites for Ru(II) on laponite.[127] At low concentrations of laponite, Ru(II) is adsorbed on outer layers and is in contact with the aqueous phase. Ru(II) is incorporated in the interlayer space by the layering silicate sheets at high concentrations of laponite.

Turro et al. reported that the addition of $MgCl_2$ and tetrabutylammonium chloride leads to an increase in the internal surface area due to flocculation and formation of clay aggregates and leads to an increase in the contribution of the interlayer species.[126] From the time-resolved luminescence and excited-state resonance Raman study, they concluded that the effects of laponite on the excited state of Ru(II) are primarily due to surface–probe interactions.

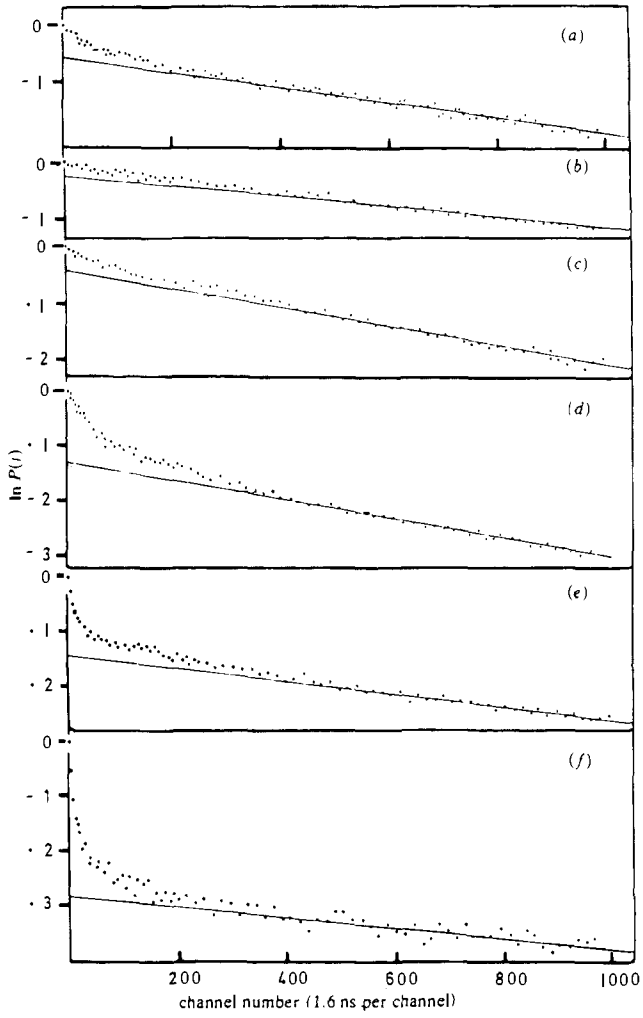

Figure 13. Normalized luminescence decay curves of Ru(II) adsorbed on (a) hectorite, (b) laponite, (c) sepiolite, (d) kaolinite, (e) montmorillonite, and (f) nontronite in aqueous suspension. (Reproduced from ref 123. Copyright 1984 The Royal Society of Chemistry.)

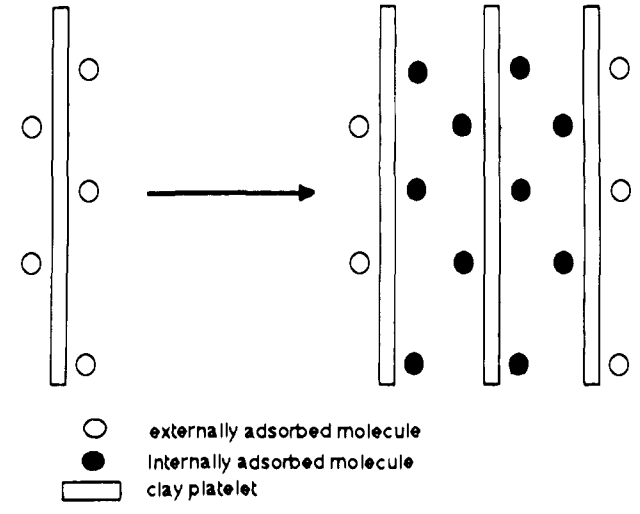

Figure 14. Idealized scheme showing the effect of clay aggregation on the distribution of probe molecules. (Reprinted from ref 126. Copyright 1987 American Chemical Society.)

Kuykendall and Thomas have deconvoluted the time-resolved luminescence of Ru(II) into two components and showed that they had two different emission maxima (Figure 15).[128] This observation

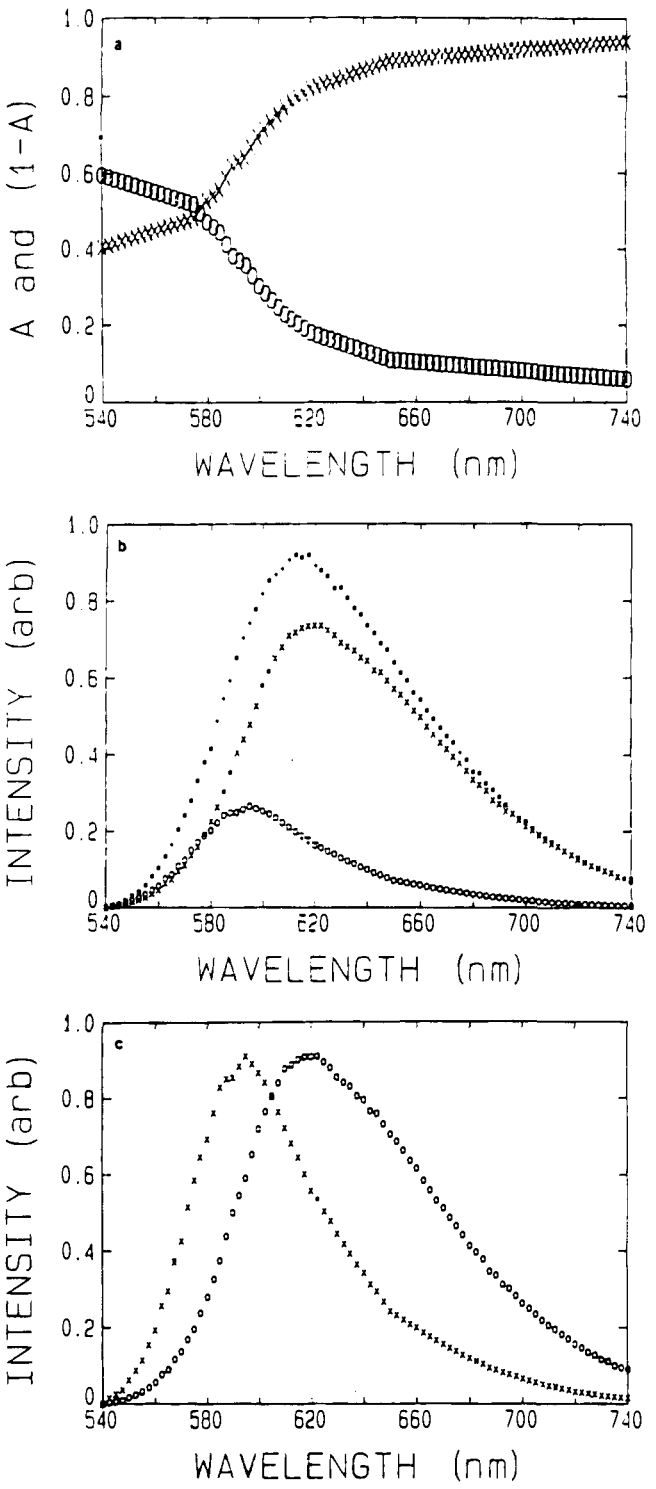

Figure 15. (a) A (×) and (1 − A) (○) parameters obtained as a function of wavelength from the biexponential model for the laponite date. (b) Deconvoluted emission spectra showing observed spectrum (*) and two-component spectra obtained from the kinetic model. Short-lived species (○); long lived species (×). (c) Normalized comparison of deconvoluted spectra obtained from the model. (Reprinted from ref 128. Copyright 1990 American Chemical Society.)

suggested the existence of two distinct adsorption sites for Ru(II) on laponite. In one type of adsorption zone the water is held rigidly and presents an environment to the Ru(II) probe that results in a short lifetime and a blue-shifted emission. The second absorption zone involves a stronger interaction directly with the clay surface so that the photophysics are less influenced by the nature of the surrounding water. This explanation was supported by a direct comparison of photophysical properties of the luminescence probe on the clay and in ice at −20 °C.

Cationic (i.e. cupric ion) and ionically neutral (i.e. dimethylaniline and nitrobenzene) quenchers have been added in the colloidal clay system to see the dynamic behavior of the adsorbed species on the clay surfaces.[127] Quenchers as exchangeable cations behaved similarly to those in solutions while the quenching rate constant was smaller by about 2 orders of magnitude on the clay than in solutions for O_2. In addition, the effect of the M^{3+} ions was stronger when they were present as substitution ions in the lattice than when they were exchangeable ions. This was due to the difference in the distance between the species and the mobility of the ions. Cu^{2+} was adsorbed strongly and the kinetics were simplified due to the strong adsorption. Stern−Volmer-type kinetics were observed, and a quenching rate constant was obtained which was lower than that in an aqueous solution, which gave an estimate of the degree of the movement of cupric ions on the clay surfaces. (The Stern−Volmer plots are shown in Figure 16.) Dimethylaniline and nitrobenzene are weakly adsorbed on a clay around the Ru(II), in a zonelike effect, rather than being adsorbed randomly throughout the system.

From these studies, the following general conclusions for the adsorption of Ru(II) on smectites have been derived.

(1) There are more than two adsorption sites with different chemical environments on smectites; one is exposed externally (outer surface) and the other is rather confined in the sheets (intercalated).

(2) There are strong interactions between the surface of the silicate sheets and Ru(II) adsorbed on the surface of smectites and those between adjacent Ru(II) complexes.

Photophysical and photochemical studies on hydroxyaluminum-pillared montmorillonite and hectorite and tetraalkylammonium-pillared hectorite have been reported. The proper choice of pillaring agents allows for the tailoring of the adsorptive property. Photochemical quenching studies utilizing gas-phase reagents (oxygen) revealed the microporosity of the pillared clays.[131]

Yamagishi and Soma have shown that optical isomers of ruthenium and iron polypyridine and phen (phen = 1,10-phenanthroline) chelate complex ions have different adsorption behaviors toward montmorillonite.[132] When a racemic mixture of ferric tris(phen) complex ions ($[Fe(phen)_3]^{2+}$) is adsorbed by a clay, the ions are adsorbed as a unit of racemic pair rather than in a random distribution of optical isomers. Otherwise enantiomeric $[Fe(phen)_3]^{2+}$ would also be adsorbed beyond CEC when the chelate is added in excess over a clay. The adsorption of racemic mixture occurs in two successive steps, the initial adsorption within CEC and the succeeding adsorption beyond CEC. When a tris(phen)metal chelate is placed on a silicate sheet of montmorillonite with its 3-fold symmetry axis perpendicular to the silicate surface, the three bottoms of the coordinated

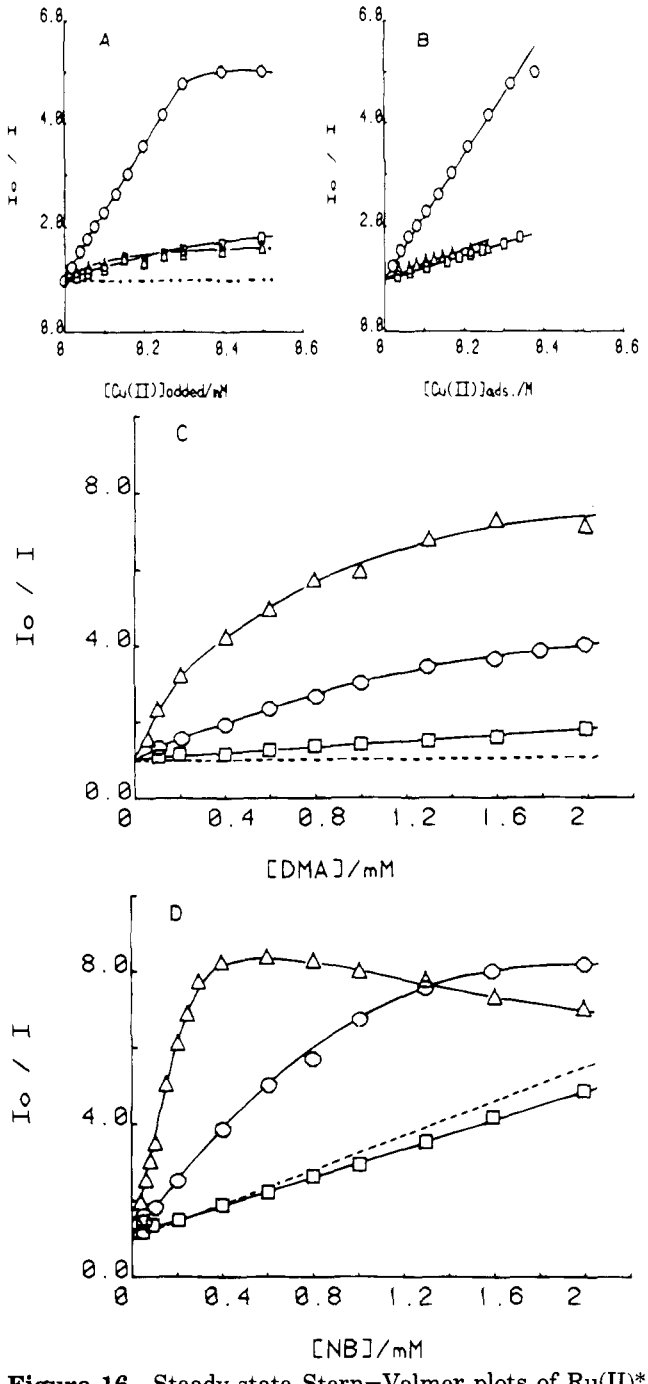

Figure 16. Steady-state Stern–Volmer plots of Ru(II)* luminescence quenching by various quenchers: (A) Cu^{2+}; (B) Cu^{2+}, I_0/I is plotted vs concentration of Cu^{2+} adsorbed; (C) dimethylaniline; (D) nitrobenzene. Symbols are as follows: (○) laponite, (△) hectorite, and (□) gelwhite. Broken lines are the data obtained in water. (Reprinted from ref 127. Copyright 1985 American Chemical Society.)

phenanthroline ligands make a regular triangle with the side length of about 6.5 Å. Since this distance is close to the distance between the centers of neighboring SiO_4 hexagonal holes (5.5 Å) on a silicate sheet, it is possible for the bound chelate to have its three hydrogen atoms of the ligands buried into the silicate surface. As a result, it is supposed that the chelate is rigidly fixed on the surface under the definite orientation. From molecular model consideration, it has been concluded that racemic adsorption by metal chelates on a solid surface can be achieved under the following conditions. (1) A bound chelate should be adsorbed up to such a density that it interacts with its neighbors stereochemically. In the case of cation exchanging by a clay, a molecule carrying two positive charges is required to have a molecular radius larger than 5 Å. Otherwise, it does not interact sterically with its neighbors. (2) A surface should be two-dimensional and capable of fixing a bound chelate under a definite orientation. Otherwise the strict stereochemical restriction does not arise in the stacking of a chelate as a molecular aggregate.

Joshi and Ghosh utilized luminescence probe for the study of the racemic adsorption on the clay–$[Ru(phen)_3]^{2+}$ systems and concluded that layered clays promote recognition between optical antipodes of cationic poly(pyridine) metal complexes.[133-136] The absorption and emission spectra and time-resolved luminescence decay profiles of enantiomeric and racemic $[Ru(phen)_3]^{2+}$ adsorbed on hectorite at ca. 3.5% loading indicate differences in the binding modes of the two forms. The quenching effect of coadsorbed $[Co(phen)_3]^{2+/3+}$, $[Ni(phen)_3]^{2+}$, and $[Rh(phen)_3]^{3+}$ were also discussed. From these data they concluded that such chiral interactions which are partly responsible for the spectral shifts of the racemic complexes upon adsorption occur spontaneously on clay and are not a steric constraint imposed on the system at high packing density. Spontaneously chiral interactions, which presumably occur via $\pi-\pi$ overlap of partially oriented chelates, also account for many of the intriguing absorption and emission spectral results of $[Ru(phen)_3]^{2+}$ in the presence of $[M(phen)_3]^{n+}$ coadsorbates, and such interactions have been thought to be the driving force for the optical resolution.

Intercalation of ruthenium poly(pyridine) complexes into other layered materials has been reported.[137-144] It has been stated that the intercalation of the complexes is not so easy compared with the case of smectite systems partly due to the higher charge densities of the host materials. Consequently, quantitative ion exchange of ruthenium complexes with the interlayer cations is difficult. Synthetic efforts have been made to introduce ruthenium polypyridine chelate complexes into ZrP, LDH, $MnPS_3$, and a transition metal oxide and to control the adsorption states.

Three types of Ru(II)–zirconium phosphates have been prepared by three different methods.[138] By ion exchange or impregnation of Ru(II) on ZrP, the complex ions have been adsorbed only on the external surface. When the mixture of zirconium oxy chloride ($ZrOCl_2 \cdot 8H_2O$), H_3PO_4, and $Ru(II)Cl_2$ was refluxed, a compound formed which emits at 590 nm and the emitting species has been thought to be $[Ru(bpy)_2(bpyH)]^{3+}$. Vliers et al. have also prepared stable aqueous suspension of HZrP and hexylammonium–ZrP. In the case of HZrP there is no interlamellar adsorption of Ru(II) and the cations are located on the external surface. On the other hand, in the case of hexylammonium–ZrP, Ru(II) was adsorbed both in the interlamellar space and the external surface. By quenching with $[Fe(CN)_6]^{3-}$, it has reportedly been possible to distinguish between Ru(II) on the external surface and in the interlamellar space.[139]

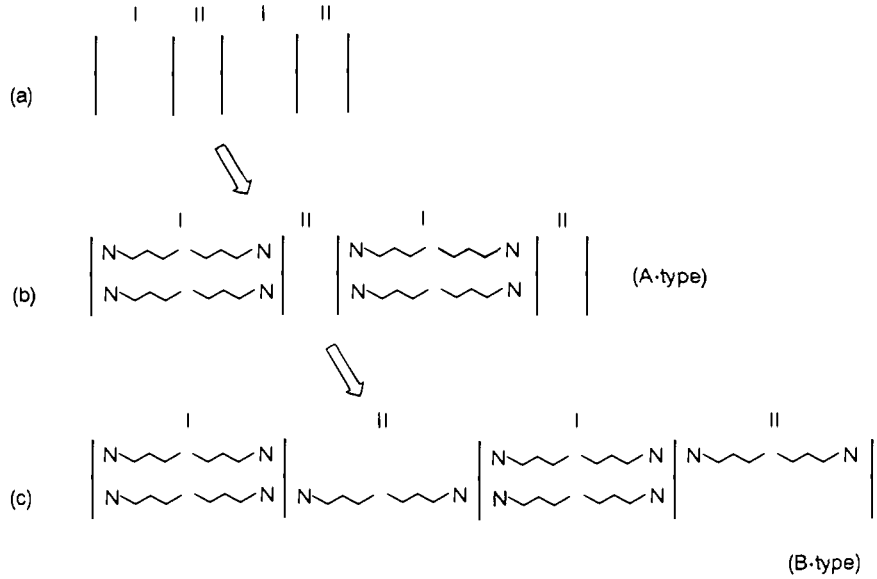

Figure 17. Schematic diagram showing the stepwise intercalation of alkylammonium ions into the two interlayer regions of $K_4Nb_6O_{17}$. Alkylammonium ions are first intercalated into interlayer I only (b). With extension of reaction time or raising of temperature, intercalation into interlayer II will take place (c). (Reprinted from ref 69. Copyright 1992 Chemical Society of Japan.)

The photophysics of Ru(II) has been used to investigate the chemical microenvironment within a sulfonated derivative of the layered solid zirconium phosphate, zirconium phosphate sulfophenylphosphonates (ZrPS).[140,141] Similar spectral shifts have been observed for Ru(II) in other chemical microenvironments (e.g., micelles, clays), and the shifts have been concluded to be the result of interactions of the complex ions with the phenyl rings of the host and the bpy rings of neighboring complexes. The movement of Ru(II) in the interlayer space of ZrPS is restrained to some extent, but diffusion leading dynamic quenching reaction can occur. A model combining diffusional quenching and sphere of action quenching accounts for the quenching of Ru(II) by MV^{2+} in ZrPS.

The photoprocess of ruthenium tris(4,7-diphenyl-1,10-phenanthrolinedisulfonate) complex anion ($[Ru(BPS)_3]^{4-}$) intercalated in a layered double hydroxide has been studied.[142] The compound was prepared by coprecipitation of Mg/Al LDH from an aqueous NaOH solution containing the metal chloride salts and $[Ru(BPS)_3]^{4-}$ and subsequent hydrothermal treatment. Multiexponential decay profiles have been observed for the $[Ru(BPS)_3]^{4-}$ adsorbed on LDH. From the effects of "surface dilution" by $[Zn(BPS)_3]^{4-}$ on the luminescence, the decay profile has been attributed to self-quenching processes similar to those for the Ru(II)–smectites systems.

The intercalation of Ru(II) into $MnPS_3$[143,144] and niobate ($K_4Nb_6O_{17}\cdot 3H_2O$)[69] has been reported. From the spectroscopic studies of the Ru(II)–$MnPS_3$ system, it was concluded that the intercalated Ru(II) bound weakly with the host lattice. Nakato et al. have preparaed two types of intercalation compounds of $K_4Nb_6O_{17}$ with Ru(II); one involves Ru(II) only in the interlayer I, and the other involves Ru(II) both in interlayer I and II.[69] Two types of alkylammonium-intercalated $K_4Nb_6O_{17}$ (the schematic structures are shown in Figure 17) were used as intermediates. Since the electronic properties of the hosts (both niobate and $MnPS_3$) are quite different from those of smectites, one may observe unique photoprocesses such as photocatalytic activity for these systems. (See section IV.A.)

B. Luminescence of Pyrenes and Other Aromatic Hydrocarbons

Aromatic hydrocarbons such as pyrene and anthracene have also successfully been employed as a luminescence probe of polarity and microviscosity in a variety of organized assemblies.[145] Among them, pyrene and its derivatives are the molecules studied most extensively. The vibronic fine structure of pyrene monomer is sensitive to surrounding polarity.[146,147] More over, when pyrene is forced into close proximity or in high concentration solution, excited-state dimers (excimers) are observed. The ratio of excimer to monomer fluorescence intensity obtained from emission spectra is often utilized as a measure of pyrene mobility and proximity. These molecules have been utilized to probe organized assemblies such as micelles,[9,146,147] polymers,[148] metal oxides,[149] cyclodextrins,[150] zeolites,[151] sol–gel-derived materials,[152] monolayers,[153] and lipid membranes.[154] Pyrene and anthracene themselves are poorly adsorbed on the hydrophilic surface of smectites but are readily adsorbed by organoammonium-intercalated clays.

Cationic pyrene derivatives, (1-pyrenyl)trimethylammonium (PN^+), [3-(1-pyrenyl)propyl]trimethylammonium ($P3N^+$), [4-(1-pyrenyl)butyl]trimethylammonium ($P4N^+$), and [8-(1-pyrenyl)octyl]trimethylammonium ($P8N^+$) ions have been used to study the anionic surface of silicate sheets.[155–159] DellaGuardia and Thomas studied the emission properties of $P4N^+$ adsorbed on colloidal montmorillonite and found that excimers formed even at low concentrations of $P4N^+$.[155] Figure 18 shows the emission spectra of $P4N^+$ adsorbed on colloidal montmorillonite particles. This indicates a clustering of adsorbed $P4N^+$ on the surface.

Figure 18. Emission spectra of P4N^{-} adsorbed on colloidal montmorillonite particles. Note the low concentration at which excimer is formed. (Reprinted from ref 155. Copyright 1983 American Chemical Society.)

Coadsorption of cetyltrimethylammonium ions (CTA; the amount is 20% of CEC) was carried out by adding an aqueous solution of CTAB (cetyltrimethylammonium bromide) to the colloidal montmorillonite suspension containing P4N^{+} (the amount is 0.5% of CEC).[156] By the addition of CTA, the P4N^{+} can be dispersed over the silicate surface which causes the emission from the pyrene monomer to increase and the excimer to decrease. Excited-state P4N^{+} exhibited a double-exponential decay, suggesting that there exists two different regions of the particles though the origin is unclear. The quenching study demonstrated that the surfactants reduced the accessibility of quenchers not adsorbed by the clay to the montmorillonite. When quenchers are adsorbed on the montmorillonite, the quenching rate constant is reduced by at least 1 order of magnitude compared to a homogeneous solution.

The fluorescence quenching of P4N^{+} adsorbed on colloidal laponite by coadsorbed alkylpyridinium ion showed unusual behavior. Figure 19 shows the influence of the alkyl chain length of various alkylpyridinium ions on the P4N^{+} fluorescence.[156] Increasing the quencher concentration led to an efficient quenching of P4N^{+} fluorescence, but increasing the quencher concentration further produced a reverse effect, whereby the fluorescence started to recover, only to be followed by a smaller degree of quenching. The alkyl chain length of the alkylpyridinium ions affects the degree of the recovery (Figure 19B). From these observations, a schematic model for PN^{+} fluorescence quenching by alkylpyridinium ions is proposed. Thus, it has been revealed that the geometry or arrangements of reactants affect the quenching of the excited adsorbed chromophore on colloidal clay.

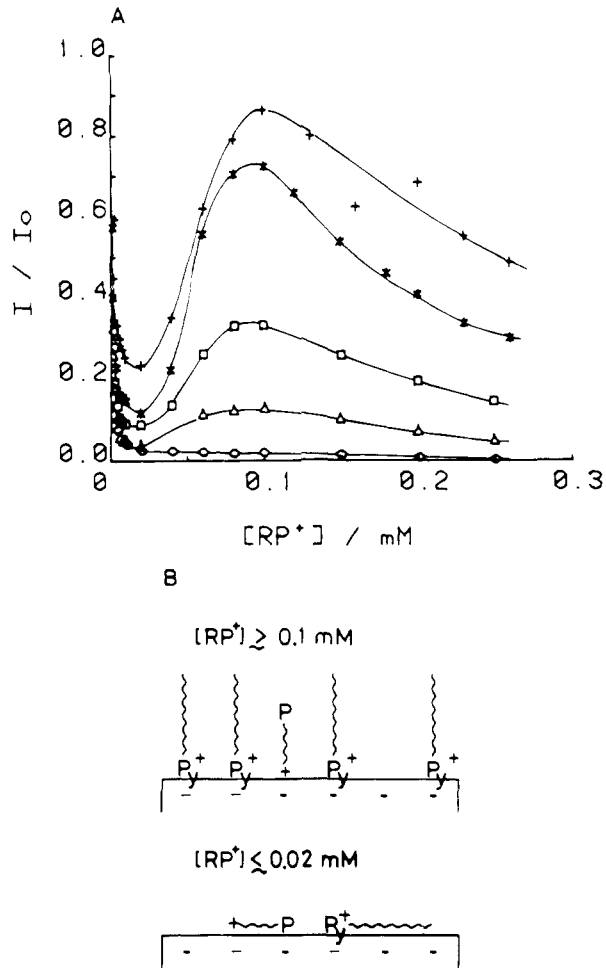

Figure 19. (A) Influence of the alkyl chain length of various alkylpyridinium ions on the P4N^{+} fluorescence quenching behaviors in laponite colloids (5 g/L): (○) ethyl-, (△) pentyl-, (□) octyl-, (*) dodecyl-, (+) hexadecyl-; [P4N^{+}] = 5×10^{-7} M. (B) Schematic model for P4N^{+} fluorescence quenching by alkylpyridinium ions: Py^{+}〰, alkylpyridinium ions; +〰P, P4N^{+}. (Reprinted from ref 156. Copyright 1986 American Chemical Society.)

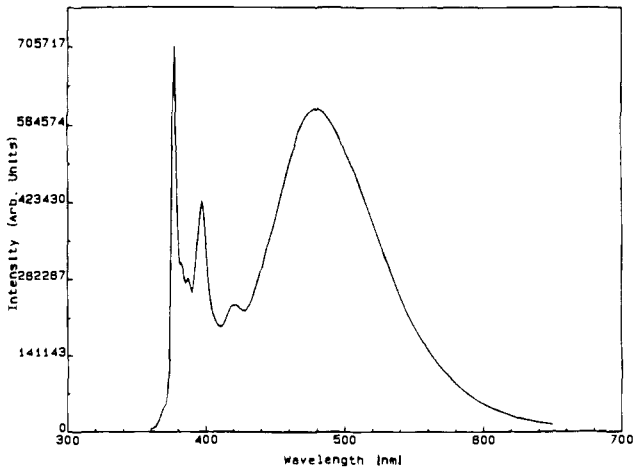

Figure 20. Fluorescence spectrum of P3N^{+} adsorbed on a clay surface. The loading amounts to 0.5% of the CEC. (Reprinted from ref 157. Copyright 1987 American Chemical Society.)

Viane et al. studied the adsorption of P3N^{+} bromide on hectorite, barasym, and laponite by an ion exchange mechanism.[157,158] Figures 20 and 21 show the emission and excitation spectra of P3N^{+} adsorbed on

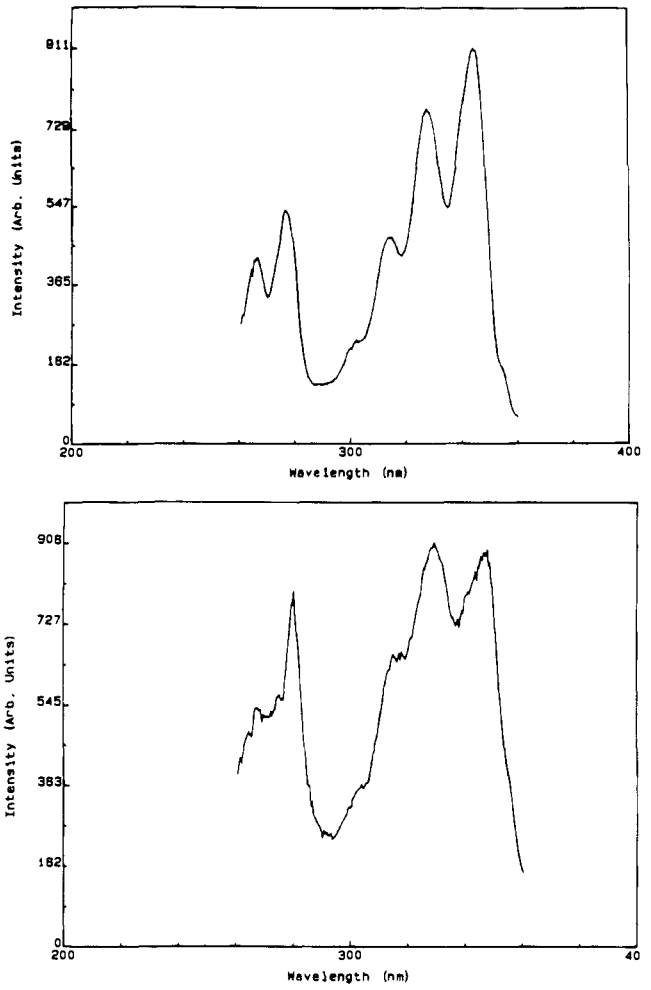

Figure 21. (Top) Excitation spectrum of monomer fluorescence of $P3N^+$ adsorbed on a clay surface. (Bottom) Excitation spectrum of the 480 nm fluorescence of $P3N^+$ adsorbed on a clay surface. (Reprinted from ref 157. Copyright 1987 American Chemical Society.)

a clay surface, respectively. Even at very low concentrations, a 480 nm emission was observed due to ground state interactions of the adsorbed $P3N^+$ ions, resulting in efficient excimer formation. This indicated a clustering of the adsorbed $P3N^+$ on the silicate surface. The 480 nm emission was suppressed by detergent molecules or Ca^{2+} ions. In the former case, detergent molecules solubilized $P3N^+$ on the surface of laponite as observed in the $P4N^+$–montmorillonite system. On the other hand, the mobility of $P3N^+$ was restricted in the latter case because of the ordering of silicate particles in suspension. Nonhomogeneous distribution of $P3N^+$ ions and a minimization of the contact surface between hydrophobic pyrene derivatives and the surrounding water phase were proposed to explain the excimer formation.

In order to see which was the major determining factor, suspensions in different solvents were studied in their subsequent work.[158] In that study, they used three pyrene derivatives, PN^+, $P3N^+$, and $P8N^+$ bromides. In nonaqueous suspension, no excimer emission was observed. Since the efficient intermolecular excimer formation in aqueous suspension had been ascribed to a cluster formation, the absence of excimer emission indicated the absence of clusters on the clay surface when the clays were suspended in nonaqueous media. These observations suggested that the distribution of the adsorbed ions is determined by the surrounding medium and not by the distribution of negative adsorption sites and that the bonding between the positive probe and negative site on the clay surface is not strong enough to inhibit diffusion of the adsorbed ions on the clay surfaces.

The PN^+ ions are initially adsorbed on the external surface and a redistribution over the interlamellar surface occurs on a time scale of 0–2000 s. Interparticle exchange of PN^+ ions is also observed on the same time scale.[161]

The effects of coadsorbed detergent have also been studied using the nonionic pyrene molecule as a probe.[160,161] The relative ratio, alkyl chain length of probes and detergents, etc. affect the adsorption states. As mentioned in the previous section, the hydrophilic surface properties of smectites are changed to become strongly organophilic by replacing the interlayer cation with long chain alkylammonium ions. The spectroscopic studies of these organophilic clays have been reported. Nakamura and Thomas studied a stable aqueous suspension of hexadecyltrimethylammonium chloride (CTAC)/laponite system.[160] The suspension contained 2 mmol of CTAC and 1 g of laponite (the amount of CTAC is two times as much as the cation exchange capacity of laponite). It should be noted that the suspension was able to dissolve 0.1 mmol pyrene. The kinetics of pyrene quenching and pyrene excimer formation reactions suggests that the CTAC forms a cluster-like double layer on the clay surface. Since the amount of CTAC is two times as much as the CEC of laponite in this system, the effects of Cl^- on the photophysics of adsorbed pyrene can not be excluded.

DellaGuardia and Thomas reported the incorporation of 1-dodecanol and pyrene in the interlamellar space of montmorillonite, which has been revealed from the fluorescence of pyrene and the basal spacing of the compound (interlayer spacing of 13 Å). Upon suspension of the powders in water, a fraction of 1-dodecanol and pyrene are released into the aqueous phase, forming dodecanol micelles into which released pyrene is solubilized.[161]

In order to apply these methods to solid samples, the intercalation of anthracene and pyrene into two types of alkylammonium–montmorillonites (octadecyltrimethylammonium- and dioctadecyldimethylammonium-types) has been carried out by solid–solid reactions.[162] The arene molecules are solubilized at extremely high concentrations in the two-dimensional interlayer spaces of the alkylammonium–montmorillonites while retaining the ordered structure which was evidenced by the X-ray diffraction studies. Fluorescence spectra of the intercalated arenes as well as the X-ray diffraction patterns show that two different types of adsorption occurred. The arenes in the octadecyltrimethylammonium–montmorillonite are aggregated and those in the dimethyldioctadecylammonium–montmorillonite are rather dispersed between the alkyl chains in the interlayer spaces. This difference in the adsorption state is due to the arrangements of the interlayer alkylammonium ions. If the cations are arranged parallel to the silicate sheets, adsorbed arenes tend to aggregate. The arene intercalated into the alkylammonium–

smectites with paraffin-type arrangement of the interlayer organoammonium ions tends to solubilize the hydrocarbons molecularly. Labbé and Reverdy reported the adsorption of pyrene on laponite by the drying of a water-filled laponite paste containing a dispersion of pyrene microcrystals or the crushing of a mixture of powdered laponite and pyrene crystals.[163]

The surface properties of laponite following thermal activation have been investigated recently by Liu et al. and the following conclusions have been derived.[164,165]

(i) The polarity of the laponite surface changes on preactivation from polar to less polar.

(ii) The lateral surface of laponite is activated at a temperature in the range of 115–440 °C acting as an electron acceptor with pyrene.

(iii) At high pyrene concentrations, pyrene dimer cation radicals form on the surface.

(iv) Adsorbed pyrene molecules migrate and form dimers on exposure of the sample to water.

They have also suggested that there is a distribution of the electron-accepting sites on the surface which ionized the surface adsorbed pyrene molecules. The location of the active sites has been studied by pretreating the clay with polymetaphosphate. Most of the active sites are located on the lateral surface, while others are located elsewhere in the regions that are unaffected by adsorbed water, polymetaphosphate, and basic molecules such as NH_3.

Thomas et al. have used the spectral shifts as a means of measuring molecular refractive indices and dielectric constants for the local microregion of systems.[166] The adsorption of (9-anthracenylmethyl)-ammonium ions (abbreviated as AMAC) and $P4N^+$ to ZrP in the presence of butylamine hydrochloride and their binding behavior has been studied.[167,168] AMAC tends to aggregate at the surface of ZrP, while $P4N^+$ gives monomer emission when adsorbed on ZrP at low surface coverage. The excimer formation of $P4N^+$ on ZrP depends upon the concentration of the phosphate, additives as well as probe. However, the origin of the difference in the binding behavior between AMAC and $P4N^+$ has not been clarified.

C. Other Luminescence Probes

Villemure studied the fluorescence of methylviologen (MV^{2+}) in a colloidal clay system and proposed that there are two adsorption sites for methylviologen; one is the external surface in which MV^{2+} retained some internal flexibility and the other is the interlayer surface where the MV^{2+} dication was rigidly bound.[169,170] This observation is consistent with those made for the Ru(II)–smectite systems.

The emission properties of rhodamines[171–175] and proflavin[176] adsorbed on colloidal suspension of smectites have also been reported. Energy transfer from the excited state of rhodamine 6G to cationic dye acceptors (rhodamine B, cresyl violet, thionine, crystal violet) on laponite has been investigated to indicate the concentrating effect of adsorption on clays.[177]

D. Metachromasy

The metachromasy of dye molecules can also be important information on the aggregation of dye molecules. Matachromasy is a gradual replacement of the principal band in the visible region by a band with a shorter wavelength. In an aqueous dye solution the shift of the absorption peak in the visible region to shorter wavelengths occurs as the dye concentration increases and has been ascribed to the formation of dimers and higher polymers. From the change in the absorption spectra, adsorption behavior of the dye molecules has been investigated. The adsorption of cationic dyes such as methylene blue,[178–184] pyronine Y,[185] acridine orange,[186,187] rhodamines,[171–175] proflavine,[176] thionines,[188,189] and crystal violet[190,191] on montmorillonite and/or laponite has been investigated. The concentrations of dyes and hosts, the relative amounts of dye to hosts, as well as the nature of the hosts, affect the adsorption state of the dyes employed and the differences have been detected by visible spectroscopy. In some cases, X-ray diffraction data supported the findings on adsorption sites and states.

The adsorption of methylene blue from aqueous solution has been utilized to measure the cation exchange capacity of clay minerals.[178] The adsorption has also been studied by means of visible absorption spectroscopy, and spectral shifts upon adsorption on clay minerals have been observed. Cenes et al. studied the adsorption of methylene blue on various clay minerals and concluded that dye aggregation was responsible for the metachromatic effects.[182] The distribution of the dye ions over the surface was determined not only by the electrostatic interaction between the negatively charged exchange sites and methylene blue, but also by dye–dye interactions.

Acridine orange has been intercalated in the interlayer spaces of various homoionic–montmorillonite by a cation exchange mechanism.[186] The adsorption leads to metachromasy of the dye molecule and a shift of the absorption bands to lower wavelengths in the visible range. Two types of association of the dye ions were proposed. One is a monolayer of the dye in the interlayer space with the aromatic rings parallel to the aluminosilicate layer; the other is a bilayer in the interlayer space or tilting of the dye ions relative to the aluminosilicate layer. The interactions between the oxygen plane of the aluminosilicate and the aromatic ring of the dye and the association of the adjacent dyes are responsible for the shifts of absorption bands in the former and latter case, respectively.

The adsorption of N-alkylated acridine orange cation on a colloidally dispersed montmorillonite[187] and zirconium phosphate[192] has been investigated. The effects of alkyl chain length on the spectroscopic properties revealed that the orientation of the adsorbed acridine oranges changed depending on the alkyl chain length.

The effects of hosts on the adsorption states of pyronin Y were observed by Grauer et al.[185] In montmorillonite, adsorption led to metachromasy of the dye and the appearance of a new band at shorter wavelength than the original band (480 and 545 nm, respectively) even at very small coverages. In laponite, on the other hand, no metachromasy was observed with small amounts of dye. In montmorillonite, the organic cation was oriented with the plane

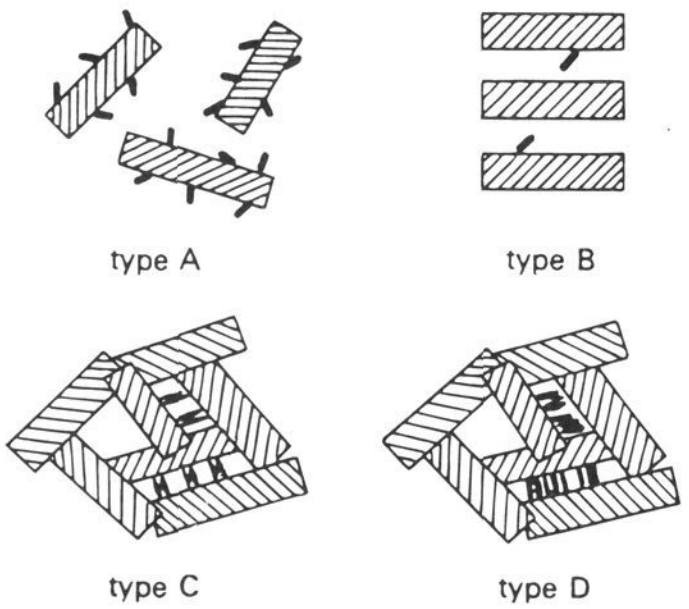

Figure 22. Possible model for the four types of adsorption of crystal violet by laponite. (Reprinted from ref 191. Copyright 1990 The Royal Society of Chemistry.)

of the rings parallel to the silicate layer and π interaction between the oxygen plane of the silicate layer and the aromatic dye gave rise to metachromasy of the dye. In laponite, the plane of the aromatic ring was tilted relative to the silicate layer and π interactions between the oxygen plane and the aromatic dye did not occur. They ascribed the different behavior to the difference in the location of the isomorphous substitution; the negative charge of laponite results from octahedral substitution, whereas in montmorillonite, tetrahedral substitution occurs. Such a substitution is thought to lead to increasing basic strength of the oxygen plane in montmorillonite compared to laponite.

Yariv et al. have studied the adsorption of crystal violet on laponite and montmorillonite.[191] On the basis of the spectroscopic characteristics of crystal violet on laponite, they proposed the adsorption model in relation to the so-called card house structure of laponite (Figure 22).

The adsorption of thionine and tetraethylthionine on montmorillonite, vermiculite and laponite has been studied.[188,189] No metachromasy has been observed in the laponite system, suggesting that Na–laponite undergoes a simple exchange reaction with the dye ion involving no π interactions because of its large swelling property and very low charge density.

In the case of the adsorption of rhodamines (6G and B) on montmorillonite or laponite, steric hindrance prohibited π interactions of rhodamines with the oxygen plane of the silicate layer. In the dyes, the phenyl ring is sterically constrained to be roughly perpendicular to the planar xanthene group. Therefore no metachromasy has been observed due to π interactions. However, metachromasy due to aggregation of dyes has been observed for the rhodamine 6G–montmorillonite and laponite systems. The dispersion degree of the clay suspension as well as the relative dye/clay concentration is reported to affect the aggregation state.

Thus, the metachromatic effects have been observed upon adsorption of dye on smectites. Factors such as the molecular structure of the dye, the surface charge density of the hosts, and the dispersion degree of hosts in suspension have been reported to affect the state of adsorption.

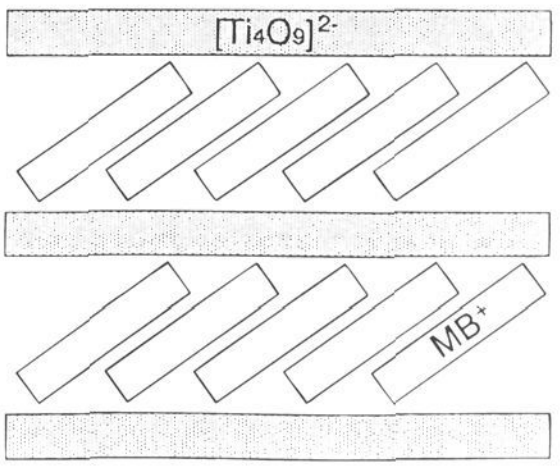

Figure 23. Schematic model of the arrangement of methylene blue cations (MB^+) in the interlayer space of $H_2Ti_4O_9$. (Reprinted from ref 194. Copyright 1992 Kluwer.)

Intercalation compounds of LDH with indigo carmine,[84] new coccine,[84] and naphthol yellow S[193] have been synthesized by anion exchange or a direct synthesis method. An intercalation compound of $H_2Ti_4O_9$ with methylene blue has been prepared by Nakato et al.[194] (The schematic structure of the intercalation compound is shown in Figure 23.) Since these systems extend the variation in the materials, further systematic studies on the spectroscopic properties of these compounds are important.

E. Photoprocesses of Porphines and Phthalocyanines

Porphines and phthalocyanines are well known not only for biological but also for catalytic, conductive, and photoactive properties. There has been an increased interest in the organization of porphines, metalloporphines, and phthalocyanines into well-defined molecular architecture because of the possibility of controlling their attractive properties. Along this line, the intercalation of porphines[87,195–204] and phthalocyanines[205–215] into layered solids has been reported. Since porphines undergo reversible protonation–deprotonation reactions depending on the acidity of the environment, they can be a probe of the interlayer environment of host lattices.

Cady and Pinnavaia reported the reactions of *meso*-tetraphenylporphyrin ($TPPH_2$) with interlayer exchangeable cations of montmorillonite. The acidity of the interlayer cations affect the adsorption state of $TPPH_2$.[195] Strongly acidic hydrated Fe^{3+} and VO^{2+} ions react quantitatively with the free base porphyrins to afford the protonated porphyrin cations and the cations form monolayers in the interlayer space of the silicate sheets. On the other hand, weakly acidic hydrated Na^+ and Mg^{2+} afford only a trace amount of $TPPH_4^{2+}$. $TPPH_2$ reacts with $(n\text{-}C_3H_7)_4N^+$, Co^{2+}, Cu^{2+}, and Zn^{2+} to give mainly metalloporphyrin in solutions and a hydronium-exchanged form of the montmorillonite. They have also reported the formation of porphyrin from aldehyde and pyrrole catalyzed by the Bronstead acidity of hydrated cations. Van Damme et al. have reported the reaction of $TPPH_2$ and *meso*-tetra(4-pyridyl)porphyrin with montmorillonite.[196] There is an equilibrium between various species on montmorillonite surface and the equilibrium is a function of the hydration state of the surface. Carrado and Winans investigated ion exchange of two simple water-soluble *meso*-substituted

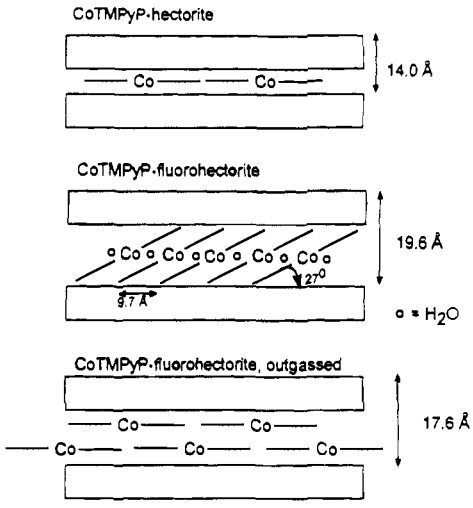

Figure 24. Schematic model of the arrangement of CoTMPyP in the interlayers of (a) hectorite (wet or outgassed), (b) air-dried fluorohectorite, and (c) outgassed fluorohectorite. (Reprinted from ref 200. Copyright 1994 American Chemical Society.)

porphyrins (tetrakis(1-methyl-4-pyridiniumyl)porphyrin and tetrakis(*N,N,N*-trimethyl-4-anilinumyl)-porphyrin) and the corresponding metalloporphyrins Fe^{2+}, Fe^{3+}, and Co^{2+} with montmorillonite, hectorite, and fluorhectorite and proposed similar effects of the exchangeable cations on their adsorption state.[197]

The metalation–demetalation reaction of tin tetrakis(4-pyridyl)porphyrin in Na–hectorite has been investigated.[198] The UV–vis and luminescence spectra revealed that the adsorbed complex was demetalated forming the tetrakis(4-pyridyl)porphyrin dication as the clay was dehydrated. This process was reversible, indicating that the Sn^{4+} ion remains in the vicinity of the porphyrin upon demetalation.

The molecular orientation of copper(II) tetrakis(1-methyl-4-pyridyl)porphyrin (CuTMPyP) in the interlayer space of Na–hectorite and Li–fluorhectorite has been studied by X-ray diffraction and anisotropic ESR spectroscopy of oriented thin film samples.[199] In the fluorhectorite, the long axis of the porphyrin cross section becomes inclined to the silicate sheet with a tilt angle of 35°. This difference in the arrangements of the intercalated porphyrin was ascribed to the different charge density of the host materials. The intercalation of cobalt(II) tetrakis(*N*-methylpyridiniumyl)porphyrin (CoTMPyP) into the interlayer space of hectorite and fluorohectorite and the arrangements of the intercalated CoTMPyP has been studied by X-ray diffraction and EPR spectroscopy.[200] The proposed orientations of CoTMPyP in the interlayer spaces are shown in Figure 24. It has been reported that the orientations of the intercalated porphyrins are affected by the layer charge density. When intercalated on the low charge density hectorite, CoTMPyP orients with the molecular plane parallel to the silicate layers and has no water in axial coordination site of Co^{2+}. In contrast, CoTMPyP orients with its ring at 27° to the silicate layer with water molecules coordinated to Co^{2+} in the high charge density fluorohectorite. Vacuum dehydration decreases the basal spacing of CoTMPyP–fluorohectorite from 19.6 to 17.6 Å, causing a rearrangement

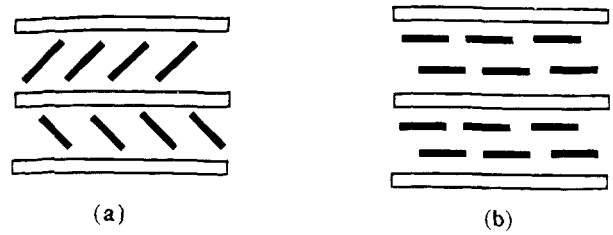

Figure 25. Stylized depictions of (a) a canted porphyrin monolayer and (b) a planar porphyrin bilayer. (Reprinted from ref 87. Copyright 1993 American Chemical Society.)

of the intercalated CoTMPyP into a staggered bilayer with no axial water bound to Co^{2+}.

Kuykendall et al. studied the photophysics of tetrakis(*N*-methylpyridyl)porphyrin adsorbed on colloidal smectite and proposed that the photophysics can be a convenient method to monitor the degree of dispersion or extent of deflocculation of a clay dispersion to produce primary particles or single sheet.[201]

Recently, Nakato et al. have reported the intercalation of a free-base prophyrin, 5,10,15,20-tetrakis-(1-methyl-4-pyridinio)porphyrin (H_2TMPyP^{4+}), into layered tetratitanic acid.[202] In order to insert the bulky ions, *n*-propylammonium–$H_xTi_4O_9$ was used as an intermediate. Spectroscopic investigations showed that the H_2TMPyP^{4+} ions were present as the monomeric free-base ions. Judging from the observed *d* values, which indicated the expansion of the interlayer space by 1.05 nm and the spectroscopic characteristics, the intercalated porphyrin ions inclined with the tilt angle of their molecular plane to be about 35° normal to the layer. Luminescence decay profile revealed the self-quenching due to the interaction between prophyrin ions.[202]

The aminophenyl (TAPP)- and pyridinium (TMPyP)-substituted porphyrins were intercalated into the α-zirconium hydrogen phosphate by exchanging the porphyrins into the *p*-methoxyaniline (PMA) preintercalated compound ($Zr(O_3POH)_2 \cdot 2PMA$).[87] Powder X-ray diffraction patterns and the EPR spectra of the anisotropic of uniaxially ordered thin films of the products suggests that the *p*-TAPP derivatives consisted of a monomolecular porphyrin layer in which the heme planes were tilted nearly 45° relative to the host lamellae (Figure 25a), whereas *o*-TAPP derivatives predominantly assembled into a porphyrin bilayer in which the heme macrocycles lay parallel with the host sheets (Figure 25b).

The intercalation of 5,10,15,20-tetra(4-sulfonatophenyl)porphine into the interlayer space of a layered double hydroxide has been reported by an anion exchange.[203] The powder X-ray diffraction pattern of the product showed that the intercalated porphyrin anions are arranged with their molecular planes perpendicular to the host lamellae (Figure 26). Photochemical hole burning properties of cationic porphine–saponite intercalation compounds have been reported and the results will be discussed in section IV.E.[204] Porphyrins have been used as templates for the hydrothermal synthesis of smectites.[205]

The intercalation of phthalocyanines into anionic and cationic layered materials and the orientation of the intercalated species have been investigated by means of X-ray diffraction and EPR. The orientation of the intercalated species has been reported to

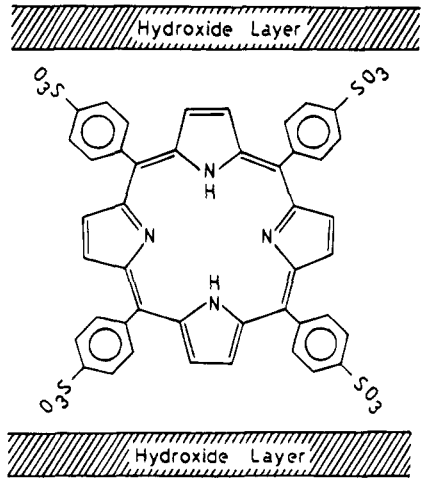

Figure 26. Postulated configuration of intercalated 5,10,-15,20-tetra(4-sulfonatophenyl)porphyrin anion in the interlayer space of the LDH. (Reprinted from ref 203. Copyright 1994 The Chemical Society of Japan.)

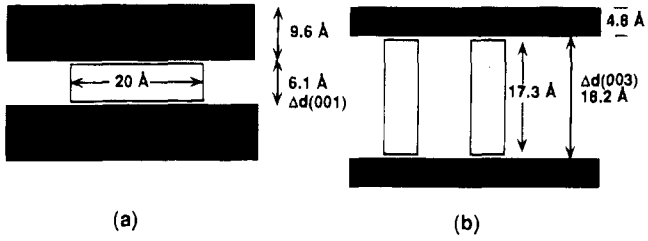

Figure 27. Schematic representation of the arrangements of phthalocyanine molecules (a) alcian blue, pyridine variant in hectorite cationic clay, and (b) copper(II) phthalocyaninetetrasulfonate in Mg/Al LDH. (Reprinted from ref 211. Copyright 1993 American Chemical Society.)

change depending on the layer charge density of the host materials.[197,200] Carrado et al. reported the incorporation of phthalocyanines and metal phthalocyanines into the interlayer space of anionic (Mg/Al LDH) and cationic (hectorite) clays via ion exchange or in situ crystallization of the synthetic host layers.[211] The phthalocyanines are oriented parallel to the silicate layer of hectorite and perpendicular to the anionic layer of LDH in correlation with their hosts' layer charge density (Figure 27). EPR studies on the cobalt(II) tetrasulfophthalocyanine (CoPcTs)–Mg/Al LDH system indicated the existence of Co^{2+} with water in axial coordination sites. Outgassing the sample results in the disappearance of the Co^{2+} spectrum and the original spectrum has been restored upon rewetting the sample with water. However, the orientation of the phthalocyanines ring, which was determined by XRD, could not be verified because attempts to prepare well-oriented films of the CoPcTs–LDH were unsuccessful.

Thus, intercalation of porphyrins and phthalocyanines into layered solids results in the organization of macrocycles with variable arrangements. The charge density of the host layer, the charge and molecular size of the guest porphines and phthalocyanines, etc. are the factors to control their states. The oriented films of the intercalation compounds have been proved to be very important for the determination of the orientation in the interlayer spaces. Although porphines and phthalocyanines are well known for biological, catalytic, conductive, and photoactive properties, only a limited number of studies have been made to investigate the properties of the intercalation compounds. Didodecyldimethylammonium–montmorillonite–metal phthalocyanine intercalation compounds[212,213] and a CoPcTs–Mg/Al LDH intercalation compound[214] have been prepared and their catalytic activities have been reported. Systematic studies on the structure–property relationships of these systems can provide indispensable information of both practical and scientific importance.

The intercalation of metal phthalocyanines into superconductive solids Bi-2212 and 2223 cupric oxides has been reported.[215] Compared with those of other organic species, porphyrins and phthalocyanines possess unusual thermal stability. Therefore, further studies on these materials and the application of the preparing procedure may lead to new research fields to which conventional soft chemical processes have no access.

F. Chemical and Photochemical Reactions of Adsorbed Organic Species Studied by Visible Absorption Spectroscopy

The reaction of adsorbed organic species with host, mainly smectites, has been investigated by means of absorption spectroscopy.[47,216–221] The adsorption of some aromatic molecules and their transformations, complex formation, etc. have been reported. The protection of pesticides from photodegradation by complexation with montmorillonite has also been reported.[222]

Photochemical reactions of organic species intercalated in the interlayer space have been reported.[223–228] Photochemial reactions of biphenyl, dioxin, and its chlorinated derivative on laponite surface have been investigated by means of diffuse reflectance spectral studies.[223,224] Cenes et al. reported the photooxidation of tryptophan, photosensitized by methylene blue exchanged on hectorite, Wyoming bentonite, and laponite.[225] Three factors have been proposed to affect the reactions: (i) Fe(III) in the structure, which quenches the excited state of methylene blue; (ii) the adsorption site of methylene blue, as photooxidation only takes place with methylene blue on the external surface; (iii) dye aggregation, which reduces the yield.

It has been reported that photolysis of intercalation compound of α-$Zr(HPO_4)_2 \cdot H_2O$ with an amine-substituted organometallic carbonyl complex led to a surface-supported organometallic complex.[226]

Photocatalytic and photochromic reactions will be reviewed in the next section.

G. Photochemical Cycloaddition of Aromatic Olefins

The interlayer spaces of clay minerals have been shown to provide a stable and characteristic reaction field suitable for spatially controlled photochemical reactions. Regioselective photocycloaddition of stilbazolium cations, intercalated in the interlayer space of saponite, have been reported.[227–230] There are four possible reaction paths of the photochemical reactions of the stilbazolium ion (Figure 28). Upon irradiation

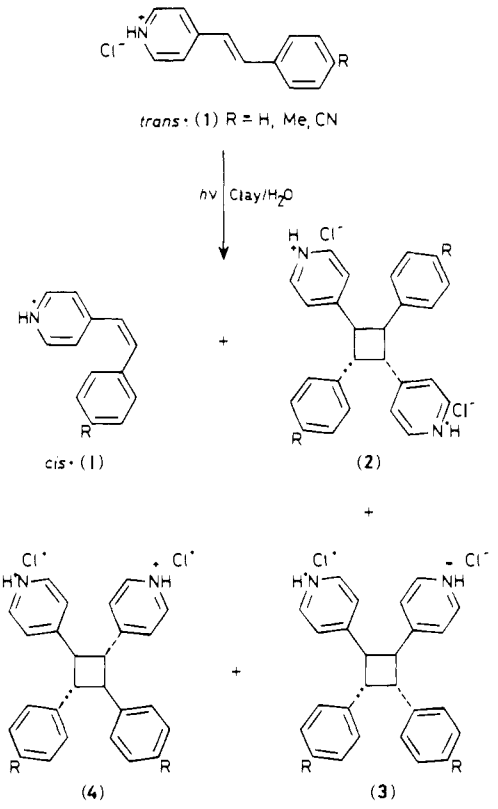

Figure 28. Four possible reaction paths of the photochemical reactions of the stilbazolium cation. (Reproduced from ref 227. Copyright 1989 The Royal Society of Chemistry.)

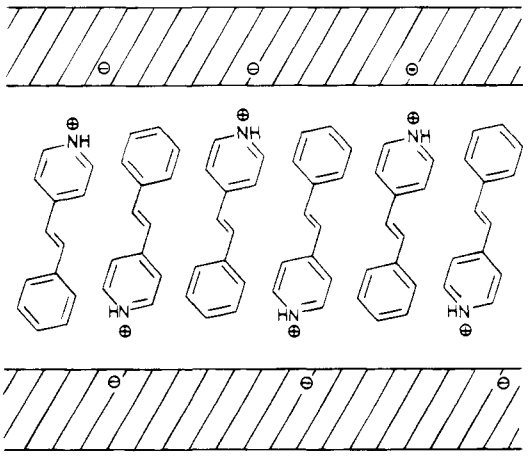

Figure 29. A schematic representation of the alkene packing in the interlayer space of saponite. (Reprinted from ref 227. Copyright 1989 The Royal Society of Chemistry.)

of UV light to the suspension of the stilbazolium–saponite system, *syn*-head-to-tail dimers were predominantly formed at the expense of *cis–trans* isomerization which is a major path in a homogeneous solution. The selective formation of head-to-tail dimers suggests that the intercalation occurs in an antiparallel fashion, as is shown in Figure 29. Since the dimer yields were barely dependent on the loading amount of the guest ions, stilbazolium ions were adsorbed inhomogeneously to form aggregates with antiparallel alternative orientation even at very low loading (e.g. 1% of CEC). This aggregation was supported by the fluorescence spectrum of the dye adsorbed on saponite, in which excimer fluorescence

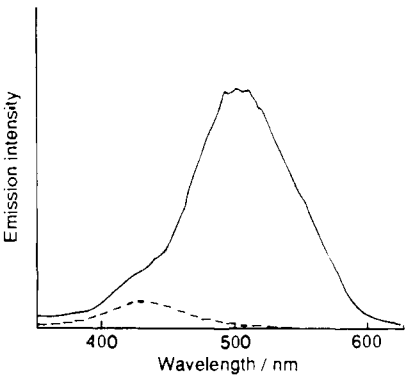

Figure 30. Emission spectrum of a stilbazolium cation adsorbed on saponite (solid line) and without saponite (broken line). Excited at 330 nm. (Reprinted from ref 228. Copyright 1990 The Royal Society of Chemistry.)

was observed at 490–515 nm at the expense of the monomer fluorescence at ca. 385–450 nm (Figure 30). The selective formation of *syn*-head-to-tail dimers indicates the formation of aggregates owing to hydrophobic interaction between the adsorbate ions.

The change in the aggregation state of a stilbazolium ion, γ-stilbazolium (4-(2-phenylvinyl)pyridinium) ion, on saponite by coadsorption of alkylammonium ions (C_n^+) has been investigated.[230] Figure 31 shows the effect of C_n^+ on photoreactivity of preintercalated stilbazolium ions on clay. On coadsorbing C_n^+ longer than the stilbazolium ion, the major photoreaction was changed from cyclodimerization to *E–Z* isomerization and the excimer emission of the intercalated stilbazolium ions was dramatically reduced. The formation of dimer or cluster of adsorbent is adequately simulated by a Monte Carlo method for a two-dimensional lattice site model. Similar trends have been observed for the adsorption and clustering of cationic pyrene derivatives on smectites (heading B of this section).

Photochemical cycloaddition for several unsaturated carboxylates has been studied in the presence of hydrotalcite (Mg/Al LDH).[231] *syn*-Head-to-tail cyclodimers were selectively formed upon irradiation of sodium cinnamate hydrotalcite system, while two isomers of *syn*-head-to-head and *syn*-head-to-tail cyclodimers were formed for the case of *p*(2-phenylethenyl)benzoates. The packing of the intercalated carboxylate and the effect of coadsorbates have been studied. X-ray diffraction analysis revealed that the carboxylate anions are intercalated as a monolayer, which suggests an alternate antiparallel packing since the interlayer of LDH possesses two ionic surfaces, top and bottom. The product selectivity was shown to be controlled by the relative distance of double bonds from the ionic surface of LDH (Table 3). Figure 32 shows the proposed orientation of the intercalated *p*-phenylcinnamate and *p*-(2-phenylethenyl)benzoate in the interlayer space of LDH.

The addition of sodium *p*-phenethylbenzoate, a photochemically inactive coadsorbate, affected significantly the product distribution in the photolysis. Figure 33 shows the effects of coadsorbates on product selectivity for the irradiation of intercalated *p*-(2-phenylethenyl)benzoate on LDH. The ratio of head-to-head and head-to-tail dimers decreased with an increasing amount of coadsorbate and the major

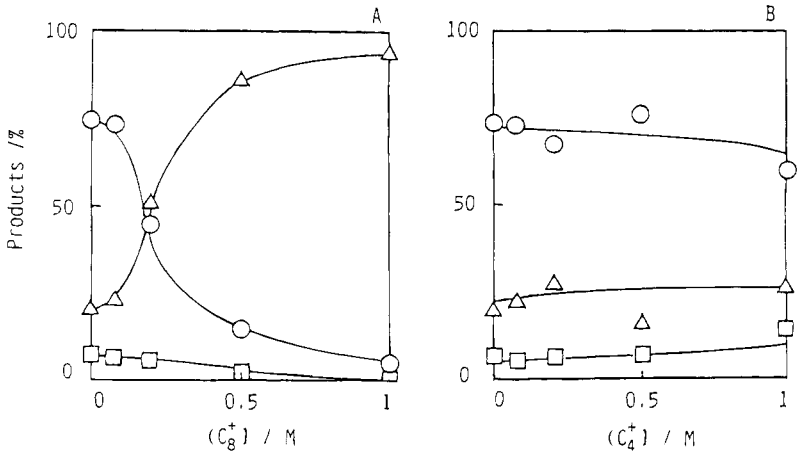

Figure 31. Effect of alkylammonium ions on photoactivity of preintercalated γ-stilbazolium ion on saponite: (○) *syn*-head-to-tail dimer; (□) *syn*-head-to-tail dimer (3); (△) *Z*-isomer. Intercalated γ-stilbazolium–saponite complex was suspended in 5 mL of aqueous solution of alkylammonium ions: (A) octylammonium (C_8^+); (B) butylammonium (C_4^+). (Reprinted from ref 230. Copyright 1991 The Chemical Society of Japan.)

Table 3. Correlation between Gallery Height of Intercalated Clays and the Resulting Cylodimer Selectivity (Reprinted from Ref 231. Copyright 1994 American Chemical Society)

intercalated carboxylate	molecular length (Å)[a]	gallery height (Å)[b]	distance between two double bonds (Å)[c]		major products[d]
			*d*HH	*d*HT	
1a (sodium cinnamate)	9.10	13.6	0	7.58	*syn*-HH
1b (sodium *p*-phenylcinnamate)	13.1	17.5	0	11.5	*syn*-HH
5a (sodium *p*-(2-phenylethenyl)benzoate)	13.2	17.5	0	2.78	*syn*-HH + *syn*-HT
5b (sodium *p*-[2-(*p'*-chlorophenyl)ethenyl]benzoate)	14.8	18.5	0	3.68	*syn*-HH + *syn*-HT

[a] Molecular lengths of carboxylates were estimated from an AM1 molecular orbital calculations. [b] Gallery heights were calculated by subtracting the $Mg(OH)_2$ sheet thickness (4.77 Å) from the interlayer distances obtained from X-ray diffraction analysis. [c] Differences between two double bonds in distances from the interlayer surface. The *d*HT (head-to-tail) values were calculated from the gallery heights and the distances of double bonds from the carboxylate groups (see Figure 32). The *d*HH (head-to-head) values for HH packing are 0 as listed. [d] Stereochemistries of the major cyclodimers formed in the photocycloaddition of intercalated olefinic carboxylates.

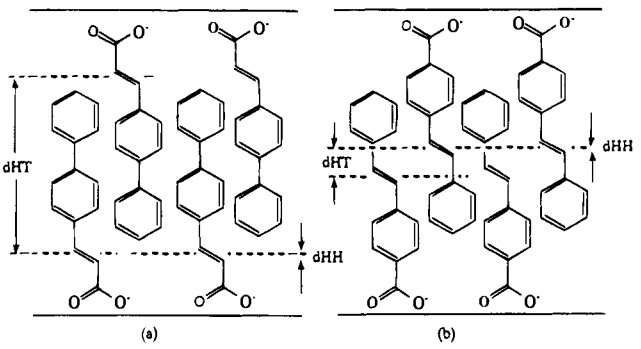

Figure 32. Simplified drawing of antiparallel packing of (a) *p*-phenylcinnamate and (b) stilbene carboxylate ions. (Reprinted from ref 231. Copyright 1993 American Chemical Society.)

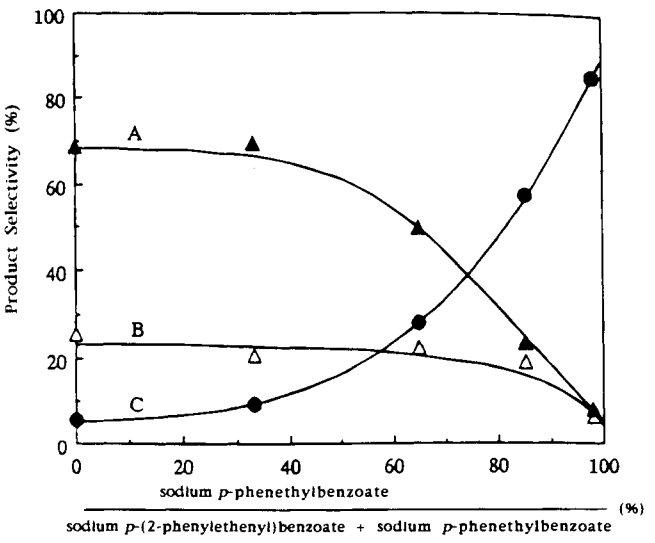

Figure 33. Effect of coadsorbate *p*-phenethylbenzoate on product selectivities for the irradiation of intercalated stilbene carboxylate ions in water: (A) formation of head-to-head dimer (▲); (B) formation of head-to-tail dimer (△); and (C) isomerization to *cis*-isomer (●). (Reprinted from ref 231. Copyright 1993 American Chemical Society.)

reaction shifted from cyclodimerization to *cis–trans* isomerization, suggesting the increasing amount of isolated unsaturated carboxylate molecules.

The dilution effect was also noticed in an excimer fluorescence study. Figure 34 shows the fluorescence spectra of a powdered sample of *p*-(2-phenylethenyl)-benzoate with coadsorbed sodium caprate. The excimer fluorescence of *p*-(2-phenylethenyl)benzoate at 430 nm decreased and the monomer fluorescence at 390 gradually increased with the addition of sodium caprate as coadsorbate.

This series of investigations shows that the organization of organic species into the interlayer space of layered materials is a way of crystal engineering in which controlled reactions can be obtained. In other words, the discussion based on the selectivity of the reactions and the interlayer spacing is a method of probing the geometric relationships between intercalated species.

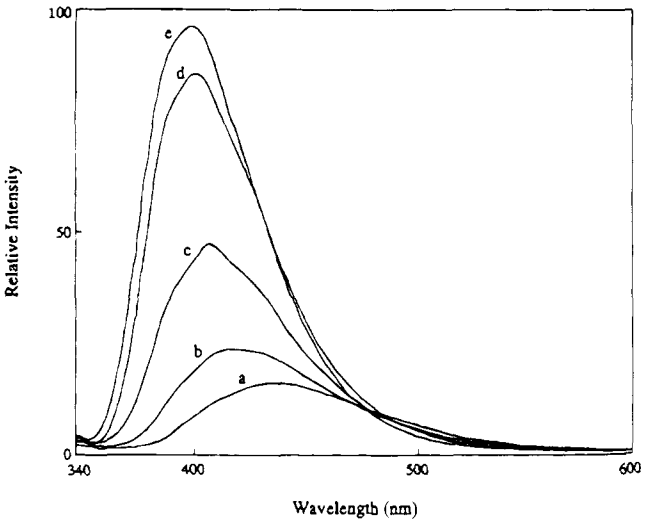

Figure 34. Diffuse reflectance fluorescence spectra of powdered samples on excitation at 325 nm. Intercalation ratios of stilbene carboxylate ions and sodium caprate: (a) 100:0, (b) 50:50, (c) 25:75, (d) 10:90, (e) 5:95. (Reprinted from ref 231. Copyright 1993 American Chemical Society.)

From these spectroscopic studies on the adsorbed species, the following general conclusions can be derived:

(1) Host–guest interactions such as electrostatic interactions and interactions between π-electron and surface oxygen layers, as well as guest–guest interactions such as hydrophobic ones, are important factors which determine the adsorption states.

(2) The charge density of the host layers and the size of the guest species significantly affect the orientation of the guest species in the interlayer space.

(3) The aggregation of guest species in the interlayer space do not originate from inhomogeneous charge distribution on the host surfaces, but from the guest–guest interactions. Appropriate coadsorbates such as surfactants and organic solvents can alter the aggregation states of photoactive species.

(4) Naturally occurring clay minerals contain impurities such as Fe^{3+} which quench the excited state of the adsorbed species through energy transfer mechanism.

(5) The rotation and diffusion of guest species depend on the host–guest systems. Factors involving host–guest interactions, guest–guest interactions, coadsorbates etc. seem to be concerned.

IV. Photofunctions of Intercalation Compounds

A. Photocatalysis

There are many reactions which can be promoted by light-activated solids which are not consumed in the overall reactions. Such solids are called photocatalysts. The construction of highly organized systems is very important to obtain higher efficiency and selectivity in photocatalytic reactions.[232]

Among photocatalytic reactions, the photocatalytic splitting of water with transition metal complexes as sensitizers has attracted much attention. Numerous homogeneous and heterogeneous systems are currently being investigated. The heterogeneous and microheterogeneous ones offer an improved possibility of avoiding back-reactions, of stabilizing high-energy intermediates, or of catalyzing difficult redox reactions. Catalytic oxidation or reduction of water has been achieved with colloidal metal or oxide particles in numerous systems. In order to achieve the separation of the H_2- and O_2-producing systems at a molecular level, the use of heterogeneous character of solid surface has been investigated. Along this line, the photooxidation of water catalyzed by metal complexes within the adsorbed layers of clays has been investigated.[233–240] The possible role of electrostatic effects between negatively charged clay minerals and photocatalysts for photoreduction of water has been reported.

Newsham et al. have reported the excited state properties of *trans*-dioxorhenium(V) ions immobilized in the intercrystalline environments of three complex-layered oxides.[241] Intercalation of *trans*-$ReO_2(py)_4^+$ to the negatively charged interlayer spaces of hectorite and fluorohectorite and that of *trans*-$ReO_2(CN)_4^{3-}$ into the positive layer of Mg/Al LDH were conducted. Despite structurally similar intercalated *trans*-ReO_2 cores, steady state and time-resolved luminescence experiments have revealed that the three intercalation compounds are quite distinct: $ReO_2(py)_4$–hectorite is highly emissive and the luminescence spectrum is similar to that of the native ion; $ReO_2(py)_4$–fluorohectorite exhibits broad and featureless emission whose intensity is attenuated by a factor of 50 relative to that of the $ReO_2(py)_4$–hectorite; no luminescence has been observed for the $ReO_2(CN)_4$–hydrotalcite. From the exited state properties and the X-ray diffraction results, the arrangements of the intercalated oxoions have been proposed, as is shown in Figure 35. It is supposed that the arrangements are responsible for the differences in the excited state properties. Although the catalytic properties have not been reported, the observed differences in the excited state properties suggest the important role of supports.

Uranyl-exchanged smectites have been used to photooxidize alcohols to ketones.[242] Interlayer uranyl ions have been thought to be catalytically active sites. The selectivity for ketone production by uranyl clay is less than that by uranyl-loaded zeolites and the stability of the clay photocatalysts is not as high as that of the zeolite catalysts. However, unusual radical coupling products can be formed on the uranyl–clay catalysts. One important observation is that the excitation wavelength can be significantly changed by changing the hosts.

Uranyl-containing pillared clay has also been used as photocatalysts.[243] Uranyl ions in the clay pillars produce more selective catalysts than materials obtained by inserting uranyl ions in the interlamellar space of the clay. A comparison of the photocatalytic properties of uranyl–clays, uranyl-containing pillared clay, and uranyl–zeolites showed that photochemical selectivity can be controlled by choosing a support with different pore size and surface area.

The photophysical and photochemical properties of small semiconductor crystallites have been a subject of interest.[14,26] The small size of these particles endows them with unusual optical properties due to

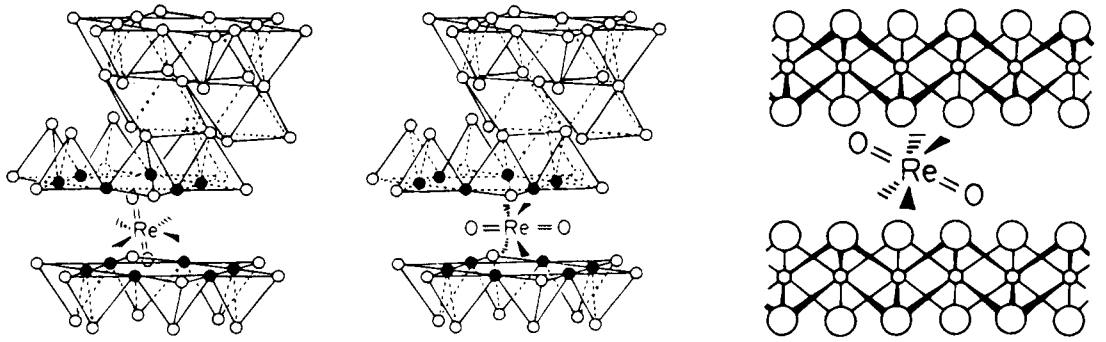

Figure 35. Proposed orientation of the *trans*-dioxorhenium(V) core in (a) hectorite, (b) fluorohectorite, and (c) LDH. (Reproduced from ref 241. Copyright 1988 American Chemical Society.)

quantum size effects that may find application in photocatalysts and nonlinear optical materials. Crystallites with nanometer sizes are inherently unstable due to their high surface tensions and the crystallites tend to grow larger under conventional nucleation conditions. Thus, terminating or stabilizing reagents or matrix are indispensable for the preparation of clusters with controlled size. Constrained systems such as proteins,[244] cellulose,[245] ion exchange resin,[246] micelles,[244] porous Vycor glasses,[247] and zeolites[14,26,248] have been used as matrices. Among them, semiconductor quantum particles formed with one constrained dimension and two free dimensions are likely to be highly anisotropic, potentially giving rise to unusual photophysical properties. On this basis, layered materials have been utilized as a support of the clusters and the resulting materials have been characterized by optical properties as well as TEM observations. There are two possible approaches: one is the incorporation of semiconductor colloidal particles and the other is the formation of the clusters in the interlamellar space.

The incorporation of TiO_2 into montmorillonite has been reported by two different methods.[249-252] One is the oxidation of the intercalated Ti(III) and the other is the direct intercalation of TiO_2 colloid. Yoneyama et al. studied the photocatalytic activities of microcrystalline TiO_2 incorporated int the interlayer space of montmorillonite. The X-ray diffraction pattern showed that the TiO_2 pillar has a 15 Å height. The pillared TiO_2 showed a ca. 0.58 eV blue shift in its absorption and fluorescence spectra compared with TiO_2 particles. The excited electronic states of the pillared TiO_2 were determined to be 0.36 eV more negative than those of the TiO_2 powder particles. It was found that the TiO_2–clay system exhibited higher photocatalytic activity than TiO_2 powder for decomposition of 2-propanol to give acetone and hydrogen, and that of *n*-carboxylic acids with up to eight carbons (from acetic acid to capric acid) to give the corresponding alkanes and carbon dioxides. They explained that the higher excited electronic state contributes to the higher activity. One important in this study is that the pillared TiO_2 exhibited lower catalytic activities for decomposition of capric acid, having 10 carbons in a molecule. It was thought that the space of the TiO_2–montmorillonite interlayers is too narrow to accommodate large molecules, resulting in the poor photocatalytic activity. Thus, the incorporation of TiO_2 small particles into montmorillonite led to the enhancement of the photocatalytic activities as well as guest selectivity in the reaction due to its defined pore size.

The photocatalytic activity of TiO_2–montmorillonite in the reduction of *N,N'*-dimethyl-4,4'-bipyridinium with oxidation of triethanolamine[252] and the oxidation of several aliphatic alcohols have also been reported.[250] The photodegradation of dichloromethane, which is not readily degraded or hydrolyzed in an aquatic environment, to hydrochloric acid and carbon dioxide using titanium-exchanged montmorillonite, titania-pillared montmorillonite, and titanium–aluminum polymeric cation–pillared montmorillonite has been reported.[251]

The photocatalytic decomposition of acetic acid, propionic acid, and *n*-butyric acid on iron oxide incorporated in the interlayer space of montmorillonite has been studied.[253,254] TEM observation showed an interlayer spacing of 0.66 nm, which is in agreement with X-ray diffraction analysis. The iron oxide prepared in montmorillonite had a greater band gap and exhibited remarkable photocatalytic activities being in marked contrast to α-ferric oxide bulk powder. These observations indicate the formation of size quantized iron oxide particles on montmorillonite. The catalytic activities were reported to be greatly dependent on solution pH.

The preparation of CdS and CdS–ZnS mixture in the interlayer space of montmorillonite,[255] laponite,[256-258] and Mg/Al LDH[259] has been reported so far. In the case of montmorillonite and laponite, the particles have been prepared by ion exchange of interlayer exchangeable cation with Cd^{2+} ions and subsequent treatment with H_2S. For the LDH system, cadmium ethylenediaminetetraacetic acid complex ions were introduced into the interlayer space and the compound was allowed to react with an Na_2S solution. The interlayer spacing of the CdS incorporated materials has been determined to be ca. 0.5, 0.2, and 0.3 nm for montmorillonite, laponite, and Mg/Al LDH respectively. Spectral shifts in the visible absorption spectra suggested that the formed CdS particles were confined to some extent.

Quantum-size ZnSe, PbS, CdS, and CdSe particles with the diameter of 3–5 nm in the interlamellar region of the layered host material $Zr(O_3PCH_2CO_2H)_2$ has been prepared by reaction of H_2S or H_2Se with $M(II)[Zr(O_3PCH_2CO_2)_2]$.[254] The semiconductor par-

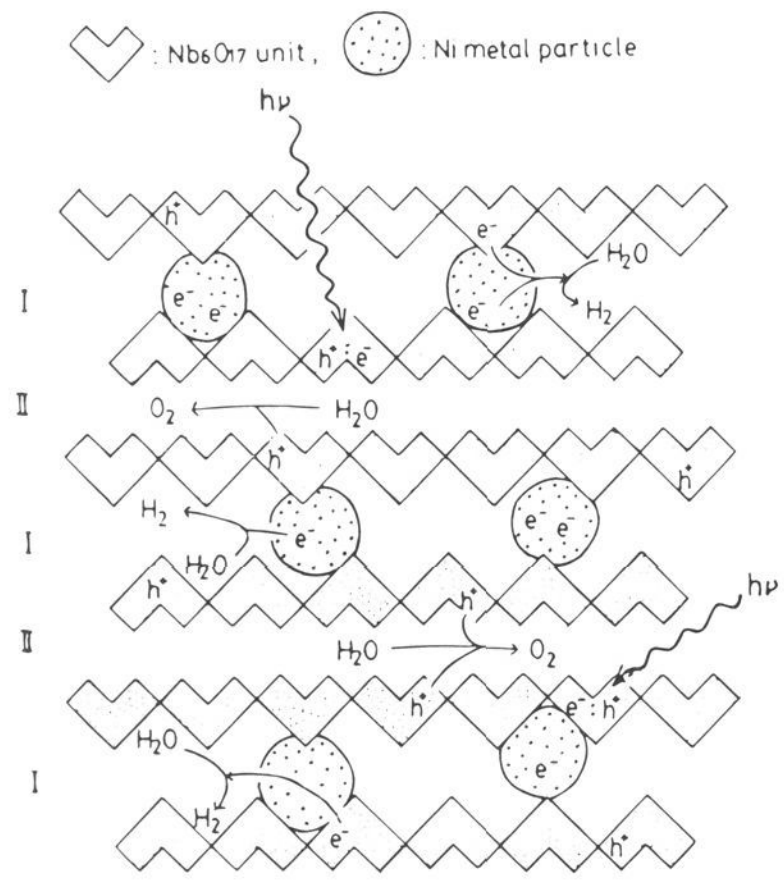

Figure 36. Schematic structure of the active NiO (0.1 wt %)−$K_4Nb_6O_{17}$ photocatalyst and the reaction mechanism of H_2O decomposition into H_2 and O_2. (Reprinted from ref 265. Copyright 1986 Academic.)

ticles exhibit quantum size shifts in their electronic absorption spectra relative to bulk semiconductors. The correlation between the size and the magnitude of blue shifts agrees closely with that reported in the literature for well-characterized "cappred" semiconductor particles. The growth of ZnS and CdS particles in a silica-pilliared layered phosphate has recently been investigated.[261] The studies on photocatalytic and nonlinear optical properties of the semiconductor particles doped in layered materials may lead to novel photofunctional materials. Detailed characterization of the shape and size of the clusters on the layered solids and development in the preparation of clusters with more defined structures are necessary.

Domen et al. studied the photocatalytic activities of several layered metal oxide semiconductors, mainly $K_4Nb_6O_{17}$, for water cleavage by bandgap excitation.[262−268] As mentioned in section II.C, $K_4Nb_6O_{17}$ possesses two different kinds of alternating interlayer space, i.e. interlayer I and II, with K^+ ions are located. This unique structure has successfully been utilized for efficient photocatalytic reactions. In some cases, metal clusters have been fixed on the $K_4Nb_6O_{17}$.

Nickel-loaded $K_4Nb_6O_{17}$ is the catalyst studied most extensively. XPS, EXAFS, TEM, and XRD results have revealed that the loaded nickel is predominantly located in interlayer I as ultrafine metal particles of ca. 5 Å in the active catalysts which was pretreated by H_2 at 773 K for 2 h and reoxidized by O_2 at 473 K for 1 h. Only a small amount of nickel was observed over the external surface of $K_4Nb_6O_{17}$. On the basis of the structure, a mechanism for the photodecomposition of H_2O into H_2 and O_2 has been proposed; intercalated water is reduced to H_2 in interlayer I and is oxidized to O_2 in interlayer II, as schematically shown in Figure 36.[265]

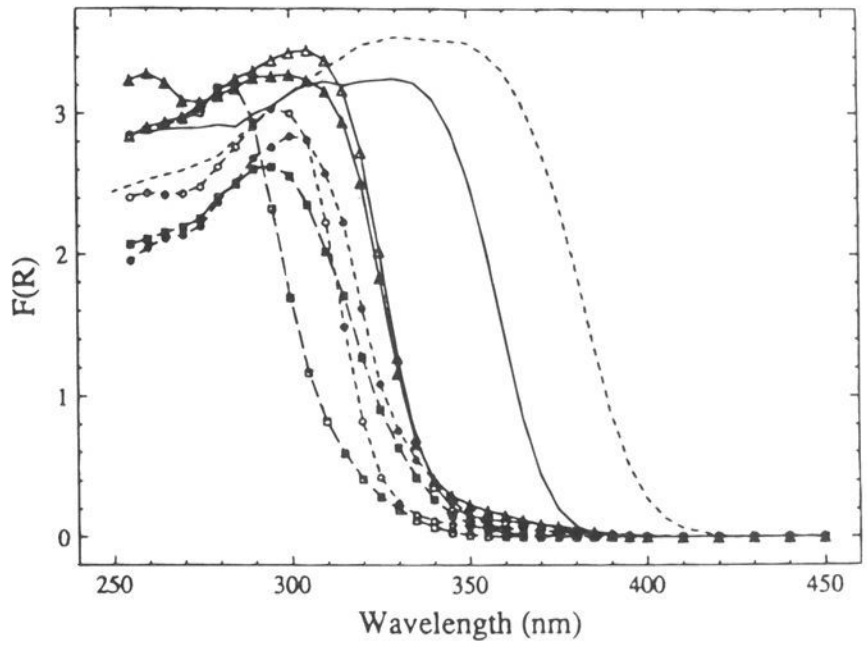

Figure 37. Diffuse reflectance UV spectra of several layered semiconductor oxides, $K_4Nb_6O_{17}$ (△), $KNbO_3$ (▲), $KTiNbO_5$ (●), $CsTi_2NbO_7$ (○), $Na_2Ti_3O_7$ (■), and $K_2Ti_4O_9$ (□), compared with anatase TiO_2 (solid line), and Nb_2O_5 (broken line). (Reprinted from ref 269. Copyright 1993 American Chemical Society.)

The loading amount of NiO on $K_4Nb_6O_{17}$ affected the catalytic activity; NiO(0.1 wt %)−$K_4Nb_6O_{17}$ showed higher activity than NiO(1 wt %)−$K_4Nb_6O_{17}$. Ultrafine Ni metal particles of ca. 5 Å were observed in NiO(0.1 wt %)−$K_4Nb_6O_{17}$ catalysts by TEM, while larger Ni metal particles of ca. 30−150 Å also existed in NiO(1 wt %)−$K_4Nb_6O_{17}$ catalysts. Ultrafine metal particles were thought to be responsible for the photodecomposition of water.[265]

Pt-intercalated $K_4Nb_6O_{17}$ was prepared by ion exchange between $[Pt(NH_3)_4]^{2+}$ and K^+ ions followed by H_2 reduction.[267] The catalysts were treated by aqua regia to remove the platinum on the external surface of $K_4Nb_6O_{17}$ completely. The catalysts showed an activity for photocatalytic overall water splitting without a reverse reaction. The reaction mechanism of the catalytic evolution of H_2 and O_2 over Pt-intercalated $K_4Nb_6O_{17}$ was considered to be similar to that proposed for the reactions over Ni-loaded $K_4Nb_6O_{17}$ catalysts. Note that Pt particles were located only on the external surface when $PtCl_6^{2-}$ anions were used instead of $[Pt(NH_3)_4]^{2+}$ cation; consequently, the reverse reaction from evolved H_2 and O_2 to form H_2O was catalyzed efficiently.

Along this line, Kim et al. investigated the various alkali metal titanates ($Na_2Ti_3O_7$ and $K_2Ti_4O_9$), niobates (KNb_3O_8 and $K_4Nb_6O_{17}$), and titanoniobates ($KTiNbO_5$ and $Csti_2NbO_7$) as photocatalysts for the production of H_2 and I_3^- from acidic alkali metal iodide solutions.[269,270] Diffuse reflectance UV spectra of the hosts are shown in Figure 37. The layered materials were internally platinized, acid exchanged, and sensitized with ruthenium polypyridyl complexes. The schematic structure of the modified layered oxide semiconductor photocatalysts is shown in Figure 38. The titanates were inactive as photocatalysts, whereas the niobates and titanoniobates were active with quantum efficiencies up to 0.3% for HI photolysis with visible light. This difference was discussed from the viewpoint of conduction band energetics. Laser flash photolysis/transient diffuse reflectance spectra established that iodide reduces the oxidized sensitizer, forming $I_2^{\bullet-}$, which subse-

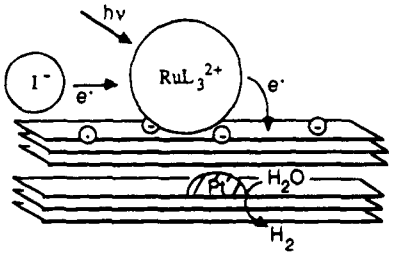

Figure 38. Schematic structure of the sensitized layered oxide semiconductor. (Reprinted from ref 270. Copyright 1991 American Chemical Society.)

quently decays in a bimolecular reaction to form I_3^-.

Two factors were proposed to be responsible for hydrogen evolution from a nonsacrificial donor, iodide, in these systems. First, the structure and anionic framework separate the anionic electron donor from internal catalytic sites, and second, their conduction band edge potentials are significantly more negative than the hydrogen/water formal potential. Since their conduction band-edge potentials depend on the interlayer composition of alkali metal ions and protons, the acid-exchange equilibria of these materials seem to play a role in hydrogen production. The inefficiency of HI photolysis was attributed to charge recombination between I_3^- and conduction band electrons for the niobates and titanoniobates. The low interlayer conductivity in hosts favors charge recombination at the external surface over electron migration to platinum clusters contained within the semiconductor particles. They also observed a strong dependence of the hydrogen production rate on the interlayer spacing. This observation supported the importance of interlayer conductivity on the reactions.

It seems that the structures of the photocatalysts made up from layered solids have not been fully elucidated. The fixation and the characterization of clusters on layered semiconducting materials with variable geometry would give further understanding of the photocatalytic reactions. The preparation and the characterization of novel host materials are also of importance.

B. Energy Storage

Thompson and his co-workers have reported efficient photoinduced charge separation in layered zirconium viologenphosphonate compounds [ZrPV(X)] in both powdered and thin film samples.[271-275] The powdered nature of the samples leads to severe scattering losses in optical studies. In order to overcome the scattering problem associated with powder, transparent multilayer thin films of ZrPV(X) were grown directly onto fused silica substrates from aqueous solution.[61,62]

The sequential growth method has been applied in the preparation of ZrPV(X) films. In this case, fused-silica slides are treated with $(et)_3SiCH_2CH_2CH_2NH_2$, followed by treatment with $POCl_3$. This procedure leads to a phosphonate-rich surface, suitable for treatment with $ZrOCl_2$. The slides are then allowed to react with $H_2O_3P-CH_2CH_2-$bipyridinium$-CH_2-CH_2-PO_3H_2X_2$. In order to accelerate the reaction, which is slow at room temperature, the solution is heated to 85 °C. The schematic structure of the film is shown in Figure 39.

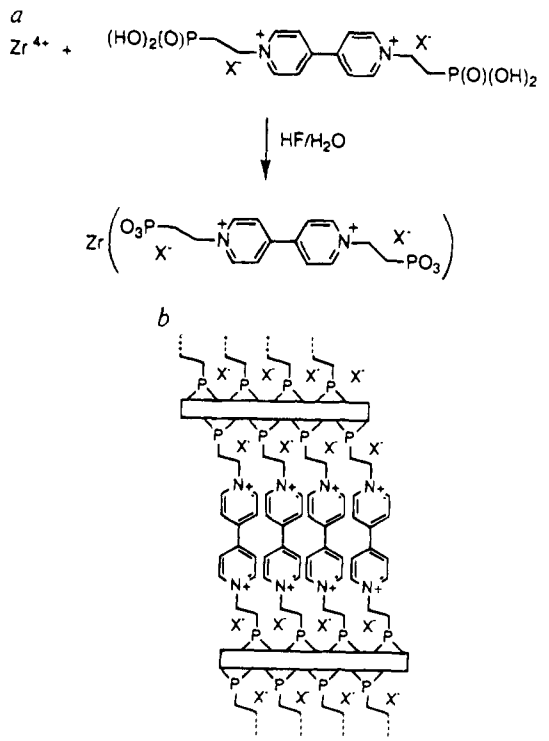

Figure 39. Proposed structure of ZrPV(X). Bars represent the phosphonate oxygen and zirconium atoms. (Reprinted from ref 271. Copyright 1992 Nature.)

Photolysis of $Zr(O_3PCH_2CH_2$(bipyridinium)$CH_2-CH_2PO)X_2$ (X = Cl^-, Br^-, I^-), ZrPV(X), results in the formation of blue radical cations of viologen which are stable in air. The transparent thin film sample makes it possible to conduct detailed photophysical studies. The photoreduction of viologen in these thin film samples is very efficient (quantum yields = 0.15), showing simple isobestic behavior in the electronic spectra. Contrary to bulk solids, photoreduced thin films are very air sensitive.

The mechanism for the formation of charge-separated states in these materials involves both irreversible and reversible components. An irreversible component is proposed to involve hydrogen atom abstraction by photochemically formed halide radicals, followed by structural rearrangements. Optimization of the reversible process may make it possible to use these materials for efficient conversion and storage of photochemical energy.

The energy-transfer among naphthyl-, anthryl- and pyrenylalkylammonium bound to zirconium phosphate and photoinduced electron transfer from 5,10,-15,20-tetrakis(4-phosphonophenyl)porphyrin to *N,N'*-bis(3-phosphonopropyl) 4,4'-bipyridinium organized in Zr based self-assembled multilayers have been reported.[274,275] Zirconium phosphate based layered structures play an important role in the organization of reactants to control important energy/electron transfer.

C. Photoluminescence

Organic laser dyes have found an increasing variety of applications in spectroscopy, optics, and lasers. One of the key problems in the investigation and

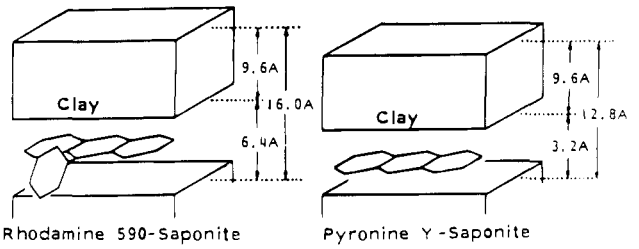

Figure 40. Schematic illustration on the conformation of rhodamine 590 and pyronin Y in the interlayer space of saponite. (Reprinted from ref 277. Copyright 1988 Elsevier.)

application is their fixation into matrices, because the spectral characteristics are largely affected by the nature of matrices. On this basis, Endo et al. studied the fluorescence properties of rhodamine 590 and 640 adsorbed on montmorillonite and those of rhodamine 590, pyronine Y, and coumarine dyes incorporated into the interlayer space of saponite.[276-278] The dyes employed in these studies are known to show high quantum efficiency of fluorescence and are used as a tunable laser. The fluorescent properties of the resulting intercalation compounds have been discussed on the basis of the arrangements of dyes in the interlayer space.

The incorporation of the dyes into smectites has been accomplished by a cation exchange mechanism. The TG-DTA curves of the intercalation compounds show that the dyes are immobilized and thermally stabilized. Saponite is a better host material because of the transparency partly due to the absence of Fe^{3+} impurities which quench the excited state of the dyes. On the basis of the observed basal spacings of 16.0 and 12.8 Å at maximum loading level for the rhodamine 590− and pyronine Y−saponite intercalation compounds, respectively, the configuration of the intercalated dyes has been estimated as shown in Figure 40.[277]

In the coumarine−, rhodamine 590−, and pyronine Y−saponite systems, the change in the fluorescence intensity accompanied with the shifts of fluorescence maxima as a function of the dye contents was observed. Taking into account the change in the X-ray diffraction pattern, Endo et al. ascribed the change in the emission intensity to the conventional concentration quenching and proposed the arrangements of the intercalated dyes. Figure 41 shows the proposed arrangements of pyronin Y intercalated in the interlayer space of saponite.[277]

However, the observed X-ray diffraction patterns showed the splitting of the $d(001)$ reflection peaks. As has already been observed in the studies of the intercalation of $Ru(II)^{2+}$ into smectites, aggregation of $Ru(II)^{2+}$ tends to occur even at a low concentration loading. In the dye−saponite systems, the possibility of segregation can not be excluded thoroughly.

We have prepared Ru(II)−fluortetrasilicic mica (TSM)−poly(vinyl pyrrolidone) (PVP) intercalation compounds with variable concentration of Ru(II) by cation exchange of sodium ions in the preformed TSM−PVP intercalation compound with Ru(II).[279,280] Since naturally occurring clay minerals contains Fe^{3+} which quenches the excited state of Ru(II), a synthetic swelling mica (TSM) was used as the host

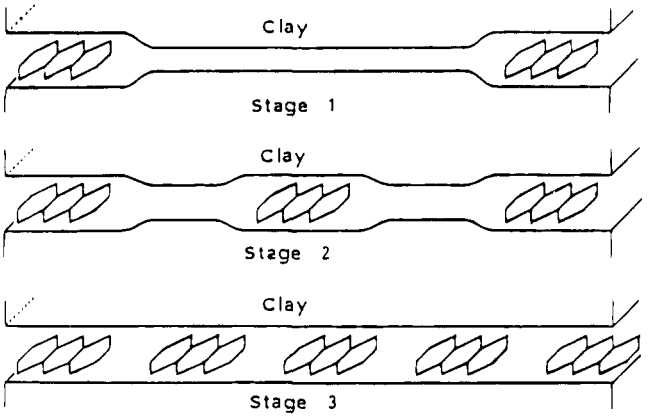

Figure 41. Schematic illustration of the model concerning the intercalation process of pyronin Y into the interlayer space of saponite. (Reprinted from ref 277. Copyright 1988 Elsevier.)

material. Ru(II) ions tend to aggregate even at low concentrations of loading upon adsorption on smectites. PVP was added in order to avoid aggregation of Ru(II).

The compounds showed unique photoluminescent properties. The luminescence maxima of intercalated Ru(II) shifted gradually toward blue with the decrease in the loading of Ru(II), reflecting the change in the polarity and/or rigidity of the microenvironment of Ru(II), which was caused by cointercalated polar PVP. Moreover, Ru(II) was isolated effectively to suppress self-quenching even at its high concentration loading. It was supposed that cointercalated PVP was forced to surround Ru(II) in close contact in the sterically limited interlayer spaces. The schematic structures are shown in Figure 42. X-ray diffraction studies supported the conclusion. When the Ru(II) intercalated in the TSM without PVP, the diffraction peaks split into two, suggesting segregation.

Thus, immobilization of fluorescence dyes into layered materials is of great significance in understanding the matrix effects on the fluorescence properties as well as controlling them. Since these composites can be obtained as thin films, they have potential applicability as light-emitting devices.

The luminescence properties of rare earth ions are a subject of interest, owing to their broad range of applications in such fields as laser materials, optical recording materials, solar concentrations, and even biological structure probes. Consequently, the complexation of rare earth ions into solids may result in novel luminescence materials. The luminescence of Eu^{3+} and Tb^{3+} ions intercalated in the interlayer space of montmorillonite, hectorite,[281] $H_2Ti_3O_7$, and $H_2Ti_4O_9{\cdot}nH_2O$[282] has been reported. The luminescence intensity of the montmorillonite sample is weak if compared with that of the hectorite sample. This difference has been attributed to energy transfer to Fe^{3+} ions of the montmorillonite lattice. It has been shown that the interaction between silicate layer and rare earth ions as well as those between coadsorbed water molecules and rare earth ions affects the luminescence.

Recently, the photoluminescence of layered alkali metal titanates ($A_2Ti_nO_{2n+1}$, A = Na, K) and potas-

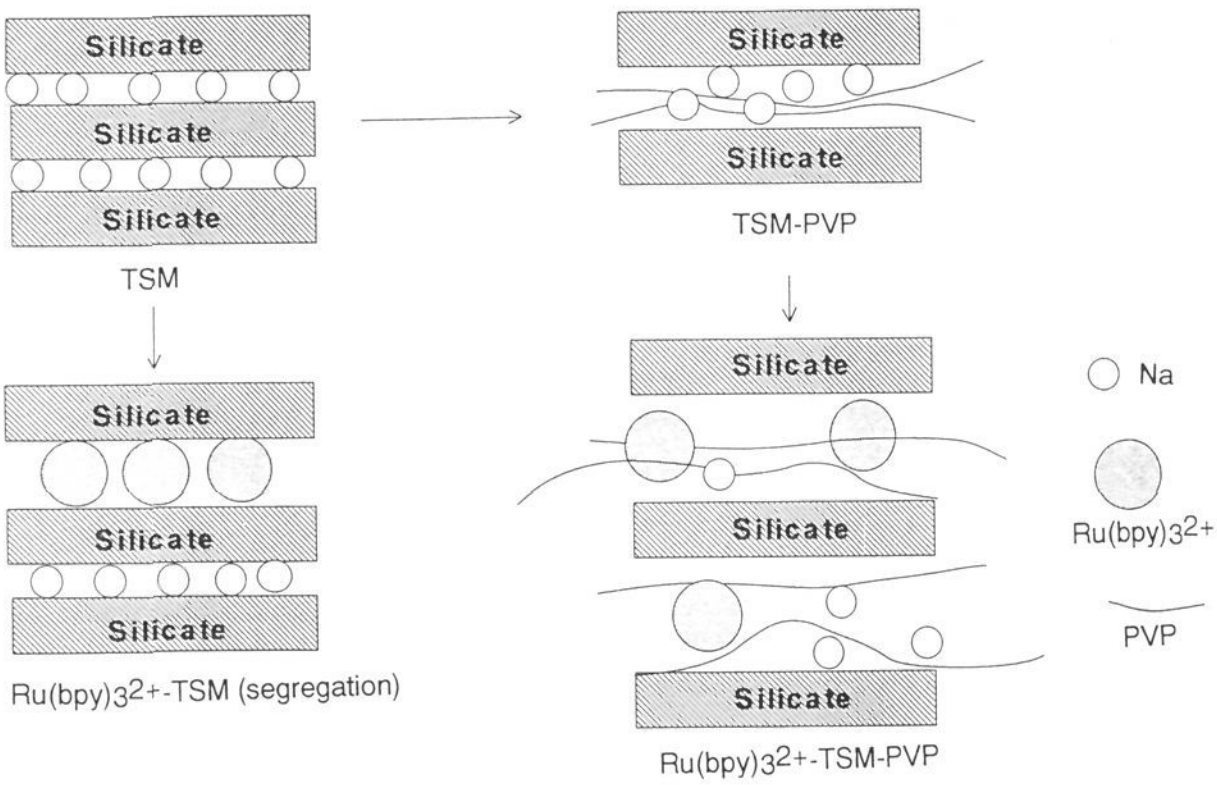

Figure 42. Schematic structure of (a, top left) Na–TSM, (b, bottom left) Ru(II)–TSM intercalation compound, (c, top right) TSM–PVP intercalation compound, and (d, bottom right) Ru(II)–TSM–PVP intercalation compound. (Reprinted from ref 280. Copyright 1993 American Chemical Society.)

sium niobates ($K_4Nb_6O_{17}$ and KNb_3O_8) has been investigated.[283] One important observation reported in this study is that the photoluminescence of $K_2Ti_3O_7$ is affected by interlayer conditions such as water content. The origin of the different emitting properties seems to be of interest.

D. Photochromism

Photochromism, dealing with photochemical reactions which are thermally or photochemically reversible, has received considerable attention ever since its discovery in 1876 and still is an active field of research mainly because of its actual and potential applications and for its paramount importance in biological phenomena.[284] Studies on photochromic reaction behaviors and their controls in solid media have significance for practical applications such as in optical recording as well as in probing host–guest systems. Recently, matrix effects for the photochromic reactions have been explored in media having ordered structures such as thermotropic and lyotropic liquid crystals,[285] bilayer membranes,[286] and Langmuir–Blodgett (LB) multilayers.[287] Studies of photochromic reactions of organic species incorporated in ordered matrices have advantages in that reaction behaviors may be understood from physical and chemical properties on a molecular level. On this basis, photochromism of fulgide,[288] azobenzene,[48] spiropyrans,[289–292] and viologens,[293] intercalated in the interlayer space of smectites and other layered materials has been reported.

Adams et al. studied the photochromism of fulgide α-2,5-dimethyl-3-furylethylidene (isopropylidene) succinic anhydride; the molecular structure of fulgide is shown in Scheme 1, in the presence of smectites.[288] The mixture of predried clay minerals and reactants solution was irradiated and the reactions were monitored.

Figure 43 shows reactions of fulgide in the absence (upper) and presence of smectites by the irradiation. Conversions which are normally accomplished with

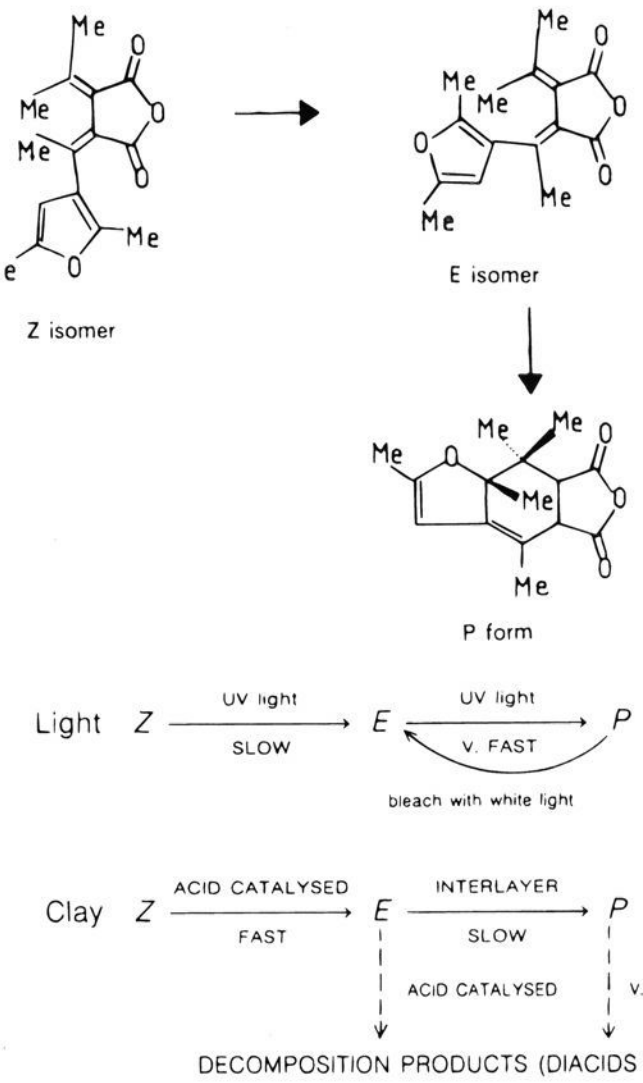

Figure 43. Schematic representation of reaction processes of flugide with and without smectites. (Reprinted from ref 288. Copyright 1990 Kluwer.)

Scheme 1. Molecular Structure of Fulgide

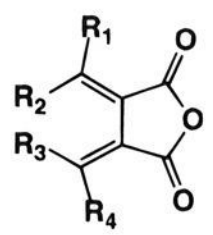

light are obtained over clays in the dark; they are thermally activated. Both the *Z*–*E* isomerization and decomposition reactions are acid catalyzed. Weight of clay, concentration of the fulgide, tempera-

Scheme 2. *Cis–Trans* Isomerization of Azobenzene

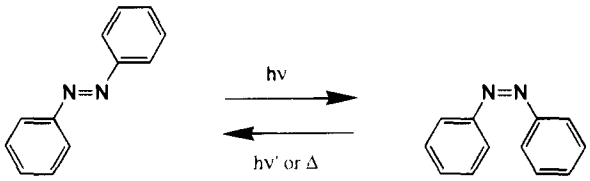

Scheme 3. Isomerization of Spiropyran to Merocyanine

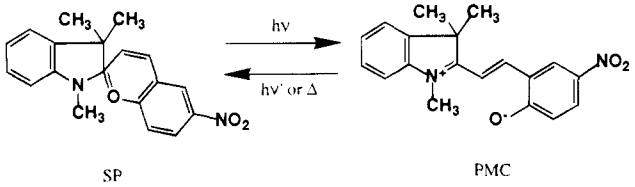

SP PMC

ture, interlayer water content, solvent, and interlayer cation affected the reaction rate, although no sufficient explanation has been given.

We have reported the incorporation and photochemical behavior of an azobenzene derivative (*p*-aminoazobenzene, abbreviated as *p*-AZ) into the hydrophobic interlayer space of *n*-dodecylammonium–montmorillonite.[48] Photochromism of azobenzene (Scheme 2) and its derivatives due to *cis–trans* isomerization has been widely investigated. Photocontrol of chemical and physical functions of crown ethers,[294] LB films,[295] etc. has been vigorously studied using the photochemical configurational change of azobenzene derivatives. Photoisomerization of azobenzene derivatives in the interlayer spaces of layered materials can induce the change in the basal spacings.

Solid-state reaction was used for the intercalation of *p*-AZ into the hydrophobic interlayer space of an organophilic montmorillonite. The basal spacing of the product increased from 18 Å to ca. 30 Å, indicating the intercalation of *p*-AZ. The absorption spectrum of the intercalation compound showed an absorption band at 395 nm ascribable to *trans*-*p*-AZ. By irradiation of UV light, the band intensity decreased. The intensity of the band increased gradually, when the sample was stored in the dark after the irradiation, and the reversible spectral change was observed repeatedly. Therefore, this was ascribed to the photoisomerization of the intercalated *p*-AZ. The high concentration of *p*-AZ and relatively slow thermal *cis* to *trans*-reaction are worth noting. Although the needs to be further systematic studies on the change in the properties and the structures of the intercalation compounds upon irradiation, these materials would be a novel photoresponsive system with controllable absorptive properties.

The photochromism of spiropyran and its derivatives in the interlayer spaces of montmorillonites and a Mg/Al LDH has been reported.[289–292] The interconversion between spiropyran (SP) and merocyanine (MC) (Scheme 3) has been known as a typical example of photochromic reactions as a possible recording medium for information storage and retrieval devices. A number of media have been investigated in which the kinetics of the photochromic reactions may be controlled. Takagi et al. reported the intercalation of 1′,3′,3′-trimethylspiro-[2*H*-1-benzopyran-2,2′-indoline] (H-SP) and its 6-nitro (NO_2SP) and 6-nitro-8-(pyridinium methyl) (Py^+-SP) derivatives into montmorillonite, and photochromic behavior has been studied for colloidal systems.[289] The effects of the intercalation on the rate of thermal coloration and decoloration have been compared with those in other systems such as colloidal silica, cetyltrimethylammonium bromide (CTAB), and sodium dodecyl sulfate (SDS) micelles.

Py^+-SP was intercalated into montmorillonite quantitatively as an equilibrium mixture with the corresponding MC with the ratio of Py^+-SP:Py^+-MC of 35:65 and exhibited reversed photochromism. It is known that thermal equilibria between SP and MC are dependent on the polarity of surroundings; MC becomes the major product with increasing polarity. Therefore, the observed reverse photochromism has been explained in terms of the polar interlayer of montmorillonite. The thermal isomerization of Py^+-SP intercalated in aqueous colloidal montmorillonite exhibited a linear combination of two components of first-order kinetics, indicating the presence of two adsorption environments. It has been suggested that one is due to molecularly separated species and the other is due to aggregated species.

In contrast, a preferential adsorption as SP was observed when CTAB was coadsorbed with Py^+-SP, H-SP, and NO_2-SP, and normal photochromism has been observed in these systems. Single first-order kinetics has been observed for the Py^+-SP–CTAB–montmorillonite system. The effects of coadsorbing CTAB on the photochromic behavior showed that the CTAB surround Py^+-SP to cause hydrophobic surrounding of Py^+-SP.

The formation of stable *H* (parallel type) and *J* (head-to-tail type) aggregates of photomerocyanines has been suggested in the study on the photochromism of a series of 1′-alkyl-3′,3′-dimethyl-6-nitro-8-(alkanoyloxymethyl)spiro(2*H*-1-benzopyran-2,2′-indoline) derivatives with different length of alkyl chains in $2C_{12}2C_1^+$–montmorillonite.[290] Bilayer-forming amphiphiles intercalated montmorillonites, dioctadecyldimethylammonium bromide ($2C_{18}2C_1N^+Br^-$), and didodecyldimethylammonium chloride ($2C_{12}2C_1^+Cl^-$) have been used to immobilize SPs.[290,291] A cast film consisting of the SP incorporated into a bilayer intercalated into a clay was prepared on a glass plate by slowly evaporating a solution of the SP and $2C_{12}2C_1^+$–montmorillonite. The results of the photochromism of spiropyran in $2C_{12}2C_1^+$–montmorillonite film are summarized in Table 4. When longer R^1 alkyl chains were introduced, new very sharp absorption peaks at around 500 nm appeared in addition to the absorption at 570 nm due to the monomeric PMC upon UV light irradiation. A new sharp absorption band appeared at a longer wavelength region around 610 nm when SPs bearing longer alkyl chains were exposed to UV light. These new absorption bands are ascribable to aggregates of PMCs which are reported to form occasionally in organized molecular assemblies. The absorption bands around 500 and 610 nm have been ascribed to *H* and *J* aggregates of PMC, respectively. A high activation energy and highly positive activation entropy for *J* and *H* PMCs, which directly correlate

Table 4. Photochromism of Spiropyrans in DDAC–Montmorillonite Cast Film. (Reprinted from Ref 290. Copyright 1994 Royal Society of Chemistry)

			DDAC–mont film			λ_{max} (nm)[b]	
SP	R^1	R^2	λ_{max} (nm)[b]	$10^4/k$ (s^{-1})[c]	T (°C)	EtOH	n-C_6H_{14}
0100	Me	H	552	1.21	37	540	580
1800	$(CH_2)_{17}Me$	H	574	19.3	37	542	576
0112	Me	$CH_2OCOC_{11}H_{23}$	550	2.90	37	542	620
1012	$(CH_2)_9Me$	$CH_2OCOC_{11}H_{23}$	580	11.2	37	547	576
1612	$(CH_2)_{15}Me$	$CH_2OCOC_{11}H_{23}$	493(H),570	17.5,25.9	60	547	577
1812	$(CH_2)_{17}Me$	$CH_2OCOC_{11}H_{23}$	497(H),570	16.7,25.0	65	549	580
0822	$(CH_2)_7Me$	$CH_2OCOC_{21}H_{43}$	578	12.7	37	546	578
1822	$(CH_2)_{17}Me$	$CH_2OCOC_{21}H_{43}$	615(J),566	16.0,16.5	70	553	579
0130	Me	$CH_2OCOC_{29}H_{59}$	565	1.50	37	543	576
1230	$(CH_2)_{11}Me$	$CH_2OCOC_{29}H_{59}$	576	4.58	37	548	577
1830	$(CH_2)_{17}Me$	$CH_2OCOC_{29}H_{59}$	617(J),566	5.35,2.35	70	548	578

[a] The SP/DDAC–mont molar ratio is 1/2. [b] Absorption maximum of PMC. [c] The first-order rate constants for the thermal isomerization of PMC to SP at the indicated temperature.

Table 5. Kinetic Data of Thermal Decoloration of PMC (Reprinted from Ref 291. Copyright 1994 American Chemical Society)

	k at 30 °C (s^{-1})			factor of rate jump at T_c[a]	E_a (kJ mol^{-1})	
film	k_{film}	k_{sol}	k_{film}/k_{sol}		below T_c	above T_c
$2C_{18}N^+2C_1$–PSS[b]	1.6×10^{-2} (fast)	2.2×10^{-2} [c]	0.72	2.6		
	7.6×10^{-4} (slow)		0.035	4.9	14.2	38.5
$2C_{18}N^+2C_1$–mont[b]	6.8×10^{-4} (fast)	7.9×10^{-3} [d]	0.086	2.0		
	4.8×10^{-5} (slow)		0.0061	14	53.5	89.9

[a] For the evaluation of the rate jump at T_c, see the text. [b] Annealed films. [c] In water–1,4-dioxane (3/97), λ_{max} = 565 nm. [d] In water–1,4-dioxane (7/93), λ_{max} = 555 nm.

with the thermal stability of these aggregates (slow decoloration), have been observed.

Although the origin of aggregate formation as well as the nature of the aggregates is not clear at present, the aggregate of organic dyes may exhibit enhanced optical properties. Therefore, systematic studies on the aggregation of dyes on the layered materials may give new insights for understanding the nature of the aggregation of dyes and for constructing optical devices.

Seki and Ichimura have investigated the thermal isomerization kinetics of photoinduced MC to SP in solid films having multibilayer structures, which consists of ion complexes between ammonium bilayers forming amphiphiles ($2C_{18}2C_1N^+$) and polyanions (montmorillonite and poly(styrene sulfonate), PSS).[291] 1,3,3-Trimethyl-6′-nitrospiro[indoline-2,2′-*2′H*-benzopyran] (SP) was incorporated into thin film of the polyion complexes, which were prepared by casting the chloroform solution or suspension of the polyion complexes.

X-ray diffraction studies showed that the cast films were composed of a multilamellar bilayer structure whose membrane plane was preferentially oriented parallel to the film surface. The spacings corresponding to lamellar thickness and estimated tilt angles of the amphiphile are listed in Table 5. Endothermic peaks were observed in the DSC curves of the films; the observed phase transition temperature was listed in Table 4. Both DSC and X-ray diffraction results indicated that the $2C_{18}2C_1N^+$–montmorillonite film had a more ordered structure than $2C_{18}2C_1N^+$–PSS film. Since annealing the film at 60–70 °C at a relative humidity of ca. 100% for a few hours resulted in the well-structured $2C_{18}2C_1N^+$–PSS film, the photochromic behavior was investigated for the annealed films. The difference in the film structure influences the kinetic properties of the thermal decaying of MC embedded in the films.

The incorporated SP exhibited photochromism in both of the immobilized bilayer complexes with montmorillonite and PSS. Kinetic measurements of the thermal isomerization (decoloration) were carried out for the annealed film. The decoloration reaction rate is dependent on the mobility of the surroundings and, in polymer matrices, is influenced by the glass transition. It was found that the reaction rates abruptly increased near the crystal to liquid–crystal phase-transition temperature of the immobilized bilayer due to increased matrix mobility in this system. Figure 44 shows temperature dependence of the rate constants of the reaction in annealed $2C_{18}2C_1N^+$–montmorillonite and $2C_{18}2C_1N^+$–PSS films. The film prepared with montmorillonite gives more homogeneous reaction environments for the chromophore than those with the linear polymer (PSS). This leads to drastic changes in this reaction rate at the crystal to liquid–crystal phase transition of the bilayer, showing the effect of the phase transition of immobilized bilayers to be more pronounced than that of the glass transition of amorphous polymer matrices.

The intercalation of sulfonated indolinebenzopyran ($SP\text{-}SO_3^-$) into a layered double hydroxide with cointercalating toluene *p*-sulfonic acid and its photochemical behavior has been investigated.[292] The intercalation compound showed reversible photochromic behavior due to SP-MC transformation. The PMC was thermally stable probably due to the interactions between host and guest and those between $SP\text{-}SO_3^-$ and toluene-*p*-sulfonic acid, although the exact orientations of the guests in the interlayer space were not clear.

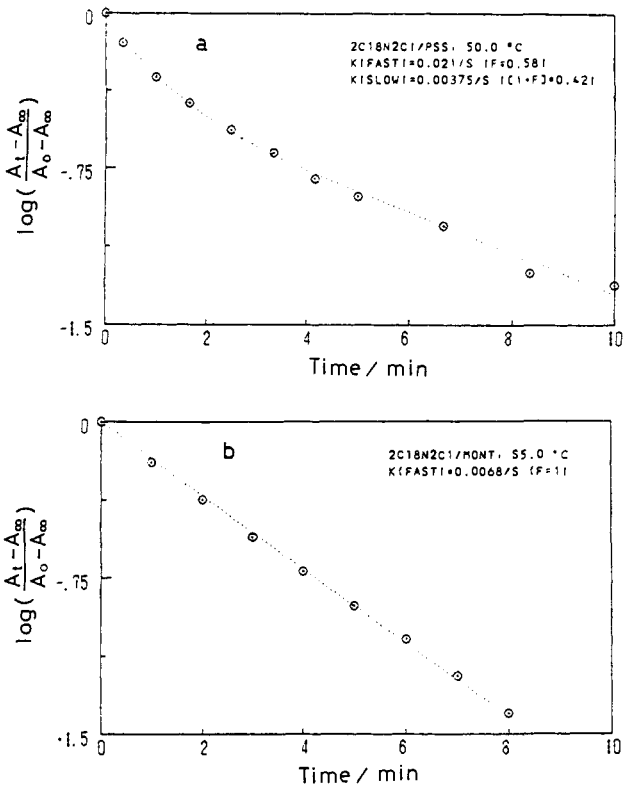

Figure 44. First-order plots for thermal decaying of PMC above T_c in annealed $2C_{18}N^+2C_1$–PSS (a) and $2C_{18}N^+2C_1$–montmorillonite (b) films. (Reprinted from ref 291. Copyright 1990 American Chemical Society.)

Scheme 4. Photochromism of Viologens

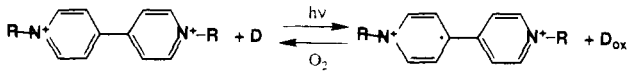

Viologens are photoreduced reversibly in the presence of an electron donor, forming blue radical cations. The color development by electrochemical reduction and UV light irradiation is shown in Scheme 4.

Miyata et al. reported the photochromism of viologens (1,1′-dialkyl-4,4′-bipyridinium ions) intercalated in the interlayer space of montmorillonite with cointercalating poly(vinyl pyrrolidone) (PVP).[293] Viologen dications were intercalated in the interlayer space of montmorillonite–PVP intercalation compound by cation exchange mechanism. Photochemical studies were carried out for self-supporting films of viologen–montmorillonite–PVP prepared by drying the samples spread on acrylic plates by irradiation with Hg lamp. Figure 45 shows the change in the absorption spectra by UV light irradiation. By the irradiation, viologen radical cations formed to show blue color and characteristic absorption bands at 610 and 400 nm in the visible spectra. Reversible color development and color fading were observed. In this system, cointercalated PVP was assumed to act as an electron donor for the reduction of the viologens. It should be noted that the color-fading required a longer period than that in a PVP matrix. Since the color-fading process in the PVP matrix was interpreted by the oxidation caused by oxygen in air, the slow color-fading reaction observed for the viologen–montmorillonite–PVP system was explained by the prevention of contact

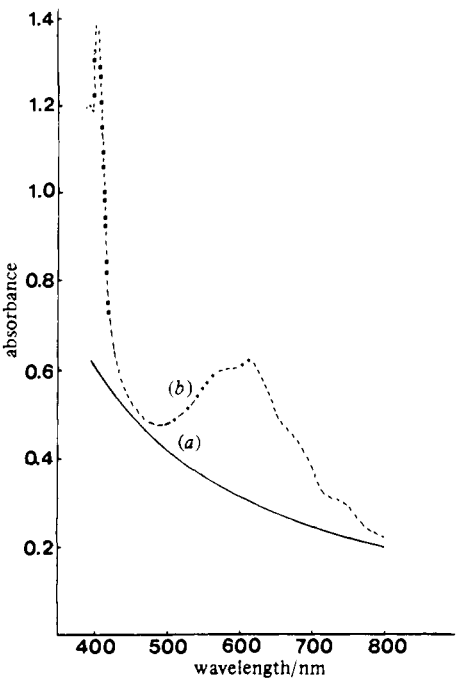

Figure 45. Absorption spectra of *n*-heptylviologen–montmorillonite–PVP intercalation compound (a) before and (b) after the irradiation. (Reprinted from ref 293. Copyright 1987 Royal Society of Chemistry.)

between the viologen radical cations and the oxidizing agent.

The photochromic behavior of the methylviologen (1,1′-dimethyl-4,4′-bipyridinium ion; abbreviated as MV^{2+}) intercalated into a series of layered transition metal oxides has been reported. $K_2Ti_4O_9$,[296] $HTiNbO_5$,[297] $K_4Nb_6O_{17}$,[298,299] HNb_3O_8,[299] and $HA_2Nb_3O_{10}$ (A = Ca, Sr)[300] were used as host materials and MV^{2+} was intercalated by cation exchange with interlayer cations. The photochemical studies were conducted for powdered sample by irradiation with Hg lamp and the reaction were monitored by diffuse reflectance spectra. Semiconducting host layers acted as an electron donor for the reduction of viologen to form radical cations of the intercalated MV^{2+} in the interlayer space. The stability of the photochemically formed blue radical cations has been discussed on the basis of their microscopic structures.

It should be noted that the photochemistry of intercalation compounds formed between the layered niobates, $K_4Nb_6O_{17}$ and HNb_3O_8 with MV^{2+}, can be controlled by changing the interlayer structures.[298] Two types of MV^{2+} intercalated compounds with different structures have been prepared for each host. In the $K_4Nb_6O_{17}$ system, two intercalation compounds, whose schematic structures are shown in Figure 46, were obtained by changing the reaction conditions. In both of the intercalation compounds, MV^{2+} are located only in interlayer I. HNb_3O_8 also gave two different intercalation compounds; one was prepared by the direct reaction of HNb_3O_8 with MV^{2+} and the other was obtained by using propylammonium-exchanged HNb_3O_8 as an intermediate. In the latter compound, propylammonium ions and MV^{2+} were located in the same layer. The schematic structures are shown in Figure 47. All the intercalation compounds formed $MV^{\cdot+}$ in the interlayers by

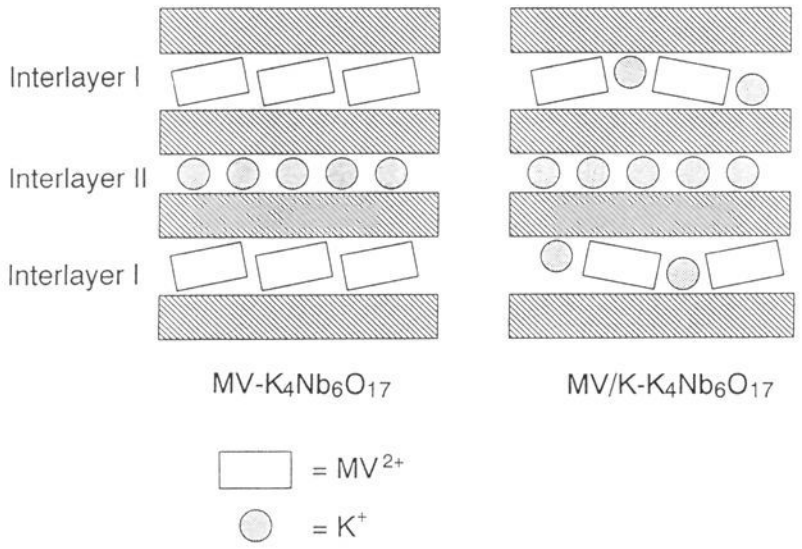

Figure 46. Schematic representation of the interlayer structure of (left) MV−$K_2Nb_6O_{17}$ and (right) MV/K−$K_2Nb_6O_{17}$. (Reprinted from ref 299. Copyright 1992 American Chemical Society.)

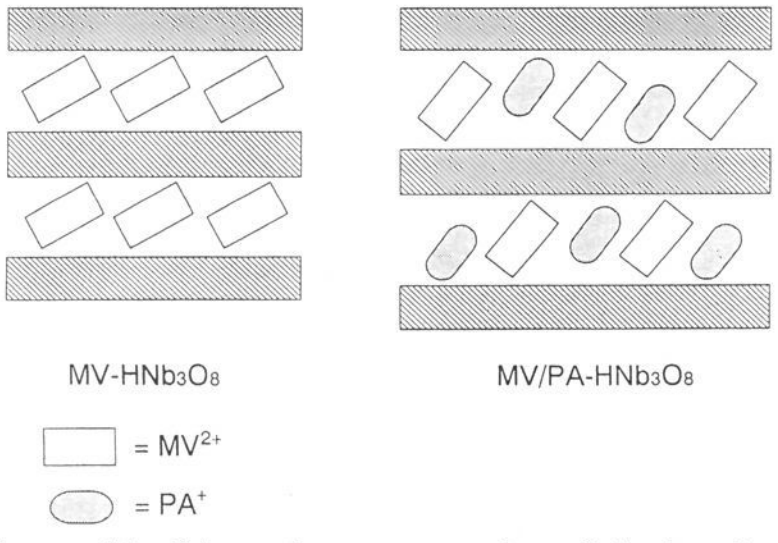

Figure 47. Schematic representation of the interlayer structure of (left) MV−HNb_3O_8 and (right) MV/PA−HNb_3O_8. (Reprinted from ref 299. Copyright 1992 American Chemical Society.)

Table 6. Half-Lives of $MV^{\bullet+}$ in Various Intercalation Compounds (Reprinted from Ref 299. Copyright 1994 American Chemical Society)

	in oxygen	in air	in argon
MV−$K_2Nb_6O_{17}$	15 min	45 min	2 h
MV/K−$K_2Nb_6O_{17}$	2 h	6 h	
MV−HNb_3O_8	3 min	4 min	10 min
MV/PA−HNb_3O_8	1 h	4 h	
MV^{2+}−H_xTiNbO_5	3 min	4 min	20 min

host−guest electron transfer. Table 6 shows the half-lives of $MV^{\bullet+}$ in the intercalation compounds. The presence of cointercalated species, K^+ and propylammonium ion in the $K_4Nb_6O_{17}$ and HNb_3O_8 systems, respectively, significantly affected the decay of $MV^{\bullet+}$. This difference was explained by guest−guest interactions which varied with the cointercalation of photoinactive guests (K^+ and propylammonium ion).

When layered niobates which have perovskite-type oxide layers have been used as host materials, the photochemical behavior of the intercalated MV^{2+} differs significantly from those of $HTiNbO_5$, $K_4Nb_6O_{17}$, and HNb_3O_8 systems.[300] Depending on the A ions, the photochemical property of the intercalation compounds varied. UV irradiation of the MV^{2+}−intercalated compounds caused electron transfer from the host to MV^{2+} in the $HCa_2Nb_3O_{10}$ system, whereas photoreduction of Nb ions in the host lattice was observed in the $HSr_2Nb_3O_{10}$ system. Such a variation

Scheme 5. Photochemical Reaction of 1,4-Dihydroxyanthraquinone (DAQ)

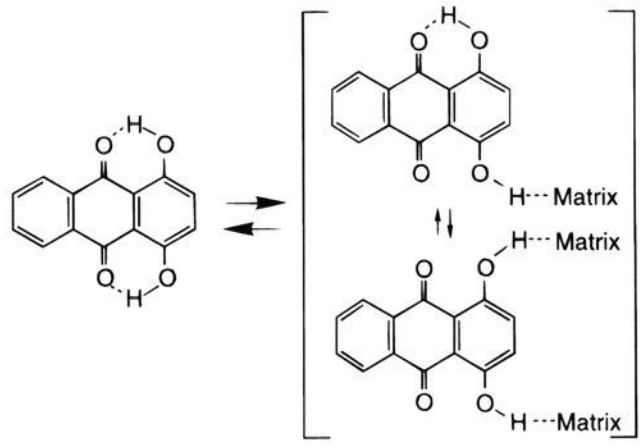

of chemical properties with A ions has also been observed in photocatalytic activities of various perovskite-related layered niobates.

E. Photochemical Hole Burning

Photochemical hole burning (PHB) is a site-selective and persistent photobleaching in an inhomogeneously broadened absorption band induced by resonant laser light irradiation at cryogenic temperatures.[301] It has attracted increasing attention recently partly due to its possible applicability to high-density frequency domain optical storage, in which a more than 10^3 times higher storage density than that of the on-going optical disk system would in principle be available. There remain, however, many obstacles to be overcome in optimization of materials as well as in the issue of the storage system and architecture. Among many efforts, a search for new materials is important because the hole formation processes depend significantly on the nature of host−guest systems. For the formation of persistent holes, the existence of both solid matrix and photoreactive molecule is essential. Since the hole formation characteristic depends significantly on the nature of host−guest systems, they can be regarded as a high-resolution solid-state spectroscopy. On this basis, two intercalation compounds, which exhibit PHB reactions, have been prepared.[204,302] In both systems, saponite was used as the host material. The photoactive centers are 1,4-dihydroxyanthraquinone (abbreviated as DAQ) and cationic porphins, both of which are typical PHB dyes, and their hole formation has been observed in amorphous matrices so far.[301]

We prepared a tetramethylammonium(TMA)−saponite−DAQ intercalation compound and investigated its PHB reaction to show the merits of an ordered matrix for a PHB material.[302] DAQ is one of the molecules most extensively used as a PHB probe and its hole formation has been observed in numerous amorphous matrices so far.[303,304] It has been suggested that the PHB reaction of DAQ is due to the breakage of internal hydrogen bond(s) and the subsequent formation of external hydrogen bond(s) to proton acceptor(s) in a matrix (Scheme 5).[303] Smectites have some attractive features as a host material for PHB reactions of DAQ; it is colorless and transparent in the visible region, and its interlayer surfaces are capable of accepting hydrogen bonds. Moreover, the surface properties of saponite such as adsorption property can be altered by cointercalation

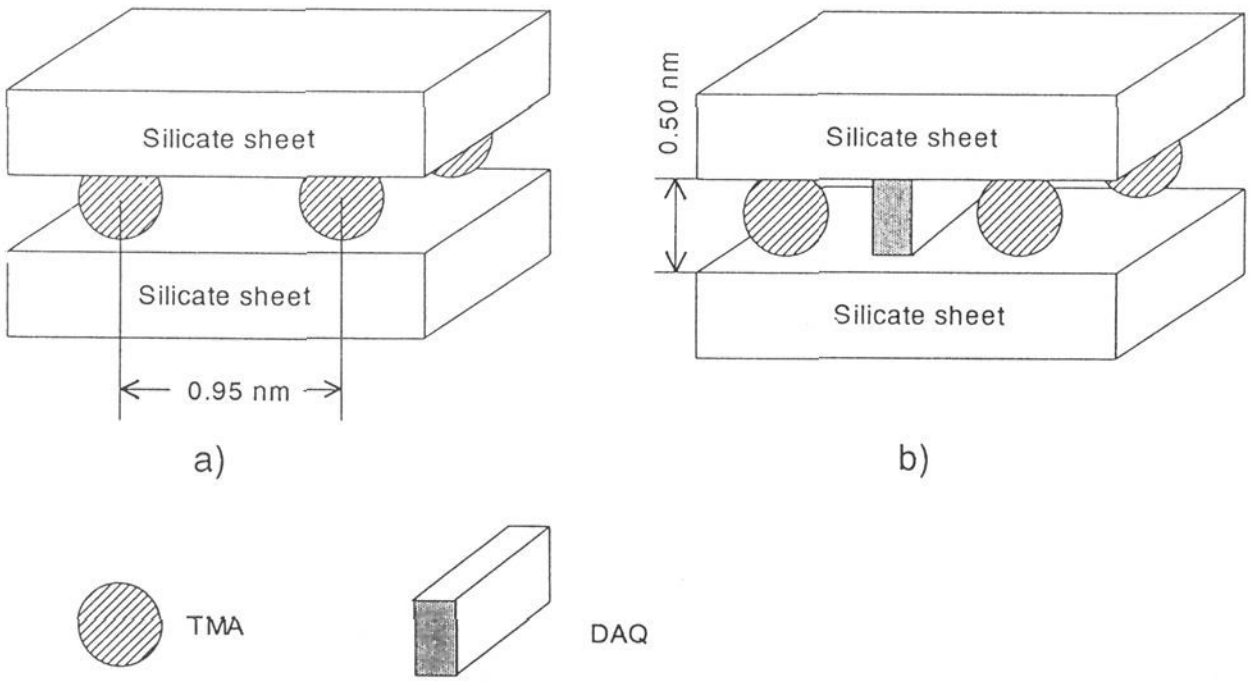

Figure 48. Schematic structures of the (a) the TMA–saponite; (b) the TMA–saponite–DAQ intercalation compound. (Reprinted from ref 302. Copyright 1992 American Chemical Society.)

of appropriate guest species. To be a molecularly dispersed system is another basic prerequisite for composing efficient PHB materials to avoid line broadening due to energy transfer. For this purpose, saponite was modified by pillaring with TMA ions to obtain independent micropores in which DAQ molecules were incorporated at a monomolecular level without aggregation. The TMA–saponite can be processed into transparent thin films by casting an aqueous suspension of the TMA–saponite on solid substrate.[305]

The schematic structure of the TMA–saponite is shown in Figure 48a. The basal spacing of the TMA–saponite was 1.43 nm, indicating that the TMA-pillared interlayer spacing was 0.47 nm. The TMA–saponite was treated with an acetone solution of DAQ, so that a TMA–saponite–DAQ intercalation compound was obtained. By taking into account the molecular size and shape of DAQ and the geometry of the micropore of TMA–saponite, DAQ was intercalated into the interlayer site of the TMA–saponite with the molecular plane nearly perpendicular to the silicate sheet (Figure 48b).

A persistent spectral zero-phonon hole was obtained at liquid helium temperatures by Kr^+ laser light irradiation (520.8 nm). Figure 49 presents a typical example of the spectra of persistent holes. In spite of the high concentration of DAQ (ca. 1.5 mol kg^{-1}), a narrow hole with the initial width of 0.25 cm^{-1} (4.6 K) was obtained. The observed initial width was apparently narrower, if compared with those (e.g. 0.4–0.8 cm^{-1}) of DAQ doped in ordinary polymers and organic glasses (e.g. PMMA, ethanol/methanol mixed glass) obtained under similar experimental conditions. We consider the associated width to be related mainly to the dephasing, but the contribution from the spectral diffusion cannot be neglected. On the other hand, a broad *pseudo*-phonon sidehole, the peak position of which is indicated by an arrow in Figure 49 and whose shift from the zero-phonon hole is 25 cm^{-1}, seems to appear only after an irradiation larger than 1500 mJ cm^{-2}. In Table 7, hole width, homogeneous width $\Delta\omega_i$, and burning efficiency obtained for 520 nm band are summarized.

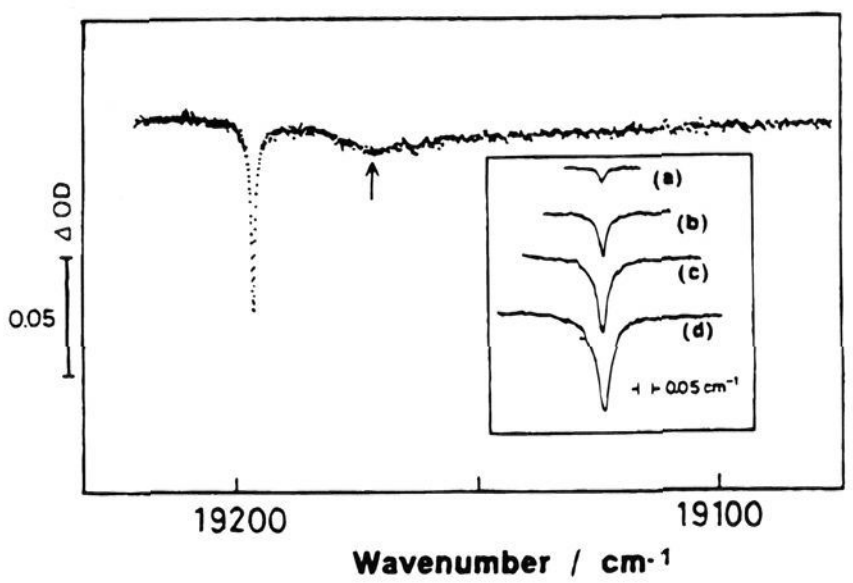

Figure 49. Zero-phonon hole and *pseudo*-phonon side hole (arrow) burned at 4.6 K by laser light (520.8 nm) irradiation. Insert: Temporal evolution of zero-phonon hole at initial stage of burning. (Reprinted from ref 302. Copyright 1992 American Chemical Society.)

Table 7. Hole Width, Inhomogeneous Width, and Burning Yield Obtained for the 520 nm Band of the TMA–Saponite–DAQ System for Wet and Dried Conditions, respectively (Reprinted from Ref 302. Copyright 1994 American Chemical Sociey)

sample	Γ_h (cm^{-1})[a]	$\Delta\omega_i$ (cm^{-1})[b]	Φ[c]	λ_B (nm)[d]	comment[e]
wet	0.25	930	8.3×10^{-4}	520.8	1.3 mJ/cm^2 1.4%
dry	0.38	940	4.5×10^{-4}	520.8	1.3 mJ/cm^2 0.5%
wet	1.38	1040	8.4×10^{-5}	547	1.5 mJ/cm^2 0.2%

[a] Γ_h, holewidth. [b] $\Delta\omega_i$, inhomogeneous width. [c] Φ, burning yield. [d] λ_B, burning wavelength. [e] Comment, the laser fluence and relative hole depth where the parameters are determined. Burning was carried out at 4.6 K.

The burning efficiency is about 8.3×10^{-4} at the initial stage of burning, estimated from the temporal evolution of the area of zero-phonon hole. This value is almost similar to or seems even higher than the typical one, 1×10^{-4}, observed in ordinary dispersed cases. By taking into account the high concentration of DAQ (ca. 0.15 mol kg^{-1} corresponding to ca. 3 mol L^{-1}) in the present system, no distinct decrease in the yield also supports the monomolecular dispersion

of DAQ within the interlayer spacing of saponite. This property is most noteworthy from the viewpoint of the fabrication of recording media, because the ability for such high dopant concentration is desirable in preparing materials in thin films. At such high concentrations, the broadening of holes and the decrease in the burning efficiency are usually inevitable in amorphous matrices prepared with conventional procedures.

We assume that the geometry of the microporous structure in the TMA–saponite intercalation compound contributes some desirable characteristics in hole formation although it is still not absolute improvement: relatively narrow zero-phonon hole compared to those in other polar and proton-accepting amorphous matrices, performance of high concentration of the PHB centers without decrease of yield, and so on.

It should be noted here that the product can be formed in a thin film by casting from an aqueous suspension. The swelling property of saponite[45] remained to some extent even after the intercalation of TMA, so that a self-supporting film was formed. The X-ray powder diffraction pattern of the film showed intensified $d(001)$ diffractions, suggesting clay particles were piled up with their ab planes parallel to the substrate. This ability to form films as an assembly of planarly oriented particles is worth noting because other porous materials such as zeolites cannot form oriented thin films by such a simple treatment.

The photochemical hole burning of cationic porphine–saponite intercalation compounds has been reported.[204] 5,10,15,20-Tetrakis(4-(*N*,*N*,*N*-trimethylammonio)phenyl)porphine tetra(*p*-toluenesulfonate) and 5,10,15,20-tetra(4-*N*-methylpyridinium) porphyrin tetraiodide were used as guest species. The intercalation of the porphines into saponite was carried out by the conventional ion exchange method. The X-ray diffraction patterns of the products showed that the porphine lay in their molecular plane parallel to the silicate layer. A photochemical hole could be burned up to at least 50 K and its half-width at this temperature was 3.7 cm^{-1}, which was fairly small compared with that of the ionic porphine–poly(vinyl alcohol) system. The amount of irreversible broadening of the hole under temperature cycle is smaller in these compounds than in a typical neutral porphine–polymer system, TPP–polymethylmethacrylate. The small irreversible broadening has been presumed to be brought about by the fact that the cationic porphins are rigidly fixed in the anionic interlayer space of saponite.

These results indicate that the modification of microscopic reaction field of PHB using layered materials is one promising way for optimizing the PHB materials. Studies on the effects of the microscopic structures on the properties of the adsorbed species using some pillared layered materials are now underway in our laboratory. Since the characteristics of the PHB reactions are very sensitive to the host–guest systems, systematic studies would provide indispensable information on the nature of the host–guest systems and also the mechanisms of the reactions.

F. Nonlinear Optics

Nonlinear optics comprises the interaction of light with matter to produce a new light field that is different in wavelength or phase.[306,307] Examples of nonlinear optical phenomena are the ability to alter the frequency (or wavelength) of light and to amplify one source of light with another, switch it, or alter its transmission characteristics throughout the medium, depending on its intensity. Since nonlinear optical processes provide key functions for photonics, recent activity in many laboratories has been directed toward understanding and enhancing second- and third-order nonlinear optical effects.

Second-harmonic generation (SHG) is a nonlinear optical process that converts an input optical wave into an outwave of twice the input frequency. Recent studies have revealed large molecular hyperpolarizabilities β of certain organic materials, leading to anomalously large optical nonlinearities relative to those of more conventional inorganic substances. Major research efforts are directed toward (a) identifying new molecules possessing large nonlinear polarizability and (b) controlling molecular orientation on a microscopic level. For purpose b, intercalation compounds have potential applicability because intercalated organic species can take unique arrangements in the interlayer space to lead to the nonlinear effects.

In order to create self-assembled aggregates of molecules that possess the noncentrosymmetry required for materials to show SHG, Langmuir–Blodgett films of host–guest complexes have been investigated. The SHG of *p*-nitroaniline organized in aluminophosphate molecular sieves (ALPO),[29] β-cyclodextrin,[308] thiourea,[309] and so on has been reported. (*p*-Nitroaniline possesses high hyperpolarizability but crystallizes in a centrosymmetric manner so that it cannot show any SHG.) Among them, crystalline inorganic materials are expected to provide stable complexes.

Compared with other host–guest systems utilized for the preparation of SHG-active compounds, layered materials have advantages such as a variation of compounds, stability, etc. On this basis, Cooper et al. have prepared intercalation compounds which exhibit SHG by the intercalation of 4-nitrohippuric acid ($NO_2C_6H_4CONHCH_2COOH$), which does not exhibit second-harmonic generation due to packing effect, into a layered lithium aluminate ($LiAl_2(OH)_6^+$).[310] (Lithium aluminate is a LDH consisting of layers of Li and Al surrounded by hydroxyl groups and the positive charge on the layer is neutralized by exchangeable anions.) From the observed basal spacing of the product (the interlayer distance was 18 Å), the guest species are thought to be stacked perpendicular to the host layer (Figure 50). It has been proposed that the 4-nitrohippuric acid molecules are held in the interlayers as carboxylic acid and the process is not by an ion-exchange process. The orientation of the 4-nitrohippuric acid molecules in the interlayers leads to an ordered arrangement of dipoles, and the material exhibits frequency-doubling

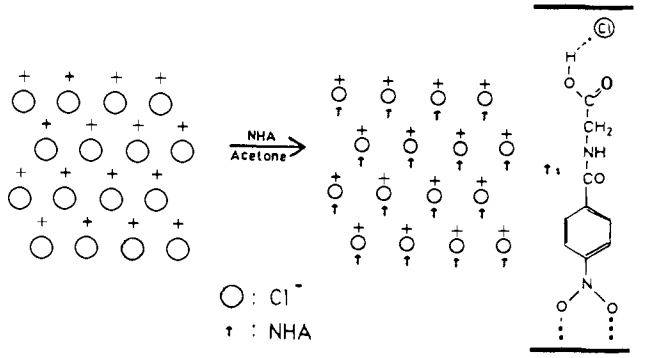

Figure 50. Schematic structure of 4-nitrohippuric acid–lithiumaluminate intercalation compound. (Reprinted from 310. Copyright 1990 American Chemical Society.)

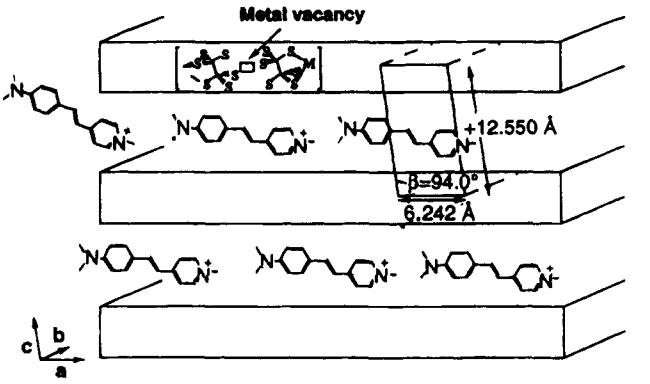

Figure 51. Model for spontaneous poling achieved by the intercalation process. (Reprinted from ref 313. Copyright 1994 American Association for the Advancement of Science.)

characteristics, generating 532 nm radiation from incident 1064 nm.

Crystals of bis(4-nitropyridine *N*-oxide)cadmium chloride and bis(4-nitropyridine *N*-oxide)cadmium iodide dihydrate have been synthesized by evaporating a solution containing purified 4-nitropyridine *N*-oxide and appropriate cadmium salts.[311] The cadmium chloride complex exhibits a second-harmonic generation signal of the same magnitude as that of $KTiOPO_4$(KTP), which is a typical inorganic SHG material. The difference in SHG activity has been ascribed to the different crystal structures. In bis(4-nitropyridine *N*-oxide)cadmium chloride complex, Cd–O bonds are short enough to cause the extension of π molecular orbital of the guest molecules to the inorganic moiety, inducing a new nonlinear entity. However, the relatively long Cd–O bonds in bis(4-nitropyridine *N*-oxide)cadmium iodide dihydrate prevent effective extension of the π molecular orbital. Thus, it has been proved that the strategy of crystal engineering using host–guest complexation is a way to build a polymeric inorganic–organic network with extended π molecular orbital of the guest species to the host besides the aligning dipoles.

Lacroix et al. have reported the intercalation of 4-[2-[4-(dimethylamino)phenyl]ethenyl]-1-methylpyridinium ($DAMS^+$) into MPS_3, where M is either Mn^{2+} or Cd^{2+}, by an ion exchange process.[312,313] In their first report on this system, they used a potassium intercalate, which was obtained by treating $CdPS_3$ with a large excess of an aqueous solution containing KCl and EDTA at pH ca. 10 fixed by a Na_2CO_3–$NaHCO_3$ buffer, as an intermediate. Subsequent treatment of the $Cd_{1-x}PS_3(K)_{2x}(H_2O)_y$ with a solution of $DAMS^+$ in 1:1 EtOH–H_2O mixture at 70 °C resulted in the insertion of $DAMS^+$. The resulting intercalation compounds gave a small SHG response on the order of that of urea.[312]

Since $DAMS^+$ chromophore can be 10^3 times more efficient than urea, the observed poor SHG signals were thought to originate from grain surface effects, and the low crystallinity of the intercalation compounds might be involved. On this basis, Lacroix et al. continued the study of this system by optimizing the intercalation process, and they then obtained two intercalation compounds ($Cd_{0.86}PS_3(DAMS)_{0.28}$ and $Mn_{0.86}PS_3(DAMS)_{0.28}$) which exhibited a significantly large SHG activity.[313] This was obtained by direct reaction between MPS_3 powder and an ethanolic solution of DAMS iodide at 130 °C in the presence of pyridinium chloride. In this reaction, pyridinium chloride played a role in generating *in situ* an intermediate pyridinium intercalated compound that underwent rapid exchange with the $DAMS^+$. Although infrared spectroscopy and X-ray diffraction showed that these compounds were structurally similar irrespective of the reaction conditions, the compounds obtained by the direct reaction were much better crystallized and did not contain residual solvents. It should be noted that the minor changes had a dramatic influence on the NLO properties.

In this case, a 1.34 μm laser was used to ensure the transparency of the samples at double frequency. (The wavelength of the maximum absorption was 0.58 μm.) $Mn_{0.86}PS_3(DAMS)_{0.28}$ exhibited an efficiency of 300 times that of urea, and the $Cd_{0.86}PS_3(DAMS)_{0.28}$ reached 750 times the efficiency of urea. Additionally, no significant decay of the NLO signal over a period of several months was observed, which is a crucial point in the search for new SHG materials based on organic NLO chromophore. The high intensity of SHG excluded the possibility of surface effects proposed in their first report and indicated that the NLO chromophore was spontaneously well aligned between the interlayer spaces. They proposed a schematic structure for the intercalation compounds based on the observed basal spacing of 12.4 Å and host–guest ratio (Figure 51). It should be noted that the intercalation did not cause significant dilution of the chromophore. There was one DAMS species in 525 Å^3 of the tosylate salt while one DAMS in 740 Å^3 of the intercalation compounds. This ability to incorporate guest species at such high concentration is one of the most attractive features of the intercalation process.

Besides the observed large value of the SHG signal, it is important to note that the SHG signal is significantly different depending on the method for preparing the compounds. (The direct reaction leads to intercalation compounds with a large SHG signal, while the SHG signal is relatively low for the compounds prepared using potassium exchanged form as an intermediate.) This difference indicates that the properties of the intercalation compounds can be significantly affected by the difference in the composition, etc.

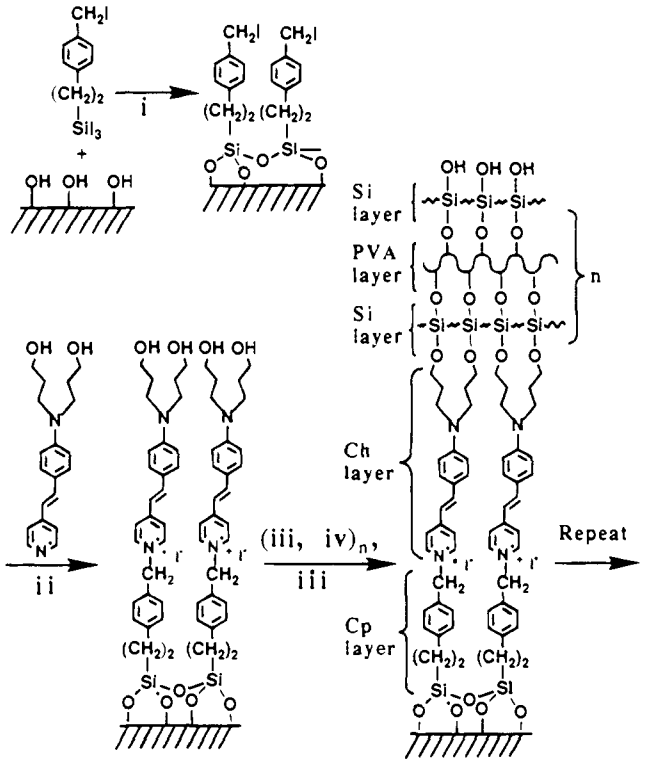

Figure 52. Schematic representation of self-assembled multilayer formation. (Reprinted from ref 315. Copyright 1990 American Chemical Society.)

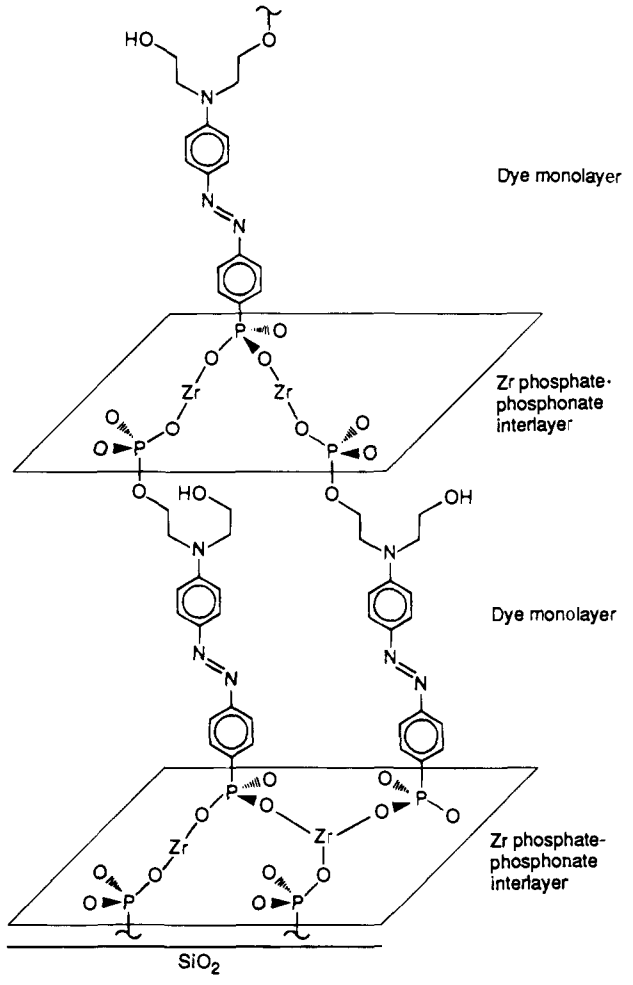

Figure 53. Idealized schematic structure of dye multilayer film based on known structure of $Zr(HOPO_3)$ and related organic Zr phosphonate salts, which feature Zr(IV) in pseudooctahedral sites between opposed hexagonal layers of phosphate or phosphonate. (Reprinted from ref 316. Copyright 1991 American Association for the Advancement of Science.)

The intercalation compounds mentioned above have been obtained as powders and the measurements of SHG intensity have been carried out by the Kurtz–Perry powder technique.[314] For the detailed characterization of optical properties of the host–guest systems as well as their practical applications as photonics devices, such materials must be available as single crystals or thin films. One of the possible resolutions for the problem is self-assembled multilayers grown on substrates. Organosilicon-derived material[315] (Figure 52) and zirconium phosphonate-derived materials[316] (Figure 53) are two typical examples. Although they are not intercalation compounds, their structures are composed of alternating inorganic and organic layers similar to intercalation compounds. Compared with the Langmuir–Blodgett film which is studied most extensively in this research field, the inorganic–organic composite systems show better stability. Therefore, they show promise for the future application of photonic materials.

To align dipoles of NLO chromophore in isotropic media such as organic polymers[317] and sol–gel derived xerogels[318] by applying an external electric field is another approach for SHG materials. Recently, "electric-field-assisted chemical vapor deposition" has been reported to prepare polyazomethine head-to-tail conjugated polymers with SHG.[319] Although excellent optical qualities have been achieved for these systems, the noncentrosymmetric alignments of the dipoles induced by an external electric field tend to randomize due to the structural relaxation of polymers. In order to overcome this limitation, we have developed a technique to prepare a novel inorganic–organic nanocomposite film, tetramethylammonium-(TMA)–saponite–*p*-nitroaniline (*p*-NA) intercalation compound.[320] The compound was prepared by a solid–gas reaction between a TMA–saponite film and *p*-NA vapor. In order to align *p*-NA dipoles in the TMA–saponite, an external electric field was applied to the host during the intercalation of *p*-NA. The TMA–saponite–*p*-NA intercalation compound prepared under an electric field exhibited SHG, while no SHG was observed for the compound prepared without an electric field. This indicates that the applied electric field caused a noncentrosymmetric alignment of the *p*-NA in the interlayer micropore of the TMA–saponite. The proposed alignment of *p*-NA dipoles in the TMA–saponite is schematically shown in Figure 54. As mentioned earlier (section IV.E), the TMA–saponite film is composed of oriented particles of TMA–saponite with their *ab* plane parallel to the substrate in which microscopic anisotropy can be directly converted into a macroscopic one. Moreover, the film shows transparency in the visible region and possesses micropores in the interlayer space. Because of the matching between the size and geometry of the micropore of the TMA–saponite and those of *p*-NA molecules, the incorporation into the TMA–saponite is a novel way to create self-as-

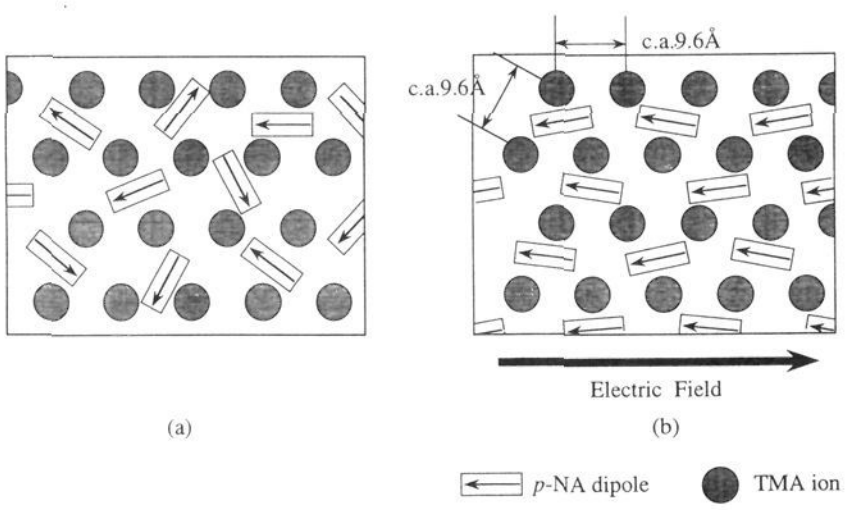

Figure 54. Schematic structure of the TMA–saponite–*p*-nitroaniline intercalation compounds (a) without and (b) with and electric field during intercalation. (Reprinted from ref 320. Copyright 1994 American Chemical Society.)

sembled aggregates of *p*-NA with noncentrosymmetry.

There are some candidates for third-order nonlinear optical materials in intercalation compounds. It seems to us that the semiconductor particles doped in layered materials and conjugated polymer intercalated layered materials are possible candidates for NLO materials. As mentioned in section IV.A, the confinement of quantum particles in the interlayer space of layered materials is not satisfactory. More effort to confine the quantum particles with narrower size distribution and to process them into films with better optical quality should be made for the optical studies. On the other hand, conjugated polymers have emerged as an important class of third-order nonlinear optical materials. However, these polymers in the film are optically loose. Their complexation into transparent solids may result in the formation of transparent composite materials. The preparation of conjugated polymers in the interlayer spaces of layered materials has been studied extensively. The optical investigation on these systems may lead to a novel class of materials with important NLO properties.

Semiconducting layered materials such as perovskite-type heavy atom halides are promising NLO materials due to their "natural quantum well" structure and the processability into oriented polycrystalline films.[75–81] The change in the optical and electronic properties upon intercalation of organic species has been investigated. It has been reported that the luminescence properties of $K_2Ti_3O_7$ were affected by the interlayer conditions.[283] Therefore, systematic studies on the optical properties of layered semiconductors such as transition metal oxides and chalcogenides upon intercalation seem to be of both fundamental and practical importance.

V. Conclusion

Studies of the organization of photoactive species on layered solids have been reviewed. The spectroscopic properties of adsorbed photoactive species have been utilized to probe surface properties as well as host–guest interactions, in the process, some indispensable information has been revealed:

(1) Host–guest interactions such as electrostatic interactions as well as guest–guest interactions such as hydrophobic ones, are important factors which determine the adsorption states of guest species.

(2) The charge density of the host layers and the size of the guest species significantly affect the orientation of the guest species.

(3) Appropriate coadsorbates such as surfactants and organic solvents can alter the aggregation of photoactive species, which originate from the guest–guest interactions.

(4) Energy/electron transfer can occur between hosts and guests.

In order to dominate the properties of intercalation compounds, host–guest interactions as well as guest–guest interactions should be precisely controlled. For this purpose, the adsorbed states of photoactive species on layered solids have successfully been changed by cointercalation of photoinactive species. Expandability of the interlayer spaces is indispensable for microscopic modifications. By this method as well as by selecting both hosts and guests, one can obtain a large variety of molecular designed host–guest systems. However, the states of adsorbed guest species such as rotation and diffusion in the interlayer spaces, and changes in the properties of hosts (mainly for conducting host materials) upon intercalation of guest species are still unclear. Further systematic studies on structure–property relationships are necessary in order to clarify them.

The properties of the intercalation compounds can be affected by a small difference in microscopic structures. For example, the SHG activity of stilbazolium–MPS_3 intercalation compounds is significantly different depending on small differences in the preparation procedure.[312,313] Another example is the effect of hydration state on the hole formation characteristics in the PHB reactions of the TMA–saponite–DAQ intercalation compound.[302] Thus, one should be very careful in preparing and characterizing photofunctional intercalation compounds to obtain reproducible results.

Although further systematic studies should be carried out, some of the observed properties can be applicable as photofunctional materials. For practical applications and further evaluations of the photofunctions, their processing into thin films or single crystals with high optical quality is necessary.[321] Developments in the synthesis of novel intercalation compounds as well as layered host materials are also very important.

References

(1) *Photochemistry in Organized & Constrained Media*; Ramamurthy, V., Ed.; VCH Publishers, Inc.: New York, 1991.
(2) *Photochemistry on Solid Surfaces*; Anpo, M., Matsuura, T., Eds.; Studies in surface science and catalysis 47; Elsevier: Amsterdam, *1989*.
(3) *Molecular Dynamics in Restricted Geometries*; Klafter, J., Drake, J. M., Eds.; Wiley Interscience: New York, 1989.
(4) Thomas, J. K. *The Chemistry of Excitation at Interfaces*; ACS Monograph 181; American Chemical Society: Washington, 1984.
(5) Thomas, J. K. *Chem. Rev.* **1980**, *80*, 283.
(6) Thomas, J. K. *J. Phys. Chem.* **1987**, *91*, 267.
(7) Thomas, J. K. *Chem. Rev.* **1993**, *93*, 301.
(8) Thomas, J. K. *Acc. Chem. Res.* **1988**, *21*, 275.
(9) Turro, N. J.; Grätzel, M.; Braun, A. M. *Angew. Chem., Int. Ed. Engl.* **1980**, *19*, 675.
(10) Ramamurthy, V. *Tetrahedron* **1986**, *42*, 5753.
(11) Eaton, D. F. In *Advances in the Synthesis and Reactivity of Solids*; Mallouk, T. M., Ed.; JAI Press: London, 1991; Vol. 1, p 81.

(12) Stucky, G. D. *Prog. Inorg. Chem.* **1992**, *40*, 99.
(13) Ozin, J. A. *Adv. Mater.* **1992**, *4*, 612.
(14) Stucky, G. D.; MacDougall, J. E. *Science* **1990**, *247*, 669.
(15) Ulman, A. *An Introduction to Ultrathin Organic Films*; Academic Press: San Diego, 1992.
(16) Ramamurthy, V.; Weiss, R. G.; Hammond, G. S. *Adv. Photochem.* **1993**, *18*, 67.
(17) Fendler, J. H. *Membrane-Mimetic Approach to Advanced Materials*; Springer-Verlag: Berlin, 1994.
(18) Smets, G. *Adv. Polym. Sci.* **1983**, *50*, 18.
(19) *Sol-Gel Optics: Processing and Application*; Klein, L. C., Ed.; Kluwer: Boston, 1993.
(20) O'Hare, D. *Inorganic Materials*; Bruce, D. W., O'Hare, D., Eds.; Wiley Interscience: Chichester, 1992; Chapter 4.
(21) *Intercalation Chemistry*; Whittingham, M. S., Jacobson, A. J., Eds.; Academic Press: New York, 1982.
(22) Barrer, R. M. *Zeolites and Clay Minerals as Sorbents and Molecular Sieves*; Academic Press: London, 1978.
(23) Suib, S. L. *Chem. Rev.* **1993**, *93*, 803.
(24) Ramamurthy, V. In *Photochemistry in Organized & Constrained Media*; Ramamurthy, V., Ed.; VCH Publishers, Inc.: New York, 1991; Chapter 10.
(25) Ozin, G. A.; Özkar, S. *Adv. Mater.* **1992**, *4*, 11.
(26) Ozin, G. A.; Kuperman, A.; Stein, A. *Angew. Chem., Int. Ed. Engl.* **1989**, *28*, 359.
(27) Yoon, K. B. *Chem. Rev.* **1993**, *93*, 321.
(28) See for example: Bein, T.; Enzel, P. *Angew. Chem., Int. Ed. Engl.* **1989**, *28*, 1692.
(29) Cox, S. D.; Gier, T. E.; Stucky, G. D.; Bierlein, J. *J. Am. Chem. Soc.* **1988**, *110*, 2986. Cox, S. D.; Gier, T. E.; Stucky, G. D. *Chem. Mater.* **1990**, *2*, 609.
(30) Feng, S.; Bein, T. *Nature* **1994**, *368*, 834.
(31) Barrer, R. M. *Hydrothermal Chemistry of Zeolites*; Academic Press: London, 1982.
(32) Kresge, C. T.; Leonowicz, M. E.; Roth, W. J.; Vartuli, J. C.; Beck, J. S. *Nature* **1992**, *359*, 710. Beck, J. S.; Vartuli, J. C.; Roth, W. L.; Leonowicz, M. E.; Kresge, C. T.; Schmidt, K. D.; Chu, C. T.-W.; Olson, D. H.; Sheppard, E. W.; McCullen, S. B.; Higgins, J. B.; Schlenker, J. L. *J. Am. Chem. Soc.* **1992**, *114*, 10834.
(33) Monnier, A.; Schüth, F.; Huo, Q.; Kumar, D.; Margolese, D.; Maxwell, R. S.; Stucky, G. D.; Krishnamurthy, M.; Petroff, P.; Firouzi, A.; Janicke, M.; Chmelka, B. F. *Science* **1993**, *261*, 1299.
(34) Huo, Q.; Margolese, D. I.; Ciesla, U.; Feng, P.; Gier, T. E.; Sieger, P.; Leon, R.; Petroff, P. M.; Schüth, F.; Stucky, G. D. *Nature* **1994**, *368*, 317.
(35) Tanev, P. T.; Chibwe, M.; Pinnavaia, T. J. *Nature* **1994**, *368*, 321.
(36) Yanagisawa, T.; Shimizu, T.; Kuroda, K.; Kato, C. *Bull. Chem. Soc. Jpn.* **1990**, *63*, 988.
(37) Jones, W. In *Photochemistry in Organized & Constrained Media*; Ramamurthy, V., Ed.; VCH Publishers, Inc.: New York, 1991; Chapter 9.
(38) Pinnavaia, T. J. *Science* **1983**, *220*, 4595.
(39) Johnson, J. W.; Jacobson, A. J.; Butler, W. M.; Rosenthal, S. E.; Brody, J. F.; Lewandowsky, J. T. *J. Am. Chem. Soc.* **1989**, *111*, 381. Cao, G.; Mallouk, T. E. *Inorg. Chem.* **1991**, *30*, 1434.
(40) Clearfield, A. *Chem. Rev.* **1988**, *88*, 125.
(41) Ruiz-Hitzky, E. *Adv. Mater.* **1993**, *5*, 334.
(42) Fitch, A. *Clays Clay Miner.* **1990**, *38*, 391.
(43) Grim, R. E. *Clay Mineralogy*; McGraw-Hill: New York, 1953.
(44) Theng, B. K. G. *The Chemistry of Clay-Organic Reactions*; Adam Hilger: London, 1974.
(45) Van Olphen, H. *An Introduction to Clay Colloid Chemistry*, 2nd ed.; Wiley-Interscience: New York, 1977.
(46) Ogawa, M.; Kuroda, K.; Kato, C. *Chem. Lett.* **1989**, 1659. Ogawa, M.; Kato, K.; Kuroda, K.; Kato, C. *Clay Sci.* **1990**, *8*, 31. Ogawa, M.; Nagafusa, Y.; Kuroda, K.; Kato, C. *Appl. Clay Sci.* **1992**, *7*, 291. Ogawa, M.; Hirata, T.; Kuroda, K.; Kato, C. *Chem. Lett.* **1992**, 365. Ogawa, M.; Handa, T.; Kuroda, K.; Kato, C. *Chem. Lett.* **1990**, 71.
(47) Ogawa, M.; Hashizume, T.; Kuroda, K.; Kato, C. *Inorg. Chem.* **1991**, *30*, 584.
(48) Ogawa, M.; Fujii, K.; Kuroda, K.; Kato, C. *Mater. Res. Soc. Symp. Proc.* **1991**, *233*, 89.
(49) Ogawa, M.; Shirai, H.; Kuroda, K.; Kato, C. *Clays Clay Miner.* **1992**, *40*, 485.
(50) Doner, H. E.; Mortland, M. M. *Science* **1969**, *66*, 1406.
(51) Boyd, S. A.; Mortland, M. M. *Nature* **1985**, *316*, 532.
(52) Soma, Y.; Soma, M.; Harada, I. *Chem. Phys. Lett.* **1983**, *94*, 475; **1994**, *99*, 153.
(53) Soma, Y.; Soma, M.; Harada, I. *J. Phys. Chem.* **1984**, *88*, 3034; **1985**, *89*, 738.
(54) Moreale, A.; Cloos, P.; Badot, C. *Clay Miner.* **1985**, *20*, 29.
(55) Soma, M.; Soma, Y. *Chem. Lett.* **1988**, 405.
(56) Thompson, D. W.; Butterworth, J. T. *J. Colloid Interface Sci.* **1992**, *151*, 236.
(57) Kitajima, K.; Daimon, N. *Nippon Kagaku Kaishi* **1974**, 685; **1975**, 991; **1976**, 597. Soma, M.; Tanaka, A.; Seyama, H.; Hayashi, S.; Hayamizu, K. *Clay Sci.* **1990**, *8*, 1.
(58) Alberti, G.; Constantino, U. In *Intercalation Chemistry*; Whittingham, M. S., Jacobson, A. J., Eds.; Academic Press: New York, 1982; Chapter 5.
(59) Alberti, G. *Acc. Chem. Res.* **1978**, *11*, 163.
(60) For example: Bujoli, B.; Pena, O.; Pavadeau, P.; Bideau, J. L.; Payne, C.; Rouxel, J. *Chem. Mater.* **1993**, *5*, 583.
(61) Cao, G.; Hong, H.-G.; Mallouk, T. E. *Acc. Chem. Res.* **1992**, *25*, 420.
(62) Lee, H.; Kepley, L. J.; Hong, H.-G.; Mallouk, T. E. *J. Am. Chem. Soc.* **1988**, *110*, 618. Lee, H.; Kepley, L. J.; Hong, H.-G.; Akhter, S.; Mallouk, T. E. *J. Phys. Chem.* **1988**, *92*, 2597.
(63) Raveau, B. *Rev. Inorg. Chem.* **1987**, *9*, 37.
(64) Izawa, H.; Kikkawa, S.; Koizumi, M. *Polyhedron* **1983**, *2*, 741.
(65) Verbaere, A.; Tournoux, M. *Bull. Soc. Chem. Fr.* **1973**, *4*, 1237.
(66) Kinomura, N.; Kumada, N.; Muto, F. *J. Chem. Soc., Dalton Trans.* **1985**, 2349.
(67) Lagaly, G.; Beneke, K. *J. Inorg. Nucl. Chem.* **1976**, *38*, 1513.
(68) Gasperin, M.; Bihan, M. T. Le *J. Solid State Chem.* **1980**, *33*, 83.
(69) Nakato, T.; Sakamoto, D.; Kuroda, K.; Kato, C. *Bull. Chem. Soc. Jpn.* **1992**, *65*, 322.
(70) Johnson, J. W. In *Intercalation Chemistry*; Whittingham, M. S., Jacobson, A. J., Eds.; Academic Press: New York, 1982; Chapter 8.
(71) Brec, R. *Solid State Ionics* **1986**, *22*, 3.
(72) Rouxel, J.; Brec, R. *Annu. Rev. Mater. Sci.* **1986**, *16*, 137.
(73) Clement, R.; Garnier, O.; Jegoudez, J. *Inorg. Chem.* **1986**, *25*, 1404.
(74) Kind, R. *Ber. Bunsen-Ges. Phys. Chem.* **1983**, *87*, 248.
(75) Carabrese, J.; Jones, N. L.; Harlow, R. L.; Herron, N.; Thorn, D. L.; Wang, Y. *J. Am. Chem. Soc.* **1991**, *113*, 2328.
(76) Dolzhenko, Y. I.; Inabe, T.; Maruyama, Y. *Bull. Chem. Soc. Jpn.* **1986**, *59*, 563.
(77) Ishihara, T.; Takahashi, J.; Goto, T. *Solid State Commun.* **1989**, *69*, 933.
(78) Ishihara, T.; Takahashi, J.; Goto, T. *Phys. Rev. B* **1990**, *42*, 11099.
(79) Al-Jishi, R.; Coleman, C. C.; Treece, R.; Goldwhite, H. *Phys. Rev. B* **1989**, *39*, 4862.
(80) Mehrota, V.; Lombarado, S.; Thompson, M. O.; Giannelis, E. P. *Phys. Rev. B* **1991**, *44*, 5786.
(81) Mitzi, D. B.; Feild, C. A.; Harrison, W. T. A.; Guloy, A. M. *Nature* **1994**, *369*, 467.
(82) Reichle, W. T. *CHEMTECH* **1986**, Jan, 58.
(83) Taylor, R. M. *Clay Miner.* **1984**, *19*, 591.
(84) Park, I. Y.; Kuroda, K.; Kato, C. *J. Chem. Soc., Dalton Trans.* **1990**, 3071.
(85) Chibwe, M.; Pinnavaia, T. J. *J. Chem. Soc., Chem. Commun.* **1993**, 278.
(86) O'Hare, D. *Chem. Soc. Rev.* **1992**, 121.
(87) Kim, R. M.; Pillion, J. E.; Burwell, D. A.; Groves, J. T.; Thompson, M. E. *Inorg. Chem.* **1993**, *32*, 4509.
(88) Lagaly, G. *Clay Miner.* **1981**, *16*, 1.
(89) Lagaly, G. *Solid State Ionics* **1986**, *22*, 43.
(90) Lagaly, G.; Beneke, K. *Colloid Polym. Sci.* **1991**, *269*, 1198.
(91) Clint, J. H. *Surfactant Aggregation*; Blackie: London, 1992.
(92) Kunitake, T. *Angew. Chem., Int. Ed. Engl.* **1992**, *39*, 709.
(93) Ringsdorf, H.; Schlarb, B.; Venzmer, J. *Angew. Chem., Int. Ed. Engl.* **1988**, *27*, 113.
(94) Jordan, J. W. *J. Phys. Colloid Chem.* **1950**, *54*, 294.
(95) Boyd, S. A.; Lee, J. F.; Mortland, M. M. *Nature* **1988**, *333*, 345. Lee, J. F.; Mortland, M. M.; Boyd, S. A. *J. Chem. Soc., Faraday Trans. 1* **1989**, *85*, 2953. Lee, J. F.; Mortland, M. M.; Chiou, C. T.; Kile, D. E.; Boyd, S. A. *Clays Clay Miner.* **1990**, *38*, 113.
(96) Bondarenko, S. V.; Zhukova, A. I.; Tarasevich, Y. I. *J. Chromatogr.* **1982**, *241*, 281.
(97) Cornelis, A.; Laszlo, P. *Synthesis* **1982**, 162. Rusling, J. F. *Acc. Chem. Res.* **1991**, *24*, 75.
(98) Jones, T. R. *Clay Miner.* **1983**, *18*, 399.
(99) Okahata, Y.; Shimizu, A. *Langmuir* **1989**, *5*, 954.
(100) Theng, B. K. G. *Formation and Properties of Clay-Polymer Complexes*; Elsevier: Amsterdam, 1979.
(101) Aranda, P.; Ruiz-Hitzky, E. *Chem. Mater.* **1992**, *4*, 1395.
(102) Liu, Y.-J.; DeGroot, D. C.; Schindler, J. L.; Kannerwurf, C. R.; Kanatzidis, M. G. *Chem. Mater.* **1991**, *3*, 992. Liu, Y.-J.; DeGroot, D. C.; Schindler, J. L.; Kannerwurf, C. R.; Kanatzidis, M. G. *Adv. Mater.* **1993**, *3*, 369. Bissessur, R.; Kanatzidis, M. G.; Schindler, J. L.; Kannerwurf, C. R. *J. Chem. Soc., Chem. Commun.* **1993**, 1582.
(103) Kyotani, T.; Sonobe, N.; Tomita, A. *Nature* **1988**, *331*, 331.
(104) Sonobe, N.; Kyotani, T.; Tomita, A. *Carbon* **1988**, *26*, 573. Sonobe, N.; Kyotani, T.; Hishiyama, Y.; Shiraishi, M.; Tomita, A. *J. Phys. Chem.* **1988**, *92*, 7029.
(105) Sonobe, N.; Kyotani, T.; Tomita, A. *Carbon* **1990**, *28*, 483.
(106) *Conjugated Polymers*; Brédas, J. L., Silbey, R., Eds.; Kluwer: Dordrecht, 1991.
(107) Inoue, H.; Yoneyama, H. *J. Electroanal. Chem.* **1987**, *233*, 291.
(108) Kanatzidis, M. G.; Tonge, L. M.; Marks, T. J.; Marcy, H. O.; Kannewurf, C. R. *J. Am. Chem. Soc.* **1987**, *109*, 3797. Kanatzidis, M. G.; Wu, C.-G.; Marcy, H. O.; Kannewurf, C. R. *J. Am.*

Chem. Soc. **1989**, *111*, 4139. Kanatzidis, M. G.; Wu, C.-G.; Marcy, H. O.; DeGroot, D. C.; Kannewurf, C. R. *Chem. Mater.* **1990**, *2*, 222. Nazar, L. F.; Zhang, Z.; Zinkweg, D. *J. Am. Chem. Soc.* **1992**, *114*, 6239.
(109) Day, P.; Ledsham, R. D. *Mol. Cryst. Liq. Cryst.* **1982**, *86*, 163. Ledsham, R.; Day, P. *J. Chem. Soc., Chem. Commun.* **1981**, 921.
(110) Cao, G.; Mallouk, T. E. *J. Solid State Chem.* **1991**, *94*, 59.
(111) *Pillared Layered Structure*; Mitchell, I. V., Ed.; Elsevier: London, 1990.
(112) Kalyanasundaram, K. *Photochemistry in Organized & Constrained Media*; Ramamurthy, V., Ed.; VCH Publishers, Inc.: New York, 1991; Chapter 2.
(113) Juris, J.; Balzani, V.; Barigelletti, F.; Campagna, S.; Belser, P.; Von Zelewsky, A. *Coord. Chem. Rev.* **1988**, *84*, 85. Kalyanasundaram, K. *Coord. Chem. Rev.* **1982**, *46*, 159.
(114) Thornton, A. T.; Laurence, G. S. *J. Chem. Soc., Chem. Commun.* **1978**, 408. Lee, P. C.; Meisel, D. *J. Am. Chem. Soc.* **1980**, *102*, 5477. Kurimura, Y.; Nagashima, M.; Takato, K.; Tsuchida, E.; Kaneko, M.; Yamada, A. *J. Phys. Chem.* **1982**, *86*, 2432. Miyashita, T.; Arito, Y.; Matsuda, M. *Macromolecules* **1991**, *24*, 872.
(115) Meisel, D.; Matheson, M. S.; Rabani, J. *J. Am. Chem. Soc.* **1978**, *100*, 117. Kunjappu, J. T.; Somasundaran, P.; Turro, N. J. *J. Phys. Chem.* **1990**, *94*, 8464.
(116) Milosauljevic, B. H.; Thomas, J. K. *Macromolecules* **1984**, *17*, 2244. Milosauljevic, B. H.; Thomas, J. K. *Chem. Phys. Lett.* **1984**, *114*, 133.
(117) Gafney, H. D. *Coord. Chem. Rev.* **1990**, *104*, 113.
(118) Wheeler, J.; Thomas, J. K. *J. Phys. Chem.* **1982**, *86*, 4540.
(119) Kajiwara, T.; Hashimoto, K.; Kawai, T.; Sakata, T. *J. Phys. Chem.* **1982**, *86*, 4516. Willner, I.; Yang, J. M.; Learne, C.; Otvos, J. W.; Calvin, M. *J. Phys. Chem.* **1981**, *85*, 3277. Memming, R. *Surf. Sci.* **1980**, *101*, 551. Perry, J. W.; McQuillan, A. J.; Anson, F. C.; Zewall, A. H. *J. Phys. Chem.* **1983**, *87*, 1480. Hashimoto, K.; Hiramoto, M.; Kajiwara, T.; Sakata, T. *J. Phys. Chem.* **1988**, *92*, 4636. Hashimoto, K.; Hiramoto, M.; Lever, A. B.; Sakata, T. *J. Phys. Chem.* **1988**, *92*, 1016.
(120) Lunsford, J. H. *Rev. Inorg. Chem.* **1987**, *9*, 1. DeWilde, W.; Peeters, G.; Lunsford, J. H. *J. Phys. Chem.* **1980**, *84*, 2306. Quayle, W. H.; Lunsford, J. H. *Inorg. Chem.* **1982**, *21*, 97. Dutta, P. K.; Incavo, J. A. *J. Phys. Chem.* **1987**, *91*, 4443. Incavo, J. A.; Dutta, P. K. *J. Phys. Chem.* **1990**, *94*, 3075. Kim, T. Il.; Mallouk, T. E. *J. Phys. Chem.* **1992**, *96*, 2879.
(121) Traynor, M. F.; Mortland, M. M.; Pinnavaia, T. J. *Clays Clay Miner.* **1978**, *26*, 318.
(122) Ghosh, P. K.; Bard, A. J. *J. Phys. Chem.* **1984**, *88*, 5519.
(123) Habti, A.; Keravis, D.; Levitz, P.; Van Damme, H. *J. Chem. Soc., Faraday Trans. 2* **1984**, *80*, 67.
(124) DellaGuardia, R. A.; Thomas, J. K. *J. Phys. Chem.* **1983**, *87*, 990.
(125) Schoonheydt, R. A.; de Pauw, P.; Vliers, D.; de Schryver, F. C. *J. Phys. Chem.* **1984**, *88*, 5113.
(126) Turro, N. J.; Kumar, C. V.; Grauer, Z.; Barton, J. K. *Langmuir* **1987**, *3*, 1056.
(127) Nakamura, T.; Thomas, J. K. *Langmuir* **1985**, *1*, 567.
(128) Kuykendall, V. G.; Thomas, J. K. *J. Phys. Chem.* **1990**, *94*, 4224.
(129) Krenske, D.; Abdo, S.; Van Damme, H.; Cruz, M.; Fripiat, J. J. *J. Phys. Chem.* **1980**, *84*, 2447.
(130) Abdo, S.; Canesson, P.; Cruz, M.; Fripiat, J. J.; Van Damme, H. *J. Phys. Chem.* **1981**, *85*, 797.
(131) Kuykendall, V. G.; Thomas, J. K. *Langmuir* **1990**, *6*, 1346.
(132) Yamagishi, A. *J. Coord. Chem.* **1987**, *16*, 131. Yamagishi, A.; Soma, M. *J. Am. Chem. Soc.* **1981**, *103*, 4640. Yamagishi, A. *J. Phys. Chem.* **1982**, *86*, 2472. Yamagishi, A.; Soma, M. *J. Chem. Soc., Chem. Commun.* **1981**, 539.
(133) Joshi, V.; Kotkar, D.; Ghosh, P. K. *J. Am. Chem. Soc.* **1986**, *108*, 4650. Kamat, P. V.; Gopidas, K. R.; Mukherjee, T.; Joshi, V.; Kotkar, D.; Pathak, V. S.; Ghosh, P. K. *J. Phys. Chem.* **1991**, *95*, 10009.
(134) Joshi, V.; Ghosh, P. K. *J. Am. Chem. Soc.* **1989**, *111*, 5604.
(135) Joshi, V.; Ghosh, P. K. *J. Chem. Soc., Chem. Commun.* **1987**, 789.
(136) Joshi, V.; Kotkar, D.; Ghosh, P. K. *Curr. Sci.* **1988**, *57*, 567.
(137) Yeates, R. C.; Kuznicki, S. M.; Lloyd, L. B.; Eyring, E. M. *J. Inorg. Nucl. Chem.* **1981**, *43*, 2355.
(138) Vliers, D. P.; Schoonheydt, R. A.; de Schrijver, F. C. *J. Chem. Soc., Faraday Trans. 1* **1985**, *81*, 2009.
(139) Vliers, D. P.; Collin, D.; Schoonheydt, R. A.; de Schryver, F. C. *Langmuir* **1986**, *2*, 165.
(140) Colón, J. L.; Yang, C.-Y.; Clearfield, A.; Martin, C. R. *J. Phys. Chem.* **1988**, *92*, 5777.
(141) Colón, J. L.; Yang, C.-Y.; Clearfield, A.; Martin, C. R. *J. Phys. Chem.* **1990**, *94*, 874.
(142) Giannelis, E. P.; Nocera, D. G.; Pinnavaia, T. J. *Inorg. Chem.* **1987**, *26*, 203.
(143) Clement, R. *J. Am. Chem. Soc.* **1981**, *103*, 6998.
(144) Poizat, O.; Sourisseau, C. *J. Phys. Chem.* **1984**, *88*, 3007.
(145) Birks, J. B. *Photophysics of Aromatic Molecules*; Wiley Interscience: London, 1970.
(146) Nakajima, A. *Bull. Chem. Soc. Jpn.* **1971**, *44*, 3272.
(147) Kalyanasundaram, K.; Thomas, J. K. *J. Am. Chem. Soc.* **1977**, *99*, 2039.
(148) Cao, T.; Munk, P.; Ramireddy, C.; Tuzar, Z.; Webber, S. E. *Macromolecules* **1991**, *24*, 6300.
(149) (a) Lochmüller, C. H.; Wenzel, T. J. *J. Phys. Chem.* **1990**, *94*, 4230. (b) Bauer, R. K.; de Mayo, P.; Ware, W. R.; Wu, K. C. *J. Phys. Chem.* **1982**, *86*, 3781. (c) Bauer, R. K.; Borenstein, R.; de Mayo, P.; Okada, K.; Rafalska, M.; Ware, W. R.; Wu, K. C. *J. Am. Chem. Soc.* **1982**, *104*, 4635. (d) Reference 1, Chapter 8.
(150) Reference 1, Chapters 7 and 16.
(151) Ramamurthy, V.; Casper, J. V.; Eaton, D. F.; Kuo, E. W.; Corbin, D. R. *J. Am. Chem. Soc.* **1992**, *114*, 3882. (b) Iu, K.-K.; Thomas, J. K. *J. Phys. Chem.* **1991**, *95*, 506. (c) Iu, K.-K.; Liu, X.; Thomas, J. K. *Mater. Res. Soc. Symp. Proc.* **1991**, *233*, 119. (d) Suib, S. L.; Kostapas, A. *J. Am. Chem. Soc.* **1984**, *106*, 7705. (e) Baretz, B. H.; Turro, N. J. *J. Photochem.* **1984**, *24*, 201.
(152) (a) Kaufman, V. R.; Avnir, D. *Langmuir* **1986**, *2*, 717. (b) Matsui, K.; Nakazawa, T.; Morisaki, H. *J. Phys. Chem.* **1991**, *95*, 976. (c) Matsui, K.; Nakazawa, T. *Bull. Chem. Soc. Jpn.* **1990**, *63*, 11. (d) Pouxviel, J. C.; Dunn, B.; Zink, J. I. *J. Phys. Chem.* **1989**, *93*, 2134. (e) Takahashi, Y.; Kitamura, T.; Uchida, K.; Yamanaka, T. *Jpn. J. Appl. Phys.* **1989**, *28*, L1609. (f) Kaufman, V. R.; Levy, D.; Avnir, D. *J. Non-Cryst. Solids* **1986**, *82*, 103.
(153) (a) Bohorquez, M.; Patterson, L. K. *Langmuir* **1990**, *6*, 1739. (b) Kano, K.; Kawazumi, H.; Ogawa, T.; Sunamoto, J. *J. Phys. Chem.* **1981**, *85*, 2204.
(154) Ahuja, R. C.; Möbius, D. *Langmuir* **1992**, *8*, 1136.
(155) DellaGuardia, R. A.; Thomas, J. K. *J. Phys. Chem.* **1983**, *87*, 3550.
(156) Nakamura, T.; Thomas, J. K. *J. Phys. Chem.* **1986**, *90*, 641.
(157) Viane, K.; Caigui, R.; Schoonheydt, R. A.; Schryver, F. C. *Langmuir* **1987**, *3*, 107.
(158) Viane, K.; Schoonheydt, R. A.; Crutzen, M.; Kunyama, B.; Schryver, F. C. *Langmuir* **1988**, *4*, 749.
(159) Kunyima, B.; Viane, K.; Khalil, M. M. H.; Schoonheydt, R. A.; Crutzen, M.; Schryver, F. C. *Langmuir* **1990**, *6*, 482.
(160) Nakamura, T.; Thomas, J. K. *Langmuir* **1987**, *3*, 234.
(161) DellaGuardia, R. A.; Thomas, J. K. *J. Phys. Chem.* **1984**, *88*, 964.
(162) Ogawa, M.; Aono, T.; Kuroda, K.; Kato, C. *Langmuir* **1993**, *9*, 1529.
(163) Labbé, P.; Reverdy, G. *Langmuir* **1988**, *4*, 419.
(164) Liu, X.; Thomas, J. K. *Langmuir* **1991**, *7*, 2808.
(165) Liu, X.; Iu, K.-K.; Thomas, J. K. *Langmuir* **1992**, *8*, 539.
(166) Kavanagh, R. J.; Iu, K.-K.; Thomas, J. K. *Langmuir* **1992**, *8*, 3008.
(167) Kumar, C. V.; Asuncion, E. H.; Rosenthal, G. *Microporous Mater.* **1993**, *1*, 123.
(168) Kumar, C. V.; Asuncion, E. H.; Rosenthal, G. *Microporous Mater.* **1993**, *1*, 299.
(169) Villemure, G.; Detellier, C.; Szabo, A. G. *J. Am. Chem. Soc.* **1986**, *108*, 4658.
(170) Villemure, G.; Detellier, C.; Szabo, A. G. *Langmuir* **1991**, *7*, 1215.
(171) Grauer, Z.; Avnir, D.; Yariv, S. *Can. J. Chem.* **1984**, *62*, 1889.
(172) Grauer, Z.; Malter, A. B.; Yariv, S.; Avnir, D. *Colloids Surf.* **1987**, *25*, 41.
(173) Estévez, M. J. T.; Arberoa, F. L.; Arberoa, T. L.; Arberoa, I. L.; Schoonheydt, R. A. *Clay Miner.* **1994**, *29*, 105.
(174) Estévez, M. J. T.; Arbeloa, F. L.; Arbeloa, T. L.; Arbeloa, I. L. *Langmuir* **1994**, *9*, 3629.
(175) Estévez, M. J. T.; Arbeloa, F. L.; Arbeloa, T. L.; Arbeloa, I. L. *J. Colloid Interface Sci.* **1994**, *162*, 412.
(176) Schoonheydt, R. A.; Cenes, J.; de Scryver, F. C. *J. Chem. Soc., Faraday Trans. 1* **1986**, *82*, 281.
(177) Avnir, D.; Grauer, Z.; Yariv, S.; Huppert, D.; Rojanski, D. *Nouv. J. Chim.* **1986**, *10*, 153.
(178) Hang, P. T.; Brindley, G. W. *Clays Clay Miner.* **1970**, *18*, 203.
(179) Yariv, S.; Lurie, D. *Isr. J. Chem.* **1971**, *9*, 537.
(180) Taylor, R. K. *J. Chem. Tech. Biotechnol.* **1985**, *35A*, 195.
(181) Saehr, D.; Dred, R. L.; Hoffman, D. C. M. *Clay Miner.* **1978**, *13*, 411.
(182) Cenes, J.; Schoonheydt, R. A. *Clays Clay Miner.* **1988**, *36*, 214.
(183) Schoonheydt, R. A.; Heughebaert, L. *Clay Miner.* **1992**, *27*, 91.
(184) Breen, C.; Rock, B. *Clay Miner.* **1994**, *29*, 179.
(185) Grauer, Z.; Grauer, G. L.; Avnir, D.; Yariv, S. *J. Chem. Soc., Faraday Trans. 1* **1987**, *83*, 1685.
(186) Cohen, R.; Yariv, S. *J. Chem. Soc., Faraday Trans. 1* **1984**, *80*, 1705.
(187) Yamagishi, A.; Soma, M. *J. Phys. Chem.* **1981**, *85*, 3090.
(188) Bose, H.; Sunwar, C. B.; Chakravarti, S. K. *Ind. J. Chem.* **1987**, *26A*, 944.
(189) Sunwar, C. B.; Bose, H. *J. Colloid Interface Sci.* **1990**, *136*, 54.
(190) Hepler, L. G.; Yariv, S.; Dobroghowska, C. *Thermochim. Acta* **1987**, *121*, 373.
(191) Yariv, S.; Nasser, A.; Bar-on, P. *J. Chem. Soc., Faraday Trans.* **1990**, *86*, 1593.
(192) Taniguchi, M.; Yamagishi, A.; Iwamoto, T. *J. Phys. Chem.* **1990**, *94*, 2534.
(193) Miyata, S. *Clays Clay Miner.* **1983**, *31*, 305.

(194) Nakato, T.; Iwata, Y.; Kuroda, K.; Kato, C. *J. Inclusion Phenom.* **1992**, *13*, 249.
(195) Cady, S. S.; Pinnavaia, T. J. *Inorg. Chem.* **1978**, *17*, 1501.
(196) Van Damme, H.; Crepsin, M.; Obrecht, F.; Cruz, M. I.; Fripiat, J. J. *J. Colloid Interface Sci.* **1978**, *66*, 43.
(197) Carrado, K. A.; Winans, R. E. *Chem. Mater.* **1990**, *2*, 328.
(198) Abdo, S.; Cruz, M. I.; Fripiat, J. J. *Clays Clay Miner.* **1980**, *28*, 125.
(199) Giannelis, E. P. *Chem. Mater.* **1990**, *2*, 627.
(200) Ukrainczyk, L.; Chibwe, M.; Pinnavaia, T. J.; Boyd, S. A. *J. Phys. Chem.* **1994**, *98*, 2668.
(201) Kuykendall, V. G.; Thomas, J. K. *Langmuir* **1990**, *6*, 1350.
(202) Nakato, T.; Iwata, Y.; Kuroda, K.; Kaneko, M.; Kato, C. *J. Chem. Soc., Dalton Trans.* **1993**, 1405.
(203) Park, I. Y.; Kuroda, K.; Kato, C. *Chem. Lett.* **1989**, 2057.
(204) Sakoda, K.; Kominami, K. *Chem. Phys. Lett.* **1993**, *216*, 270.
(205) Carrado, K. A.; Thiyagarajan, P.; Winans, R. E.; Botto, R. E. *Inorg. Chem.* **1991**, *30*, 794.
(206) Garillon, L.; Bedioui, F.; Devynck, J.; Battioni, P.; Barloy, L.; Mansuy, D. *J. Electroanal. Chem.* **1991**, *303*, 283.
(207) Garillon, L.; Bedioui, F.; Devynek, J.; Battioni, P. *J. Electroanal. Chem.* **1993**, *347*, 435.
(208) Bergaya, F.; Van Damme, H. *Geochim. Cosmochim. Acta* **1982**, *46*, 349.
(209) Kameyama, H.; Suzuki, H.; Amano, A. *Chem. Lett.* **1988**, 1117.
(210) Barloy, L.; Lallier, J. P.; Mansuy, D.; Piffard, Y.; Tournox, M.; Valim, J. B.; Jones, W. *New J. Chem.* **1992**, *16*, 71.
(211) Carrado, K. A.; Forman, J. E.; Botto, R. E.; Winans, R. E. *Chem. Mater.* **1993**, *5*, 472.
(212) Rusling, J. F.; Ahmadi, M. F.; Hu, N. *Langmuir* **1992**, *8*, 2455.
(213) Hu, N.; Rusling, J. F. *Anal. Chem.* **1991**, *63*, 2163.
(214) Chibwe, M.; Pinnavaia, T. J. *J. Chem. Soc., Chem. Commun.* **1993**, 278.
(215) Grigoryan, L.; Yakushi, K.; Liu, C.-J.; Takano, S.; Wakata, M.; Yamauchi, H. *Physica C* **1993**, *218*, 153.
(216) Theng, B. K. G. *Clays Clay Miner.* **1971**, *19*, 383.
(217) Fahn, R.; Fenderl, K. *Clay Miner.* **1993**, *18*, 447.
(218) Kovar, L.; DellaGuardia, R.; Thomas, J. K. *J. Phys. Chem.* **1984**, *84*, 3595.
(219) Sackett, D. D.; Fox, M. A. *Langmuir* **1990**, *6*, 1237.
(220) Sanchez-Martin, M. J.; Sanchez-Camazano, M. *Chemosphere* **1987**, *16*, 937.
(221) Vicente, M. A.; Sánchez-Camazano, M.; Sánchez-Martín, M. J.; Arco, M.; Martín, C.; Rives, V. *Clays Clay Miner.* **1989**, *37*, 157.
(222) Marguiles, L.; Rozen, H.; Cohen, E. *Nature* **1985**, *315*, 658. Margulies, L.; Rozen, H. *J. Mol. Struct.* **1986**, *141*, 219.
(223) Mao, Y.; Zhang, G.; Thomas, J. K. *Langmuir* **1993**, *9*, 1299.
(224) Mao, Y.; Pankasem, S.; Thomas, J. K. *Langmuir* **1993**, *9*, 1504.
(225) Cenes, J.; Schoonheydt, R. A. *Clay Miner.* **1988**, *23*, 205.
(226) Lee, C. F.; Thompson, M. E. *Inorg. Chem.* **1991**, *30*, 4.
(227) Takagi, T.; Usami, H.; Fukuya, H.; Sawaki, Y. *J. Chem. Soc., Chem. Commun.* **1989**, 1174.
(228) Usami, H.; Takagi, K.; Sawaki, Y. *J. Chem. Soc., Perkin Trans. 2* **1990**, 1723.
(229) Usami, H.; Takagi, K.; Sawaki, Y. *J. Chem. Soc., Faraday Trans.* **1992**, *88*, 77.
(230) Usami, H.; Takagi, K.; Sawaki, Y. *Bull. Chem. Soc. Jpn.* **1991**, *64*, 3395.
(231) Takagi, K.; Shichi, T.; Usami, H.; Sawaki, Y. *J. Am. Chem. Soc.* **1993**, *115*, 4339.
(232) Grätzel, M. *Energy Resources through Photochemistry and Catalysis*; Academic: New York, 1983.
(233) Casal, B.; Ruiz-Hitzky, E.; Bergaya, F.; Challal, D.; Fripiat, J.; Van Damme, H. *J. Mol. Catal.* **1985**, *33*, 83.
(234) Nijs, H.; Cruz, M.; Fripiat, J.; Van Damme, H. *J. Chem. Soc., Chem. Commun.* **1981**, 1026.
(235) Nijs, H.; Cruz, M.; Fripiat, J.; Van Damme, H. *J. Phys. Chem.* **1987**, *87*, 1279.
(236) Detellier, C.; Villemure, G. *Inorg. Chim. Acta* **1984**, *86*, L19.
(237) Detellier, C.; Villemure, G.; Kodama, H. *Can. J. Chem.* **1984**, *63*, 1139.
(238) Villemure, G.; Bazan, G.; Kodama, H.; Szabo, A. G.; Detellier, C. *Appl. Clay Sci.* **1987**, *2*, 241.
(239) Van Damme, H.; Nijs, H.; Fripiat, J. J. *J. Mol. Catal.* **1984**, *27*, 123.
(240) Van Damme, H.; Bergaya, F.; Habti, A.; Fripiat, J. J. *J. Mol. Catal.* **1983**, *21*, 223.
(241) Newsham, M. D.; Giannelis, E. P.; Pinnavaia, T. J.; Nocera, D. G. *J. Am. Chem. Soc.* **1988**, *110*, 3885.
(242) Suib, S. L.; Carrado, K. A. *Inorg. Chem.* **1985**, *24*, 863.
(243) Suib, S. L.; Tanguay, J. F.; Occelli, M. L. *J. Am. Chem. Soc.* **1986**, *108*, 6972.
(244) Fendler, J. H. *Chem. Rev.* **1987**, *87*, 877.
(245) For example: Krishran, M.; White, J. R.; Fox, M. A.; Bard, A. J. *J. Am. Chem. Soc.* **1983**, *105*, 7002.
(246) For example: Milosauljevic, B. H.; Kuczynski, J.; Thomas, J. K. *J. Phys. Chem.* **1984**, *88*, 980.
(247) For example: Kuczynski, J.; Thomas, J. K. *J. Phys. Chem.* **1985**, *89*, 2720.
(248) For example: Herron, N.; Wang, Y.; Eddy, M. E.; Stucky, G. D.; Cox, D. E.; Moller, K.; Bein, T. *J. Am. Chem. Soc.* **1989**, *111*, 530.
(249) Yoneyama, H.; Nippa, S. *Chem. Lett.* **1988**, 1807.
(250) Yoneyama, H.; Saga, S.; Yamanaka, S. *J. Phys. Chem.* **1989**, *93*, 4833.
(251) Tanguay, H. F.; Suib, S. L.; Coughlin, R. W. *J. Catal.* **1989**, *117*, 335.
(252) Fan, F.-R. F.; Liu, H.-Y.; Bard, A. J. *J. Phys. Chem.* **1985**, *89*, 4418.
(253) Miyoshi, H.; Mori, H.; Yoneyama, H. *Langmuir* **1991**, *7*, 503.
(254) Miyoshi, H.; Yoneyama, H. *J. Chem. Soc., Faraday Trans. 1* **1989**, *85*, 1873.
(255) Enea, O.; Bard, A. J. *J. Phys. Chem.* **1986**, *90*, 301.
(256) Stramel, R. D.; Nakamura, T.; Thomas, J. K. *Chem. Phys. Lett.* **1986**, *130*, 423.
(257) Stramel, R. D.; Nakamura, T.; Thomas, J. K. *J. Chem. Soc., Faraday Trans. 1* **1988**, *84*, 1287.
(258) Liu, X.; Thomas, J. K. *J. Colloid Interface Sci.* **1989**, *129*, 476.
(259) Sato, T.; Okuyama, H.; Endo, T.; Shimada, M. *React. Solids* **1990**, *8*, 63.
(260) Cao, G.; Rasenberg, L. K.; Nunn, C. M.; Mallouk, T. E. *Chem. Mater.* **1991**, *3*, 149.
(261) Cassagneau, T.; Hix, G. B.; Jones, D. J.; Maireles-Torres, P.; Rhomari, M.; Rozière, J. *J. Mater. Chem.* **1994**, *4*, 189.
(262) Domen, K.; Kudo, A.; Shinozaki, A.; Tanaka, A.; Maruya, K.; Onishi, T. *J. Chem. Soc., Chem. Commun.* **1986**, 356.
(263) Domen, K.; Kudo, A.; Shibata, M.; Tanaka, A.; Maruya, K.; Onishi, T. *J. Chem. Soc., Chem. Commun.* **1986**, 1706.
(264) Kudo, A.; Tanaka, A.; Domen, K.; Maruya, K.; Aika, K.; Onishi, T. *J. Catal.* **1988**, *111*, 67.
(265) Kudo, A.; Sayama, K.; Asakura, K.; Domen, K.; Maruya, K.; Onishi, T. *J. Catal.* **1989**, *120*, 337.
(266) Kameyama, A.; Domen, K.; Maruya, K.; Endo, T.; Onishi, T. *J. Mol. Catal.* **1990**, *58*, 205.
(267) Sayama, K.; Tanaka, A.; Domen, K.; Maruya, K.; Onishi, T. *J. Phys. Chem.* **1991**, *95*, 1345.
(268) Sekine, T.; Yoshimura, J.; Tanaka, A.; Domen, K.; Maruya, K.; Onishi, T. *Bull. Chem. Soc. Jpn.* **1990**, *63*, 2107.
(269) Kim, Y. I.; Atherton, S. J.; Brigham, E. S.; Mallouk, T. E. *J. Phys. Chem.* **1993**, *97*, 11802.
(270) Kim, Y. I.; Salim, S.; Huq, M. J.; Mallouk, T. E. *J. Am. Chem. Soc.* **1991**, *113*, 9561.
(271) Vermeulen, L. A.; Thompson, M. E. *Nature* **1992**, *358*, 656.
(272) Vermeulen, L. A.; Snover, J.; Sapochak, L. S.; Thompson, M. E. *J. Am. Chem. Soc.* **1993**, *115*, 11767.
(273) Snover, J.; Thompson, M. E. *J. Am. Chem. Soc.* **1994**, *116*, 765.
(274) Ungashe, S. B.; Wilson, W. L.; Katz, H. E.; Scheller, G. R.; Putvinsky, T. M. *J. Am. Chem. Soc.* **1992**, *114*, 8717.
(275) Kumar, C. V.; Chadhari, A.; Rosenthal, G. L. *J. Am. Chem. Soc.* **1994**, *116*, 403.
(276) Endo, T.; Sato, T.; Shimada, M. *J. Phys. Chem. Solids* **1986**, *47*, 799.
(277) Endo, T.; Nakada, N.; Sato, T.; Shimada, M. *J. Phys. Chem. Solids* **1988**, *49*, 1423.
(278) Endo, T.; Nakada, N.; Sato, T.; Shimada, M. *J. Phys. Chem. Solids* **1989**, *50*, 133.
(279) Ogawa, M.; Inagaki, M.; Kodama, N.; Kuroda, K.; Kato, C. *Mol. Cryst. Liq. Cryst.* **1992**, *214*, 141.
(280) Ogawa, M.; Inagaki, M.; Kodama, N.; Kuroda, K.; Kato, C. *J. Phys. Chem.* **1993**, *97*, 3819.
(281) Bergaya, F.; Van Damme, H. *J. Chem. Soc., Faraday Trans. 2* **1993**, *79*, 505.
(282) Izawa, H.; Kikkawa, S.; Koizumu, M. *Nippon-Kagaku-Kaishi* **1987**, 397.
(283) Kudo, A.; Sakata, T. *J. Mater. Chem.* **1993**, *3*, 1081. Kudo, A.; Sakata, T. *Chem. Lett.* **1994**, 2179.
(284) *Photochromism Molecules and Systems*; Dürr, H., Bouas-Laurent, H., Eds.; Elsevier: Amsterdam, 1990.
(285) Otruba, J. P.; Weiss, R. G. *Mol. Cryst. Liq. Cryst.* **1982**, *80*, 165. Ramesh, V.; Labes, M. M. *J. Am. Chem. Soc.* **1987**, *109*, 3228.
(286) Seki, T.; Ichimura, K. *J. Chem. Soc., Chem. Commun.* **1987**, 1187.
(287) Holden, D. A.; Ringsdorf, H.; Deblauwe, V.; Smets, G. *J. Phys. Chem.* **1984**, *88*, 716.
(288) Adams, J. M.; Gabbutt, A. J. *J. Inclusion Phenom.* **1990**, *9*, 63.
(289) Takagi, K.; Kurematsu, T.; Sawaki, Y. *J. Chem. Soc., Perkin Trans. 2* **1991**, 1517.
(290) Tomioka, H.; Itoh, T. *J. Chem. Soc., Chem. Commun.* **1991**, 532.
(291) Seki, T.; Ichimura, K. *Macromolecules* **1990**, *23*, 31.
(292) Tagaya, H.; Kuwahara, T.; Sato, S.; Kadokawa, J.; Karasu, M.; Chiba, K. *J. Mater. Chem.* **1993**, *3*, 317.
(293) Miyata, H.; Sugahara, Y.; Kuroda, K.; Kato, C. *J. Chem. Soc., Faraday Trans. 1* **1987**, *83*, 1851.
(294) See for example: Shinkai, S.; Nakaji, T.; Ogawa, T.; Shigematsu, K.; Manabe, O. *J. Am. Chem. Soc.* **1981**, *103*, 111.
(295) See for example: Tachibana, H.; Goto, A.; Nakamura, T.; Matsumoto, M.; Manda, E.; Niino, H.; Yabe, A.; Kawabata, Y. *J. Am. Chem. Soc.* **1989**, *111*, 3080.

(296) Miyata, H.; Sugahara, Y.; Kuroda, K.; Kato, C. *J. Chem. Soc., Faraday Trans. 1* **1988**, *84*, 2677.
(297) Nakato, T.; Miyata, H.; Kuroda, K.; Kato, C. *React. Solids* **1988**, *6*, 231.
(298) Nakato, T.; Kuroda, K.; Kato, C. *J. Chem. Soc., Chem. Commun.* **1989**, 1144.
(299) Nakato, T.; Kuroda, K.; Kato, *C. Chem. Mater.* **1992**, *4*, 128.
(300) Nakato, T.; Ito, K.; Kuroda, K.; Kato, C. *Microporous Mater.* **1993**, *1*, 283.
(301) See for example: Moerner, W. E., Ed. *Persistent Spectral Hole Burning: Science and Applications*; Springer-Verlag: Berlin, 1988.
(302) Ogawa, M.; Handa, T.; Kuroda, K.; Kato, C.; Tani, T. *J. Phys. Chem.* **1992**, *96*, 8116.
(303) Graf, F.; Hong, H.-K.; Haarer, D. *Chem. Phys. Lett.* **1978**, *59*, 217. Drissler, F.; Graf, F.; Haarer, D. *J. Chem. Phys.* **1980**, *72*, 4996.
(304) Iino, Y.; Tani, T.; Sakuda, M.; Nakahara, H.; Fukuda, K. *Chem. Phys. Lett.* **1987**, *140*, 76. Tani, T.; Iino, Y.; Sakuda, M.; Itani, A.; Nakahara, H.; Fukuda, K. *J. Lumin.* **1987**, *38*, 43. Friedrich, J.; Wolfrum, H.; Haarer, D. *J. Chem. Phys.* **1982**, *77*, 2309. Friedrich, J.; Swalen, J. D.; Haarer, D. *J. Chem. Phys.* **1980**, *73*, 705. Tani, T.; Itani, A.; Iino, Y.; Sakuda, M. *J. Chem. Phys.* **1988**, *88*, 1272. Tani, T.; Namikawa, H.; Arai, K.; Makishima, A. *J. Appl. Phys.* **1985**, *58*, 3559. Tani, T.; Itani, A.; Iino, Y.; Sakuda, M. *Jpn. J. Appl. Phys.* **1987**, *26*, suppl. 77. Tani, T.; Sakakibara, Y.; Yamamoto, K. *Jpn. J. Appl. Phys.* **1989**, *28*, suppl. 239. Basché, Th.; Bräuschle, C. *J. Phys. Chem.* **1991**, *95*, 7130. Basché, Th.; Bräuschle, C. *Chem. Phys. Lett.* **1991**, *181*, 179.
(305) Ogawa, M.; Takahashi, M.; Kato, C.; Kuroda, K. *J. Mater. Chem.* **1994**, *4*, 519.
(306) Prasad, P. N.; Williams, D. J. *Introduction to Nonlinear Optical Effects in Molecules and Polymers*; Wiley Interscience: New York, 1991.
(307) Munn, R. W., Ironside, C. N., Eds., *Principles and Applications of Nonlinear Optical Materials*; CRC: London, 1993.
(308) Tomaru, S.; Zembutsu, S.; Kawachi, M.; Kobayashi, M. *J. Inclusion Phenom.* **1984**, *2*, 885. Tomaru, S.; Zembutsu, S.; Kawachi, M.; Kobayashi, M. *J. Chem. Soc., Chem. Commun.* **1984**, 1207. Wang, Y.; Eaton, D. F. *Chem. Phys. Lett.* **1985**, *120*, 441.
(309) Eaton, D. F.; Anderson, A. G.; Tam, W.; Wang, Y. *J. Am. Chem. Soc.* **1987**, *109*, 1886.
(310) Cooper, S.; Dutta, P. K. *J. Phys. Chem.* **1990**, *94*, 114.
(311) Pécaut, J.; Fur, Y. I.; Levy, J.-P.; Masse, R. *J. Mater. Chem.* **1993**, *3*, 333.
(312) Lacroix, P. G.; Lemarinier, A. V. V.; Clément, R.; Nakatani, K.; Delaire, J. A. *J. Mater. Chem.* **1993**, *3*, 499.
(313) Lacroix, P. G.; Clément, R.; Nakatani, K.; Zyss, J.; Ledoux, I. *Science* **1994**, *263*, 658.
(314) Kurtz, S. K.; Perry, T. T. *J. Appl. Phys.* **1968**, *39*, 3798.
(315) Li, D. Q.; Ratner, M. A.; Marks, T. J.; Zhang, C.; Yang, J.; Wong, G. K. *J. Am. Chem. Soc.* **1990**, *112*, 7389.
(316) Katz, H. E.; Scheller, G.; Putvinski, T. M.; Schilling, M. L.; Wilson, W. L.; Chidsey, C. E. D. *Science* **1991**, *254*, 1485.
(317) For example: Singer, K. D.; Sohn, J. E.; Lalma, S. J. *Appl. Phys. Lett.* **1986**, *49*, 248.
(318) For example: Kim, J.; Plawsky, J. L.; LaPeruta, R.; Korenowsky, G. M. *Chem. Mater.* **1992**, *4*, 249.
(319) Yoshimura, T.; Tatsuura, S.; Sotoyama, W. *Thin Solid Films* **1992**, *207*, 9. Tatsuura, S.; Sotoyama, W.; Motoyoshi, K.; Matsuura, A.; Hayano, T.; Yoshimura, T. *Appl. Phys. Lett.* **1993**, *62*, 2182.
(320) Ogawa, M.; Takahashi, M.; Kuroda, K. *Chem. Mater.* **1994**, *6*, 715.
(321) Note Added in Proof: Preparation of multilayered structures from layered solids have been reported recently by two different research groups (Keller, S. W.; Kim, H.-N.; Mallouk, T. E. *J. Am. Chem. Soc.* **1994**, *116*, 8817. Kleinfeld, E. R.; Ferguson, G. S. *Science* **1994**, *265*, 370.) Exfoliated platelets of ZrP, layered metal oxide semiconductors, and laponite have been used as a building block to construct multilayer films.

CR940028R